ALMA MATER STUDIORUM - UNIVERSITÀ DI BOLOGNA

DOTTORATO DI RICERCA IN INGEGNERIA CIVILE, CHIMICA, AMBIENTALE E DEI MATERIALI

CICLO XXXIV

Settore Concorsuale: 08-A2 – INGEGNERIA SANITARIA – AMBIENTALE, INGEGNERIA DEGLI IDROCARBURI E FLUIDI NEL SOTTOSUOLO, DELLA SICUREZZA E PROTEZIONE IN AMBITO CIVILE

Settore Scientifico Disciplinare: ING-IND/30 – IDROCARBURI E FLUIDI DEL SUTTOSUOLO

COUPLED WELLBORE-RESERVOIR SIMULATION OF THERMAL EFFECTS DURING MULTIPHASE CO$_2$ INJECTION

Presentata da: **Supervisore:**

Kristina Strpić   Prof. Paolo Macini

Coordinatore Dottorato: **Co-supervisori:**

Prof. Alessandro Tugnoli   Prof. Villiam Bortolotti

                                                            Prof. Stefano Bonduà

                                                            Ing. Alfredo Battistelli

Esame finale anno 2022

Acknowledgments

Abstract

The advantages of the coupled wellbore-reservoir simulation are well known in the oil and gas industry since many decades. T2Well-ECO2M is a coupled wellbore reservoir simulator still under development at Lawrence Berkeley National Laboratory (LBNL, Berkeley, USA) with the ability to deal with a mixture of H_2O-CO_2-NaCl and includes the simulation of CO_2 phase transition and multiphase flow. So far, T2Well-ECO2M is available only as an under-development code, and thanks to the collaboration with LBNL, the Geothermal Modelling group of DICAM had an opportunity to test and verify the code. The code was originally developed for the simulation of CO_2 injection into deep saline aquifers and the modelling of enhanced geothermal systems; however, the focus of this research was to modify and test T2Well-ECO2M to simulate CO_2 injection into depleted gas reservoirs.

To this end, the original code was properly changed in a few parts and a dedicated injection case was developed to study CO_2 phase transition inside of a wellbore and the corresponding thermal effects.

In the first scenario, the injection case was run applying the fully numerical approach of wellbore to formation heat exchange calculation. Results were analysed in terms of wellbore pressure and temperature vertical profiles, wellhead and bottomhole conditions, and characteristic reservoir displacement fronts. Special attention was given to the thorough analysis of bottomhole temperature as the critical parameter for hydrate formation. Besides the expected direct effect of wellbore temperature changes caused by the phase transition on reservoir conditions, the simulation results indicated also the effect of CO_2 phase change in the near wellbore zone on BH pressure distribution. This proved the importance of the coupled-wellbore reservoir approach in the case of CO_2 injection simulations as CO_2 phase conditions inside of wellbore depend of multiple factors such as injection rate and temperature, and pressure difference between the injected CO_2 and initial wellhead pressure.

To test the implemented software changes, in a second scenario, the same injection case was reproduced with using the improved semi-analytical time-convolution approach for wellbore to formation heat exchange calculation. It is noteworthy T2Well-ECO2M is the first version of

T2Well codes with an available time-convolution option for heat exchange calculation. The comparison of the two scenarios showed that the simulation of wellbore and reservoir parameters after one year of continuous CO_2 injection are in good agreement with the computation time to solve the time-convolution semi-analytical reduced. The new updated T2Well-ECO2M version has shown to be a robust and performing wellbore-reservoir simulator that can be also used to simulate the CO_2 injection into depleted gas reservoirs.

Contents

List of Figures

List of Tables

Nomenclature

A	Connection (cross sectional) surface	(m^2)
C	Specific heat capacity	$(J\ ^{\circ}C^{-1}\ kg^{-1})$
C_0	Wellbore distribution coefficient	$(-)$
C_w	Wellbore wall friction coefficient	$(-)$
D	Distance between block nodes	(m)
d	Wellbore diameter	(m)
$\vec{F}$	Mass or energy flux	$(kg\ m^{-2}\ s^{-1})\ or\ (J\ m^{-2}\ s^{-1})$
$\vec{g}$	Gravitational acceleration	$(m\ s^{-2})$
h	Specific enthalpy	$(J\ kg^{-1})$
j	Volumetric flux of mixture	$(m^3\ s^{-1}\ m^{-2})$
k	Absolute permeability	(m^2)
k_r	Relative permeability	$(-)$
K_u	Kutateladze number	$(-)$
M	Mass or energy per volume	$(kg\ m^{-3})\ \ or\ \ (J\ m^{-3})$
N_B	Bond number	$(-)$
P	Pressure	(Pa)
P_c	Capillary pressure	(Pa)
Q	Mass or energy generation rate	$(kg\ m^3\ s^{-1})\ or\ (J\ m^3\ s^{-1})$
Q_{ex}	Heat loss/gain of the wellbore per unit length	$(W\ m^{-1})$
R	Residual	$(-)$
r	Radius	(m)
S	Saturation	$(-)$
T	Temperature	$(^{\circ}C)$
T_{∞}	Formation temperature (wellbore surrounding)	$(^{\circ}C)$

t	Time	(s)
t_D	Dimensionless time	$(-)$
U	Over-all heat exchange coefficient	$(W\ {}^{\circ}C^{-1}m^{-2})$
u	Specific internal energy	$(J\ kg^{-1})$
V	Pore volume	(m^3)
v	Velocity	$(m\ s^{-1})$
v_d	Drift velocity	$(m\ s^{-1})$
X	Mass fraction	$(-)$
α	Thermal diffusivity	$(m^2\ s^{-1})$
Γ	Surrounding surface of the volume	(m^2)
γ	Euler's constant	$(-)$
θ	Wellbore inclination angle	(rad)
κ	Component	$(-)$
λ	Thermal conductivity	$(W\ {}^{\circ}C^{-1}\ kg^{-1})$
μ	Dynamic viscosity	$(Pa{\cdot}s)$
ρ	Density	(kg/m^3)
ρ_m^*	Profile adjusted average density	(kg/m^3)
ϕ	Porosity	$(-)$
σ	Surface tension	$(N\ m^{-1})$

Abbreviations

CCS	Carbon capture and storage
CCUS	Carbon capture, utilization and storage
DFM	Drift flux model
EDM	Equivalent Darcy's media
EGR	Enhanced gas recovery

EGS	*Enhanced geothermal systems*
EOR	*Enhanced oil recovery*
EPM	*Equivalent porous media*
GHG	*Greenhouse gases*
GWP	*Global warming potential*
IFDM	*Integral finite difference method*
NEQ	*Number of equations*
NEL	*Number of grid elements (blocks)*
NK	*Number of components*
PCGO	*Gas-oil (liquid) capillary pressure*
PCGW	*Gas-aqueous capillary pressure*
REPAq	*Aqueous phase relative permeability*
REPG	*Gas phase relative permeability*
REPL	*Liquid phase relative permeability*

Subscripts and Superscripts

a	*Aqueous phase*
cem	*Cement*
co	*External casing (radius)*
cr	*Critical value*
g	*Gaseous phase*
f	*Formation*
h	*External cement sheath (radius)*
i	*I^{th} grid element (block)*
k	*Time step index*
l	*Liquid phase*
m	*M^{th} element*

n	*Nth element*
n-a	*Non-aqueous part of mixture*
R	*Rock matrix*
r	*Radiation*
s	*Solid salt*
sm	*Salt mass*
to	*External tubing (radius)*
w	*Wellbore*
β	*Phase index*

1 Introduction

There is no unique pathway for achieving global climate goals in the next 30 years and the key aspect of the global strategies is development and adaptation in various sectors. Investment in sustainable and renewable energy resources should help in the mitigation of new emissions, but at the same time, adaptation is necessary for existing high emitting sectors. Carbon capture, storage and utilization (CCUS) is considered to be critical for reaching a sustainable path in energy systems and reaching climate pledges.

1.1 Greenhouse gases and the present CO_2 issues

The concentration of greenhouse gases (GHG) in the atmosphere, well documented and recorded since many decades, its anthropogenic nature and its influence on the complex dynamics of climate change is no doubts the major environmental concern of the new millennium. The transnational social and political "climate pledge" testifies the global commitment to design a viable and sustainable "Energy Transition".

GHG have the property of absorbing infrared radiation, i.e., the net heat energy which is emitted from Earth's surface and reradiated back (Hertzberg et al., 2017). The effect of each GHG on Earth's climate depends on its chemical nature and its relative concentration in the atmosphere. The most important GHG are water vapor (H_2O), carbon dioxide (CO_2), methane (CH_4), low-level ozone (O_3, also called surface ozone), nitrous oxide (N_2O), and fluorinated gases (halocarbons). Some gases have a high capacity for absorbing infrared radiation or occur in significant quantities, whereas others have considerably lower capacities for absorption or occur only in trace amounts (Mann, 2019). Radiative forcing, as defined by the Intergovernmental Panel on Climate Change (IPCC), is a measure of the influence which a greenhouse gas has on the amount of radiant energy impinging upon Earth's surface. The "global warming potential" (GWP) of a single GHG indicates the amount of warming that gas causes over a certain time period (normally 100 years). GWP is an index, with CO_2 having the reference index value of 1, and the GWP for all other GHGs is the number of times more warming they cause compared to CO_2 (IPCC, 2007). For example, for the

1

same weight, methane, with GWP number 25, causes 25 times more warming over a period of 100 years compared to CO_2. An additional advantage of GWP determination is assigning contribution of each gas in the total GHG mixture. Climate Watch of the World Research Institute reports that CO_2 comprises 74% of greenhouse gas emissions in 2016 (Ge and Friedrich, 2020). Although there are natural sources of CO_2 such as venting volcanos or decomposing organic matter, according to IPCC's special report on Carbon Dioxide Capture and Storage (2005), the GHG making the largest contribution from human activities is CO_2. These anthropogenic sources are the massive combustion of fossil fuels and biomass as a fuel; burning of forests during land clearance, together with certain industrial and resource extraction processes (Yoro and Daramola, 2020). According to literature, fossil fuel power plants contribute about 33-40% of total CO_2 emissions, where coal is the main contributor (Tian and Yang, 2016). Other important contributors among industry sector include petrochemical plants, iron and steel industry, and cement industry in which CO_2 is partially emitted from the combustion process (40%) and partially from calcination (60%) (Barker et al., 2009).

Increase in the global average temperature is the most concerning consequence connected with the increase in GHG concentration. Agreement of the governments about limiting global warming to 1.5°C above pre-industrial levels was set on the IPCC Special Report released in October, 2018. The report draws on research conducted since nations unveiled the 2015 Paris climate agreement (UNFCC, 2015), which seeks to limit greenhouse-gas emissions and global temperature increase to between 1.5°C and 2 °C by 2100. These climate pledges were revised during COP26 annual meeting in Glasgow, 2021. Although climate targets set by the Paris Climate Agreement included pursuing efforts to limit surface warming to 1.5°C above its pre-industrial average, current emissions pledges discussed at COP26, if met, will still likely result in warming of over 2°C.

According to the IPCC 2018 report, there are four pathways for reaching these climate goal and three of them include CCUS/CCS as one of the crucial actions for climate change mitigation. Each of the pathways would require concerted effort globally, either through commitments in policies and regulations to drive down both energy demand/supply and consumption or mitigate impact of growth through a solution which would include low-carbon energy technologies and CCUS.

1.2 CCS

CCS and CCUS refers to technologies dedicated to capturing CO_2 from processes such as combustion (generally power generation) or gasification, and its permanent storage in geological structures or conversion into valuable chemical compounds (Cuéllar-Franca and Azapagic, 2018). Many industrial processes, most notably cement, iron and steel production, and -in few cases - natural gas treatment also intrinsically produce CO_2 and can be fitted with CO_2 capture technologies. For these industries, CCS offers a valuable solution for lowering CO_2 emissions (Boot-Handford et al., 2014; Rackley, 2017). Consequently, CCS has been viewed as a bridge for decarbonizing future energy. CO_2 is first captured from the flue/fuel gases, transported and then either stored permanently or reutilized industrially. CCS can reduce CO_2 emissions up to 85–90% from large point emission sources (Leung et al., 2014). However, after three decades of research, this technology has been facing barriers as the design and operation costs are still high (Karimi and Khalilpour, 2015).

Estimation of actual CCS cost is challenging, as well as expressing it is straightforward way. Part of the difficulties lies in choosing the baseline for comparing different CCS plants, costs associated with implementation of CCS on a retrofit basis and CO_2-footprint of heat and power used in CCS chain (Roussanaly et al., 2021). Significant research and development efforts are focused on the capture part of the CCS system since capture is identified as the most expensive step in CCS system (Budinis, 2018; IPCC, 2018). Technically, four main technological options are available for CO_2 capturing from large point sources such as fossil fuel power plants. These technological options include post-combustion, pre-combustion, oxy-fuelling, and capturing from industrial processes such as biogas sweetening and ammonia production (Raza et al., 2019).

Commonly, CO_2 is not stored in the same place where has been captured. There are several CO_2 transportation methods, mainly depending on the distance between the capture and storage site, and this can be done by pipelines, dedicated vessels, or tank trucks (Pires et al., 2011). Additionally, the choice of the transport will also depend on transportation cost, where operational conditions, onshore/offshore storage location, and size of the pipeline, have a major impact. During the capturing practice, non-condensable impurities which are often mixed with CO_2, such as O_2, N_2 or Ar, may also pose additional costs on the storage projects and, eventually, reduce the storage

capacity. Therefore, they should be removed before injection (Wang et al., 2011). Furthermore, captured CO_2 may contain water vapor, which should be reduced to a very low percentage as it reacts with CO_2 and other acidic compounds to form corrosive acids. The CO_2 transport in liquid or supercritical phase, which is the most common case for pipeline transport with operative pressure higher than CO_2 critical pressure. Even though CO_2 transport pipelines are primarily designed to operate in one-phase condition, two-phase conditions may occur. Some of the reasons for two-phase conditions inside of CO_2 transportation pipelines are fluctuation in CO_2 supply or transient operations such as start-up or shut-in operations (Klinkby et al., 2011; Munkejord et al., 2013). Potential leakage from the pipeline, and corresponding pipeline depressurisation, can also cause two-phase conditions. Depressurisation can lead to strong temperature drops, therefore it is important to have accurate modelling of these temperatures to have safe CO_2 transport, since pipeline materials have a minimum temperature at which they lose toughness (Munkejord and Hammer, 2015).

As already mentioned, the high CO_2 rich mixture can be transported for geological storage, or for CO_2 utilization. Regarding the utilisation, there are many research and development projects in chemical and energy industry. Captured CO_2 can be used for ammonia, methanol and urea production, production of high-quality plastics and advanced materials (Ampelli et al., 2015), and in a wide range of thermal waste treatment (Leung et al., 2014; Zhu, 2019). These direct applications for CO_2 are limited in scale and have a small effect on the overall CO_2 emissions reduction. It can also be used in large-scale industries to indirectly boost/enhance a process as in the enhanced oil recovery (EOR), enhanced gas recovery (EGR) and enhanced geothermal systems (EGS) (Rafieea et al., 2018).

Storage site selection for a CCS project is guided by basin and regional-scale suitability evaluation. Suitable candidates for CO_2 storage are sedimentary formations with oil and gas reservoirs, deep saline aquifers, unmineable coal beds, and, as documented in recent projects, in salt caverns (da Costa et al., 2020). However, active or depleted oil and gas reservoirs and deep saline aquifers have been recognized as the best CCS sites for a large-scale disposal of CO_2 (Raza et al., 2019).

The key CO_2 storage aspects include storage capacity, injectivity, trapping and containment (Bachu, 2007). Storage capacity refers to total usable storage volume of a subsurface formation. For the case of depleted oil and gas reservoirs, storage capacity estimation is usually done by using

information about reserves estimation, reservoir properties and in-situ CO_2 characteristics (Raza et al, 2018). Assessment of the storage capacity in deep saline aquifers is a challenging task because of the lack of field data. The suitability of the reservoir for CO_2 storage depends on a multitude of factors: the depth of the reservoir and lateral and vertical extents; the pressure gradient; the salinity of the reservoir fluids; and most significantly – available pore space (Rodosta et al., 2011; Potdar and Vishal, 2016). These factors deal with the initial reservoir conditions, and they provide screening criteria for a preliminary analysis of storage capacity. The next step should involve comprehension of the specific reservoir response to fluid injection and trapping mechanisms in the short and long terms (Yashvardhan et al., 2021).

Injectivity is generally referred as a ratio between injection rate and differential pressure between bottom hole pressure and reservoir pressure (Raza et al., 2016). Therefore, injectivity is strongly depended on geomechanical and stratigraphic parameters of the storage formation (Raza et al, 2016; Bacci et al, 2011). Determination of dominant trapping mechanism during the sequestration site selection is essential to prevent leakage from the storage site. There are several trapping mechanisms occurring during the life span of storage site and their importance varies with time. For instance, structural/stratigraphic refers to trapping beneath a seal, and requires the presence of structural/stratigraphic trap. During the initial phase of injection, this is the important trapping mechanism where top seal (caprock) is a structural trap preventing CO_2 from escaping the storage formation. Residual trapping, on the other hand, refers to the CO_2 that remains in a porous rock after it has been disconnected from the injected CO_2 plume (Smit et al., 2014). Solubility/dissolution trapping, is a long-term process and takes place when CO_2 dissolves into subsurface fluids while mineral trapping occurs when dissolved CO_2 reacts with mineral phases forming the rock matrix. Dissolution and mineralisation are the most stable trapping forms (Raza et al., 2016; IPCC, 2005). The reassurance of containment of injected CO_2 in storage formation is required when considering potential storage sites. The most critical element of the containment system is the caprock, confining the storage formation. Therefore, it is indispensable to have information about caprock properties and faults and fractures in wellbore surrounding formation to minimise the risk of leakage to the biosphere, atmosphere or into overlying formations (Kaldi et al., 2013). CO_2 should be retained underground for very long period; therefore, every CCS project must include monitoring activity (Leung et al., 2014). The monitoring operation includes pre-injection, during-injection and post-injection phases. There are many surface and subsurface

monitoring techniques developed, aimed to check the integrity of the reservoir and the absence of leakage. Direct monitoring tools and techniques can be used to measure concentrations of CO_2 near wellbores in the subsurface or by taking surface/water column (in case of offshore application) measurements, however, most monitoring activities includes indirect measurement methods such as seismic, gravity or electromagnetic surveys (Cooper, 2009).

1.2.1 Importance of numerical simulation in CCS project development

In the complex chain of interdependent CCS activities described in the previous paragraph, numerical simulation is present in all sectors, from modelling of CO_2 capture technologies and separation of impurities in CO_2-rich stream, design of pipeline transport networks, CO_2 flow conditions inside injection wells to the study of CO_2-rich displacement front migration inside the storage formation. When focusing on the storage site, accurate information on the storage formation stratigraphic and hydrogeological parameters is essential for modelling of CO_2-rich front propagation. However, at the same time injection conditions directly affect wellbore flow behaviour. As discussed by Wan et al., (2021), injection rate and temperature will directly affect the CO_2 phase condition inside of wellbore, and finally, CO_2-bottomhole conditions will determine conditions at which CO_2 stream enters the reservoir formation. Difference between the injected wellhead pressure and incoming CO_2 pressure, as well as difference between the bottomhole and reservoir pressure are the key driving forces for CO_2 injection (Samuel and Mahgerefteh, 2017). Therefore, only with numerical simulation tools considering also the changes during transient wellbore flow it is possible to gather a comprehensive understanding of processes involved in CCS chain of activities and optimize CO_2 injection conditions.

1.3 CO_2 storage in depleted gas reservoirs

There are numerous examples of CCS projects with storage in depleted gas reservoirs, strictly for storage purposes or in combination with EGR projects (Hannis et al., 2017). However, they are appealing candidate for CO_2 storage due to their known reservoir and caprock structure and proven containment which kept hydrocarbons underground for significant geological time. An

additional benefit is that the main infrastructure on the field site already exists. According to the IEA technical Report from 2009 (Ladbrook et al., 2009), the worldwide storage capacity of depleted gas reservoirs is estimated to be around 390 Gt, based on a conservative pore volume replacement ratio of 60%. Comparing it to the global annual CO_2 emission for 2019 (Ritchie and Roser, 2020) which was 36.42 Gt, the storage capacity of depleted gas reservoirs is ten times current world's annual CO_2 emission.

However, there are challenges connected with depleted gas reservoirs as an option for CO_2 storage concerning the residual gas in the potential storage formations and wellbore integrity issues.

1.3.1 Residual gas

One of the challenges is to determine the impact of the natural gas, which is still present in a depleted gas reservoir. There are numerous studies about the effect of residual natural gas on CO_2 injection for EGR projects, mainly focused on the delay of CO_2 breakthrough and amount and quality of the recovered gas (Feather and Archer, 2010; Narinesingh and Alexander, 2014). In CCS projects, residual gas can have impact on the phase behaviour of CO_2, the thermal aspects around the wellbore, and reservoir pressure increase. In simulation study about suitability of depleted gas reservoirs for CO_2 storage, Raza et al. (2018) performed sensitivity analysis to evaluate the variation of the injection rate and heterogeneity on CO_2 storage. The study showed that the selection of an optimum injection rate can help to accomplish high storage potential in depleted gas reservoirs, particularly in condensate gas reservoirs. In the case of wet media, hight injection rates would be beneficial to ensure good storage capacity. The results obtained also revealed that a reduction in the permeability of the storage site enhances the overall storage capacity by boosting the residual and dissolution trappings after the injection period.

1.3.2 Wellbore integrity

One of the main safety concerns about CO_2 storage in depleted gas reservoirs is the leakage from the storage formation. Potential CO_2 leakage pathways include (i) natural geological faults

or fractures present in the caprock which can be reactivated with reservoir pressure increase due to injection, including possible hydraulic fractures; (ii) poorly sealed injection or monitoring wells and improperly abandoned production wells (Pruess, 2007; Ebigbo et al., 2007; Feng et al., 2017). Although one of the main advantages of the depleted gas reservoirs for CO_2 storage is the possibility to reuse some of the existing infrastructures, existing wellbores can present a threat to the integrity of CO_2 storage. In most of the cases, those wellbores were drilled when the regulations were less restrictive and, some of the materials and methods that were used are outdated or simply not designed for the high CO_2 partial pressures related to a storage project (Watson and Bachu, 2009). As wellbores are direct connections to the subsurface, defects in their structure can become leakage pathways since CO_2, in free-phase or dissolved in the formation brine, has a potential to react with and damage the materials used in wellbore construction. Therefore, investigation of wellbore integrity is a crucial prerequisite process before starting CO_2 injection for any CCS project. Numerous field examples and experimental examples warned about the casing corrosion (Kapusta and Canter, 1994; Scherer et al., 2011; Han et al., 2012) and formation of casing-cement micro-annuli (Carey et al., 2010; Heathman, 2007) during CO_2 injection for EOR, EGR and sequestration projects. The role of thermal stress on cement bond was investigated experimentally and numerically. From the recent experimental studies, De Andrade et al. (2014) applied cyclic thermal loading on the wellbore sample and showed how any pre-existing cracks in the cement sample will extend during thermal cyclic operations or will result in cement debonding. Experiments conducted by Todorović et al. (2016) on a similar sample well section revealed that strong temperature drop can create radial fractures upon freezing the pore water. In the numerical studies of this issue, Asamoto et al. (2013) found that, apart from the cases where there is pre-existing defect in the cement domain, the risk of the tensile cracking inside of the cement is low for the commercial-scale injections. Several studies confirmed how cement debonding due to thermal stress during injection operation strongly depends on the combination of thermal expansion factors of wellbore materials (Weideman, 2014; Lavrov and Torsæter, 2016). Roy et al. (2017) studied the effect of cooling rates and found that the stresses generated by thermal loading or unloading depend on the initial material temperature and the spatial gradient of temperature, while in the following study (Roy et al., 2018) it was found that thermal stress impacts can be mitigated, even with the low temperature CO_2 injection conditions, if effective in-situ stress is large enough. In general, it has been highlighted that the wellbore damage caused by thermal stress

is dependent on the combination of various factors such as injection and formation temperature and thermal and mechanical properties of the completion materials. In studies by Samuel and Mahgerefteh (2017) and Sacconi and Mahgerefteh (2020), it is discussed the importance of accurate simulation of start-up injection conditions as the rapid expansion cooling due to CO_2 depressurisation could pose several operational and safety risks, namely:

- CO_2 hydrate and ice formation following contact of the cold CO_2 with the interstitial water around the wellbore and the formation water in the perforations at the near well zone. The former poses the risk of well blockage, while the latter may severely reduce the reservoir injectivity and ultimately its storage capacity;
- thermal stress shocking of the wellbore casing steel leading to its fracture and the escape of CO_2;
- thermal stress shocking of the reservoir rocks leading to fracture thus changing the reservoir permeability and reducing storage effectiveness.

1.3.3 Non-isothermal wellbore conditions – impact on the storage formation

Additional complexity for CO_2 injection into depleted gas reservoirs comes from the fact that reservoir pressure can be much lower than the local hydrostatic pressure of the surrounding formation, while at the same time, CO_2 is in liquid or supercritical state at the high pressures, common for pipeline transport. Strong pressure difference between the upstream conditions at high pressure and bottomhole pressure (BHP) needed for the injection, can cause undesirable presence of two-phase CO_2 during the injection. The wellhead pressure (WHP), in that case, will be lower than the pressure needed to have liquid or liquid-like supercritical CO_2 causing the flashing at the wellhead propagating to the bottomhole and eventually, inside of reservoir domain. Additionally, friction loss, heat exchange with surrounding completion and rock domain, and Joule-Thomson's (JT) heating/cooling can cause thermal effects for injected CO_2 inside of the wellbore (Piao et al., 2018). The temperature at which CO_2 enters into the reservoir affects reservoir fluid flow

processes, because thermodynamic equilibria and many fluid properties are function of temperature. Weight of the fluid inside of the wellbore has significant contribution to BHP, and BHP is interrelated with the injection rate (Lu and Connell, 2008; Paterson et al., 2008). BHP is an important parameter for injection operation as it must exceed reservoir pressure.

Importance of non-isothermal CO_2 wellbore flow for optimization of injection conditions has been investigated in numerous studies since it relates directly to the operational feasibility and economics of the project. Deeper understanding of this multiple simultaneous processes requires numerical simulation. In 2006, Curtis Oldenburg investigated Joule-Thomson cooling due to CO_2 injection into natural gas reservoirs, while injecting CO_2 at a higher pressure than initial reservoir pressure. In that study, a simplified isothermal injection model considered constant injection rate and pressure with JT's cooling effect due to an isenthalpic expansion of CO_2 after entering through low and high permeability plug into an idealized reservoir. The study has shown that JT cooling is minor effect in the case of low injection rates and high permeability reservoirs (typical for natural gas reservoirs), but in the case of hight pressure injections into low pressure reservoirs, JT's cooling up to 20°C may occur, especially in the cases where injection temperature is similar to ambient temperature. However, many authors suggest the importance of the more realistic scenario which would include wellbore flow component under non-isothermal conditions. Lu and Connell (2008) have developed a numerical procedure to evaluate flow of CO_2 and CO_2-rich mixtures in non-isothermal wells. Developed procedure allows to solve coupled heat, mass and momentum equations with various fluid and thermodynamic properties. The same numerical method was used by Paterson et al. (2008) in the study about modelling of pressure and temperature profiles in CO_2 wells, with phase transition included. According to the above numerical method, two-phase wellbore conditions are potentially significant issue for CO_2 depleted gas reservoirs shallower than 2 km because under those conditions bottom-hole calculation is less straightforward and makes pressure monitoring and interpretation challenging. These studies include only injection wellbore behaviour. Zhao and Chen (2015) developed an idealized 2D model of injection site to evaluate the effects of injection temperature on CO_2 storage in deep saline aquifers. Study showed that temperature of injected CO_2 can have significant impact on pressure behaviours in near-wellbore area. In further studies (Zhao and Chen, 2017) they found that injection temperature has remarkable impact on salt precipitation in near-wellbore zone as a result of dry-out due to brine evaporation in contact with dry CO_2. Battistelli et al. (2010) studied the contribution of wellbore

flow and JT cooling withing the reservoir of the temperature distribution in near-wellbore area and evaluated it for different CO_2 injection temperatures. Simulations results showed that wellbore flow processes should be considered for a reliable evaluation of near wellbore temperature distribution during GHG sequestration. Importance of using non-isothermal flow models for correct characterization of CO_2 flow profiles in wellbores and reservoirs was demonstrated in Lei et al. (2020). In their study, new partially coupled wellbore-reservoir model was presented through combination of wellbore flow simulator, CO2Well (Lu and Connell, 2014), and reservoir simulator TOUGH2/ECO2N (Pruess, 2005, Pan et al., 2015b). This partially coupled model was applied to the Ordos CCS project (Inner Mongolia, China), to investigate the effect of non-isothermal CO_2 behaviour during the injection. Presented results suggest that the formation of the hydrate in the near-wellbore region is a function of injection temperature and injection rate.

2 Tools and methods

2.1 Numerical reservoir simulation

Since the second half of the last century, significant progress has been made in the mathematical modelling of flow and transport processes in porous media. Research efforts, driven by the increasing need for optimization of resource production from the subsurface formations, have developed many numerical modelling approaches and techniques (Collins, 1961; Fagin and Stewart, 1966; Ames, 1969; Peery and Herron, 1969). At the end of the 1980s, numerical multi-phase models have been also applied to environmental problems, such as simulation of groundwater remediation and contamination in the unsaturated zone, and steam injection for the removal of nonaqueous phase liquids from the subsurface (Falta et al., 1992, Panday et al., 1995).

A typical numerical reservoir simulation procedure can be summarised in the following steps (Chierici, 1995):

1.   Definition of a geological model (or conceptual model) of the reservoir and, the aquifer, in terms of geometry, zonation, spatial distribution of petrophysics and thermophysical rock properties, initial saturations, pressures and temperatures for non-isothermal systems;

2.   Description of the thermodynamic properties of the reservoir fluids, including possible vertical and horizontal variations. Definition and normalisation of the relative permeability and capillary pressure curves or pseudo-curves;

3.   Configuration of the most appropriate gridding for subdivision of the reservoir into blocks and subdomains;

4.   Editing, creation and initialisation, of the numerical model: this assigns local initial values of the petrophysical, thermodynamic, thermophysical (for non-isotherm system) and dynamic parameters of the rock and fluids to each grid block, as well as the initial saturations;

5.   "History matching" or replication of the production history of the reservoir (if available) for the calibration of the numerical model. The model is run with the actual production/injection rate for each well, while pressure, water/oil ratio (WOR) and gas/oil ratio (GOR) computed at each well are compared with measured data where available. The reservoir description and model parameters can be modified within reasonable limits and the model rerun as necessary until a satisfactory match is obtained (the model is calibrated). At the successful conclusion of the history matching phase, the final version of the model is said to have been "validated'';

6.   Sensitivity analysis, to check what are the parameters of the numerical model that have a strong effect on the results of the simulations;

7.   Prediction of the reservoir behaviour under any future development program that the engineer may wish to specify - using the model in "forecast mode".

2.1.1 Numerical simulation of CO_2 sequestration in geological formations – overview

Many reservoir simulators, developed since the 90's, are used to model the phase-partitioning processes and flow behaviour during CO_2 flooding (Chang et al., 1994; Hsu et al., 1995). In early simulation, a rough approximation was used to describe oil-CO_2 phase behaviour and water-CO_2 systems. According to the overview given by Pruess (2002) in a study about multiphase CO_2 disposal into saline aquifer, important experience relevant for CO_2 sequestration in deep-saline aquifers comes from mature technologies of natural gas storages in aquifers, which were common in north-eastern USA (Katz and Lee, 1990), while comprehensive work on CO_2 PVT properties has been done in numerous studies in former Soviet Union, among which in studies by Vargaftik (Vagarftik, 1975; Vargaftik et al., 1996). Initial numerical simulation studies of CO_2 sequestration into geological formations have been performed with petroleum reservoir simulators. Jiang (2011) gave an overview of numerical simulators which had application for geological CO_2 sequestration over years, while the list of the simulators was updated in the dissertation of Pham, 2012. The updated list of simulators, together with the main application and numerical features is presented in Table 1.

Table 1: Overview of the simulators for geological carbon storage (updated from Jiang (2011) and Pham (2012)).

Simulators	Main application	Numerical features
ATHENA/ACCRETE	Thermal multi-phase 3D-reactive transport	FVM, Reaction and flow iteratively coupled
CODE-BRIGHT	Solution of the flow, heat and geo-mechanical model equations	FEM for spatial discretisation, implicit FDM for temporal discretization
COORES	Multi-component multi-phase and 3D fluid flow in heterogenous porous media	FVM for spatial discretisation; implicit temporal discretisation
COMSOL Multiphysics	Coupled thermo-hydro-mechanical modelling, groundwater flow, geochemical analysis, electrochemical analysis	FEM for spatial discretisation, FVM, particle tracing methods; implicit/explicit/generalized alpha temporal discretisation
DUMUX	Multi-scale multi-physics toolbox for the simulation of flow and transport processes in porous media	Vertex-centred FVM for spatial discretisation, implicit temporal discretisation

ECLIPSE 100/300	Three-phase and 3D fluid flow in porous media with cubic EOS	IFDM with irregular spatial discretisation; implicit temporal discretisation
FEFLOW	Groundwater flow solutions with mass and heat transfer, including multi-component chemical kinetics	FEM for spatial discretisation, implicit/explicit/Crank-Nicholson temporal discretisation
FEHM	Fully coupled heat, mass and stress balance equations for 3D, non-isothermal, multi-phase flow in porous media	Control volume FEM for spatial discretisation, implicit temporal discretisation
GEM	EOS compositional reservoir simulator	IFDM for spatial discretisation; implicit temporal discretisation
GEOSX (new, by TOTAL)	Coupled flow, thermal, and geomechanical effects modelling	FEM and hybrid FVM for spatial discretisation; implicit temporal discretisation
IPARS-CO2	Parallel multi-block, multi-physics approach for multi-phase flow in porous media	Mixed FEM for space discretisation; implicit pressure, explicit concentration sequel algorithm for temporal discretisation
MIN3P	Multi-component reactive transport modelling in variably saturated porous media	FVM for spatial discretisation; implicit temporal discretisation
MODFLOW	Flow through aquifer – groundwater flow equations solutions	FDM for spatial discretisation; implicit/Crank-Nicolson for temporal discretisation
MUFTE	Isothermal and non-isothermal multi-phase flow problems including compositional effects	Vertex-centred FVM for spatial discretisation; implicit temporal discretisation
PFLOTRAN	Parallel 3D reservoir simulator, multi-phase multi-component reactive flow problems	FEM for spatial discretisation; implicit/semi-implicit time integration
PHAST	Groundwater flow, solute transport	FDM for spatial discretisation; implicit of Crank-Nicholson for temporal discretisation
ROCKFLOW	Multi-phase and solute transport processes in porous and fractured media	FEM for spatial discretisation; implicit temporal discretisation
RTAFF2	2D/3D non-isothermal multi-phase and multi-component flow	FEM for spatial discretisation; implicit temporal discretisation
STOMP-CO2	Multi-phase flow and transport through geological media	IFDM for spatial discretisation; implicit temporal discretisation
SUTRA	Fluid movement and transport of either energy or dissolved substances in a subsurface environment	Hybrid finite element and IFDM for spatial discretisation; implicit temporal discretisation

TOUGH family of codes	Multi-phase, non-isothermal flows in porous and fractured media; Chemically reactive multi-component (TOUGHREACT)	IFDM for spatial discretisation; implicit temporal discretisation
Waiwera*	Numerical simulation of high-temperature subsurface geothermal flows, including robust phase changes	FVM for spatial discretisation; implicit temporal discretisation

* new tool, theoretically applicable for CCS simulations (Croucher, 2020)

Even from this limited list, it is possible to get an insight about the numerous existing simulation tools, using different numerical approaches, which have the capability to model CO_2 injection and storage in geological formation. Therefore, it is crucial to identify the appropriate conceptual model for a given problem. For example, modelling the pressure build-up and thermal front distribution in the near-wellbore area depends predominantly on viscous forces due to the high injection velocities and injection conditions. This can be modelled with a multiphase model neglecting geochemical reactions. On the other hand, to show the long-term CO_2 distribution and progress of trapping mechanisms, it is necessary to consider more sophisticated models which have the capacity for simulating compositional effects and geochemical reactions.

Numerical modelling of CO_2 storage is an indispensable tool for commercial scale CCS projects, considering the long period over which CO_2 should be stored and the complex nature of CO_2 storage. But although overall time scales of the problem are very large, physical processes of small timescales are still important, and sometimes crucial for operation feasibility of the project. For example, relatively short periods of transient flow during start-up and shut-in injection operation can be associated with various thermal effects and undesirable presence of two-phase conditions in the wellbore. As described in chapter 1.4., wellbore flow behaviour determines the temperature at which CO_2 enters into the reservoir, and in that way introduces a thermal aspect to the reservoir fluid flow processes, because thermodynamic equilibria and many fluid properties depends on temperature. As a lot of studies, as discussed in paragraph 1.3.3, emphasize the importance of accurate modelling of wellbore conditions for CO_2 injection projects, there is an extensive amount of research dedicated to the non-integrated coupling of wellbore and reservoir simulators and the development of integrated coupled wellbore-reservoir simulators.

2.1.1.1 Coupled-wellbore reservoir simulation for CO_2 injection – overview and research contribution

The earliest studies on the interaction between the wellbore and the reservoir domain in petroleum engineering were done in the 1980s, and were predominantly focused on well testing. Particularly, one of the first wellbore-reservoir simulators was developed by Miller (1980) to study the reservoir and wellbore fluid-flow interactions and effects of temperature changes during well testing of liquid-dominated geothermal reservoirs. Extensive review about the beginning and progress of the development of various dynamic wellbore-reservoir coupling examples in petroleum and geothermal engineering can be found in the work of Bahonar et al. (2011) and Da Silva and Jansen from 2015.

In this paragraph, only a preview of studies with significant contribution to concepts of today's coupled-wellbore reservoir tools used for simulation of CO_2 injection will be given. One of the early significant contributions for the development of coupled-wellbore reservoir simulations was proposed by Hadgu et al. (1995), for geothermal production purposes, where the TOUGH2 reservoir simulator was coupled with the one-dimensional steady-state flow wellbore simulator WFSA. In this study, the coupling was achieved through the deliverability option (production index) which related wellbore and reservoir pressure. Over the years, many field-scale simulations available in the literature use a sink/source term to represent CO_2 injection where the injection flux is directly applied to well grid blocks or in some cases, directly to the reservoir domain. Approximate approaches for wellbore flow modelling are based on the use Darcy's Law and assigning adequate rock properties to the wellbore domain. This approach is literature called equivalent porous media (EPM) or equivalent Darcy's media (EDM) and it has been widely used as a convenient approximation of wellbore flow, especially in coupled wellbore-reservoir simulations with single-phase wellbore flow and flowing fluid properties slightly changing along the wellbore (Giorgis et al., 2007, Birkholzer et al., 2011, Zhang et al., 2012). The comparison of results obtained by using the Darcy's law and the rigorous friction losses equation in the momentum balance equation are discussed by Battistelli et al. (2011) for the injection of acid gas mixtures in an undersaturated oil reservoir modelled using TOUGH2-TMGAS (Battistelli and Marcolini, 2009). Realistic wellbore flow is not expected to obey Darcy's law. Moreover,

researchers usually select high permeability for the wellbore domain in the EDM approach but the values can differ from case to case (Zhang et al., 2012). For example, In TMGAS there are options to use either: i) a constant Darcy's permeability over the tubing length; ii) compute the equivalent Darcy's permeability by iteration considering the local fluid conditions in order to have the same pressure losses of the rigorous approach; iii) use the rigorous wellbore flow equation (Battistelli and Marcolini, 2009). However, in many cases, efficient and rigorous treatment of wellbore conditions is critical for successful simulation of large-scale CO_2 storage. In 2010, Livescu et al. developed a fully coupled wellbore-reservoir simulator with an application of the heating technique for EOR simulation. Multiphase wellbore flow was represented with a one-dimensional drift flux model (DFM) elaborated by Shi et al. (2005a; 2005b) along with experimental data of multiphase flow in inclined pipes of large diameter found by Oddie et al. (2003). Pekot et al., (2011) demonstrated the drawbacks of using single-phase pure CO_2 component often present in standard petroleum and gas wellbore simulators, such as OLGA, to accurately simulate wellbore conditions during CO_2 injection. Lindeberg (2011) developed a model for simulation of transient effects of multiphase CO_2 in the wellbore during the injection, but without coupling the wellbore and reservoir domain. As shown in his study, with minor modification, the same model could be used for simulation of transient effects during CO_2 leakage from the reservoir. Fully coupled wellbore-reservoir simulator T2Well, with the capability to model non-isothermal, multiphase, and multi-component transient coupled wellbore-reservoir flow, was developed by Pan et al. (2011a) as an extension of TOUGH2. In T2Well, wellbore and reservoir are considered to be two different subdomains where flow is described with different physics and multiphase wellbore flow is represented with DFM suitable for 1D multiphase flow in cylindrical pipes. Same as in TOUGH2, T2Well can be used with a different equation of state (EOS) modules to describe different fluid properties. Over the years, it T2Well has been used in several studies for coupled wellbore-reservoir simulation of CO_2 injection and leakage (Pan et al., 2011b; Hu et al., 2012; Pan and Oldenburg, 2018b; Basirat et al., 2020). More details about T2Well will be given in the following chapters since the new experimental version of the T2Well code is used in this study.

Additionally, it is important to mention other tools and tool combinations, available in the literature, applied to simulate coupled wellbore-reservoir conditions during CO_2 injection. External coupling of a commercial wellbore and pipeline simulator OLGA with reservoir simulator ECLIPSE was presented by Klinkby et al. (2011), for simulation of fluctuating CO_2 flow in full

CCS chain during the injection into an onshore deep-saline aquifer. Torsen et al. (2018) investigated the influence of different CO_2 injection rates in a coupled wellbore-reservoir simulation of CO_2 injection into the deep-saline aquifer situated in the North Sea with an external coupling of OLGA and reservoir simulator ROCX. In the work of Lei et al. (2020), wellbore flow simulator CO2Well, developed by Lu and Connell in 2014, was coupled with TOUGH2/ECO2N for simulation of CO_2 injection at Ordos CCS site (China). Work of the CO2Well was compared and verified with T2Well on simplified CO_2 injection examples.

2.2 TOUGH2

The TOUGH2 general-purpose numerical simulator has been developed at the LBNL (Pruess et al., 1999; 2012). The code allows the modelling of non-isothermal, multicomponent, multiphase flow of fluid mixtures in porous and fractured media. TOUGH2 has a wide application in different area of subsurface engineering, some of them are geothermal reservoir engineering, unsaturated and saturated zone hydrology, CO_2 storage and radioactive waste disposal. One of the important features of TOUGH2 is its modular structure, with a main flow and transport module which can interface with different fluid properties modules (EOS modules). The modular structure of TOUGH2 code is shown in Figure 1.
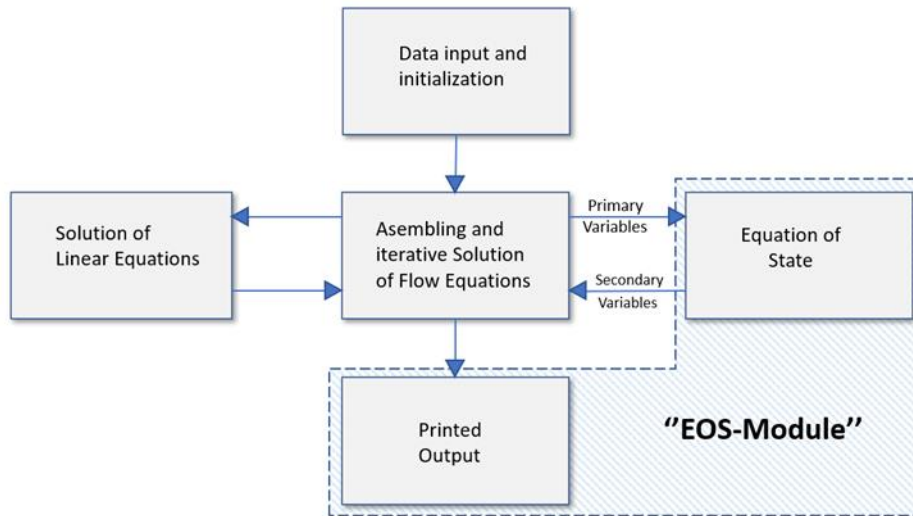
Figure 1*: Modular structure of TOUGH2 simulation architecture (adapted from Pruess et al., 1999).*

As can be noticed from the scheme in Figure 1, the main module provides the primary variables to the ''EOS-module'' while ''EOS-module'' provides the secondary parameters needed for the assemblage of balance equations with respect to the fluid mixture and thermodynamic conditions supported by the EOS module.

The equations describing the multiphase flow have the same mathematical formulation for any arbitrary number of components and phases. The nature and properties of a specific mixture affect the equations describing the system only through thermodynamic and transport parameters, such as density, dynamic viscosity, and enthalpy. Different fluid mixtures are then simulated using the same mathematical formulation of flow using appropriate EOS modules, to model the thermodynamics and evaluate the thermo-physical properties of fluid phases involved. Complete methodology and architecture of TOUGH2 code can be found in the TOUGH2 v.2.0. manual (Pruess et al., 1999; 2012).

Open architecture of the TOUGH suite of codes allowed development of numerous code extensions over the years. Since 2018, the TOUGH3 is available (Jung et al., 2018), as a solution for challenges of inconsistency between the code versions or duplicate effort to code maintenance and development. TOUGH3 incorporates improved capabilities and usability, many new features,

addresses bugs, and improves the flexibility of data handling in problems related to subsurface flow modelling. Presently, T2Well extension has not been coupled with TOUGH3.

2.2.1 EOS modules

In order to simulate a specific set of problems, an appropriate EOS module should be chosen among those available, suitable to simulate the thermodynamics and compute phase properties and composition of fluid mixture for the pressure and temperature field of interest. The EOS module, as function of the set of primary variables and assuming thermodynamic equilibrium among the phases and thermal equilibrium between the fluid and the rock formation, determines (Pruess et al., 1999; 2012):

- The thermodynamic state of the fluid mixture;

- The phase transitions occurring during the simulation;

- The composition of phases at equilibrium;

- The thermodynamic and transport properties of the fluid phases.

Table 2 lists some of the currently available EOS for the TOUGH family of codes with the focus on EOS modules suitable to simulate thermodynamics of CO_2 storage.

Table 2: *EOS modules for TOUGH family of codes.*

Name	Properties
EOS1	water, water with tracer, heat
EOS2	water, CO_2, heat
EOS3	water, air, heat
EOS4	water, air, with VPL*, heat
EOS5	water, hydrogen, heat
EOS7	water, brine, air, heat
EOS7R	water, brine, air, parent-daughter radionuclides, heat

EOS8	water, air, oil
EOS9	water (Richard' equation)
T2VOC	air, water, VOC***, heat
TMVOC	water, VOCs, NCGs, heat
TMGAS	water, NCG & hydrocarbons, salt; 1 - 300°C T, < 1200 bar P; two-phase flow
EOC7C	water, brine, NCG (CO_2, N_2 or CH_4), heat; T < 350°C, P < 1000 bar
EOS7CMA	water, brine, NCG (CO_2, N_2 or CH_4), gas tracer, air, heat; T < 350°C, P < 1000 bar
EWASG	water, salt, NCG; T < 350 °C, P < 1000 bar; low NCG partial pressure
ECO2N v1.0	water, brine, single-phase CO_2; 10 - 110°C T, 1- 600 bar P
ECO2N v2.0	water, brine, single-phase CO_2; 10 - 300°C T, 1- 600 bar P
ECO2M v.1.0	water, brine, multi-phase CO_2; 3 - 103°C T, 1- 600 bar P
ECO2M v.2.0	water, brine, multi-phase and supercritical CO_2; -20 - 300°C T, 1- 600 bar P

VPL - Vapor pressure lowering;

**NCG - non-condensable gas;

***VOC – volatile organic chemical.

Basic description of original EOSs versions is present in TOUGH2 manual (Pruess et al., 1999; 2012) but more detailed description and updated EOSs versions are available in separate reports. Only one EOS module at a time can be linked with the other TOUGH2 modules to form an executable code.

2.2.2 TOUGH2 formulation

2.2.2.1 Mass and energy balance

As already mentioned, the equations describing the multi-phase multi-component flow have the same mathematical formulation for any arbitrary number of components and phases. To amplify this, let's consider a unit formation volume, with the volume of phase β in that pore volume:

$$V_\beta = \phi S_\beta \tag{2.1},$$

where ϕ is porosity and S_β is saturation of the phase β. Mass of the single phase in the pore space is:

$$M = \phi \rho \tag{2.2},$$

and mass of component κ in that phase is:

$$M^\kappa = \phi \rho X^\kappa \tag{2.3},$$

with X^κ denoting fraction of the component.

Therefore, if we consider multi-phase multi-component system, with the mass of the phase β in pore volume:

$$M_\beta = \phi S_\beta \rho_\beta \tag{2.4},$$

mass of the component κ in that phase is:

$$M_\beta^\kappa = \phi S_\beta \rho_\beta X_\beta^\kappa \tag{2.5}.$$

Nevertheless, component κ may be partitioned in all present phases, so accumulation term for phase κ can be written as:

$$M^\kappa = \phi \sum_\beta S_\beta \rho_\beta X_\beta^\kappa \tag{2.6}.$$

Finally, the change of mass of each individual component in an arbitrary volume V_n is given by the mass fluxes through the enclosed surface of the control volume plus the contribution of internal sink/sources, while mass of the component κ in that control volume is $\int M^\kappa dV$. This is summarized in the TOUGH2's final form of mass balance for each block of the numerical model:

$$\frac{d}{dt} \int_{V_n} M^\kappa dV_n = \int_{\Gamma_n} \overrightarrow{F^\kappa} \cdot n \, d\Gamma_n + \int_{V_n} q^\kappa dV_n \tag{2.7}.$$

This basically shows that fluid mass change in volume V (grid block), $\frac{d}{dt}\int_{V_n} M^\kappa dV_n$, is the sum

of net fluid inflow across surface of the grid block, $\int_{\Gamma_n} \overrightarrow{F^\kappa} \cdot n\, d\Gamma_n$, and net gains from sinks and

sources in the grid block, $\int_{V_n} q^\kappa dV_n$.

Limiting here the term F^κ to the advective mass flux over all individual phase fluxes:

$$\overrightarrow{F^\kappa} = \sum_\beta X_\beta^\kappa \overrightarrow{F_\beta} \qquad\qquad [2.8].$$

Following the Darcy's relation for single phase flow, $\vec{F} = -\frac{k}{\mu}\left(\nabla P - p\,\vec{g}\right)$, individual phase flux

in multi-phase multi-component system can be calculated by multi-phase version of Darcy's law

as

$$\overrightarrow{F_\beta} = \rho_\beta \overrightarrow{v_\beta} = -k\frac{k_{r\beta}\rho_\beta}{\mu_\beta}\left(\nabla P_\beta - \rho_\beta \vec{g}\right) \qquad\qquad [2.9].$$

In the above's expression, $\vec{v}_\beta$ is Darcy's velocity of phase β, k is the absolute permeability, $k_{r\beta}$

is the relative permeability of phase β, $\vec{g}$ is the vector of gravitational acceleration and ρ_β and

μ_β are density and dynamic viscosity of the phase β. Pressure P_β is the fluid pressure in phase

β and refers to the sum of the pressure P of a reference phase (usually taken to be the gas phase),

and the capillary pressure $P_{c\beta}$ (≤ 0). A detailed description of mass balance formulation can be

found in TOUGH2 User's guide (Pruess et al., 1999; 2012).

For the finite number of the components specified by the user (NK), each phase will be handled

individually in the above explained mass balance formulation. In TOUGH2 formulation, as the

transport of the NK species is accounted, it is possible to account for energy transport introducing

another species, NK+1. To account for the internal energy per unit volume, TOUGH2 includes

heat contribution of rock matrix and fluid:

$$M^{NK+1} = \left(1-\phi\right)\rho_R C_R T + \phi\sum_\beta S_\beta \rho_\beta u_\beta \qquad\qquad [2.10],$$

where subscript R refers to rock and β to the fluid phase. u_β states for the internal energy of each fluid phase, C_R is specific heat of the rock and T is the temperature of the rock.

Energy transfer due to advective fluid flow is calculated by taking into account phase mass flux and associated specific enthalpies. Heat flux includes conductive and convective component:

$$F^{NK+1} = -\lambda \nabla T + \sum_\beta h_\beta F_\beta \qquad \text{[2.11]}.$$

For each Newton-Raphson iteration within each time step, the thermodynamic state equilibrium is calculated in each grid block for the updated primary variables and then phase's composition and properties are recomputed.

2.2.2.2 Space and time discretisation

The final form of continuum equation in TOUGH2 (2.7) is discretised in space using the integral finite difference method (IFDM). By following that approach, part of the equation 2.7 referring to the change in fluid mass in volume V_n (grid block), $\int_{V_n} M^\kappa dV_n$, becomes:

$$\int_{V_n} M^\kappa dV_n = V_n M_n^\kappa \qquad \text{[2.12]},$$

where M_n^κ is average value of mass of the component κ over the volume V_n. Approximation of surface integrals is formulated as discrete sum of averages over surface of the grid blocks, A_{nm}. Sum of net fluid inflow across the surface of the grid block from the equation 2.7, $\int_{\Gamma_n} \overrightarrow{F^\kappa} \cdot n \, d\Gamma_n$, can therefore be written as:

$$\int_{\Gamma_n} \overrightarrow{F^\kappa} \cdot n \, d\Gamma_n = \sum_m A_{nm} F_{nm} \qquad \text{[2.13]},$$

where F_{nm} is the average value of normal component of the flux over the connection surface (A_{nm}) between two grid blocks, V_n and V_m. Figure 2 illustrates the discretisation approach in IFDM used in TOUGH2 and main geometrical parameters.
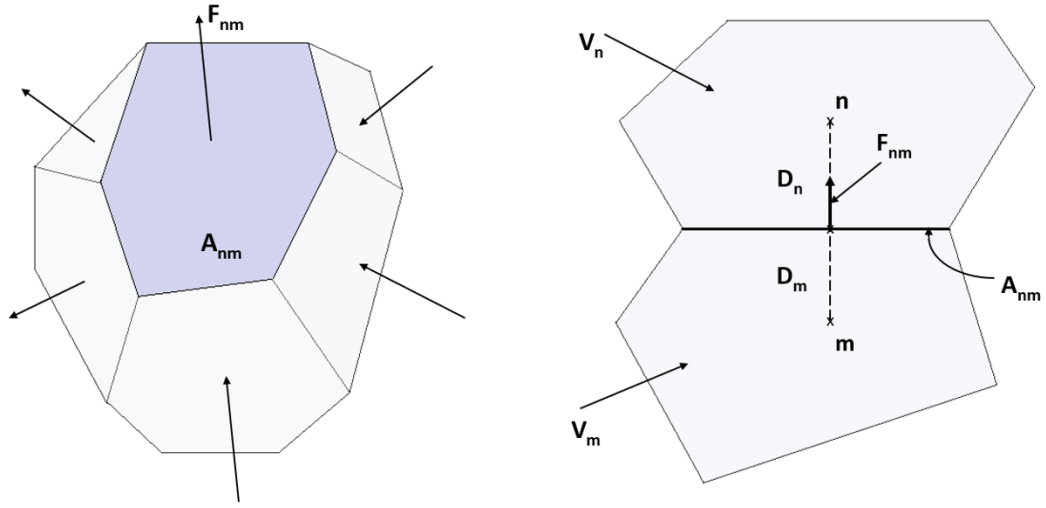
Figure 2*: Space discretization and geometry parameters in the IFDM (adapted from Pruess et al., 1999).*

In Figure 2, parameters D_n and D_m are the distances between the block nodes, n and m, and the common interface A_{nm}. Finally, equation 2.7 can be rewritten as:

$$\frac{d}{dt}M_n^\kappa = \frac{1}{V_n}\sum_m A_{nm}F_{nm}^\kappa + q_n^\kappa \qquad\qquad [2.14].$$

More detailed description of space discretisation approach in TOUGH2 can be found in TOUGH2 User guide (Pruess et al., 1999; 2012).

Time is discretised as a first-order finite difference where the flux term is processed with a fully implicit approach. Therefore, flux term along with sink and source parameter in equation 2.14 are unknow at the time t^{k+1} ($t^{k+1} = t^k + \Delta t$), but are implicitly defined in resulting equations. For more details about this method, the TOUGH2 User guide refers to the approach described by Peaceman (1977) in the study about fundamentals of numerical reservoir simulation. As a result, time discretisation is presented by the set of coupled non-linear, algebraic equations:

$$R_n^{K,k+1} = M_n^{K,k+1} - M_n^{K,k} - \frac{\Delta t}{V_n}\left(\sum_m A_{nm}F_{nm}^{K,k+1} + V_n q_n^{K,k+1}\right) = 0 \qquad\qquad [2.15],$$

for $K = 1, 2, ..., $ NEQ.

Here $R_n^{K,k+1}$ is the corresponding residual of the Kth equation, considering that the total number of the equation is *NEQ* for each grid block, and *NEQ = NK+1*. Residual $R_n^{K,k+1}$ is related to the nth grid block at the time step t^{k+1}. If we consider total number of the grid blocks/elements, NEL, the flow system can be represented with *NEL × NEQ* coupled non-linear equations with the same number (*NEL × NEQ)* of unknowns which are independent primary variables. In this way, the flow system is fully defined at the time step t^{k+1}. This set of equations in TOUGH2 is solved with the Newton-Rapson iteration method.

2.3 T2Well

As already mentioned in the previous section, T2Well is an integrated coupled wellbore-reservoir simulator with a capacity to simulate non-isothermal, multi-phase multi-component wellbore and reservoir fluid flow. T2Well was developed by Pan et al. (2011a) as an extension of TOUGH2, where wellbore and reservoir are described by two different subdomains with different flow physics. In the case of the wellbore domain, it is represented with DFM suitable for 1D multiphase flow in cylindrical or annular pipes. Same as TOUGH2, T2Well can be used with a different EOS module to describe different fluid properties. Essentially, it was coupled with ECO2N to improve understanding of CO_2 wellbore-flow and transport processes and improve the design of injection operations, but also to understand the potential danger of CO_2 leakage through wellbores (Pan et al., 2011a; Pan and Oldenburg, 2014). During the years of research and code development, T2Well has been coupled with ECO2H for the simulation of enhanced geothermal systems (Pan et al., 2015), with EOS7C for applications related to compressed air storage (Oldenburg et al., 2013), with EWASG for application on geothermal systems and reproduction of geothermal production well tests (Vasini et al., 2015; Vasini et al., 2018) and with EOS2H for the modelling of steam-like supercritical geothermal systems (Battistelli et al., 2020). In this research, a test version of T2Well coupled with ECO2M.v.2.0 has been applied for simulation of several cases of CO_2 injection with phase transition in the wellbore. A brief description of the T2Well formulation and changes implemented into the new code version, T2Well-ECO2M, are described in the following subparagraphs.

2.3.1 T2Well formulation

2.3.1.1 Mass and energy balance

Since the mass and energy balance in T2Well has the same structure as TOUGH2, this chapter will be focused on the main differences with T2Well to handle the conservation equations. Furthermore, the described formulation in this paragraph refers to the primary code version of T2Well, coupled with ECO2N, since at the moment, there is an available user guide only for that version. Changes applied to the code version used in this research will be discussed in the following paragraphs, referring to the primary code version.

The most important differences between T2Well and TOUGH2 mass and energy balance are present in the formulation of energy flux, accumulation term and computation of the phase velocity. Application of DFM for the description of flow in wellbore domain requires considering multiphase accumulation term in the equation 2.7 for the wellbore grid blocks. According to Pan et al. (2011a) the original formulation for T2Well-ECO2N for two-phase wellbore flow can be written as:

$$M^k = \sum_{\beta} S_{\beta} \rho_{\beta} X_{\beta}^{\kappa} = S_g \rho_g X_g^{\kappa} + S_l \rho_l X_l^{\kappa}$$
[2.16],

with k = 1, 2 and 3.

Here X_{β}^{κ} is the mass fraction of the component κ in the phase β and S_{β} stands for the saturation of the phase β in the two-phase system. Subscripts g and l in term on the right side of the equation 2.16 denote local accumulation terms, for gas and liquid phase respectively. The local saturation of the phase β at the certain elevation can be expressed as:

$$S_g = \frac{A_g}{A} = \frac{A_g}{A_g + A_l}$$
[2.17],

where A is the total cross-sectional area, and A_g and A_l are cross-sectional area occupied by gas and liquid phases.

Regarding the energy accumulation for the wellbore grid blocks, it is described with:

$$M^{NK+1} = M^4 = \sum\nolimits_{\beta} \rho_{\beta} S_{\beta} \left(u_{\beta} + \frac{1}{2} v_{\beta}^2 \right)$$
[2.18].

In the latter equation both, internal energy, u_{β}, and kinetic energy, $\frac{1}{2} v_{\beta}^2$, are expressed per unit mass of the phase β.

Flow inside of the wellbore is rather complex, governed by several different processes. In T2Well, the relation to compute the total advective mass transport for the component κ in one dimension is given by:

$$F^{\kappa} = \frac{1}{A} \left[\frac{\partial \left(A \rho_g X_g^{\kappa} S_g v_g \right)}{\partial z} + \frac{\partial \left(A \rho_l X_l^{\kappa} S_l v_l \right)}{\partial z} \right]$$
[2.19],

where v_{β} is the average velocity vector of phase β within the wellbore and z is the along-wellbore coordinate, considering that wellbore can be vertical, inclined, or horizontal. Including advection, kinematic energy, potential energy and lateral wellbore heat loss/gain, the overall one-dimensional energy transport term can be written as (Pan et al., 2011.a):

$$F^{NK+1} = F^4 = -\lambda \frac{\partial T}{\partial z} - \frac{1}{A} \sum\nolimits_{\beta} \frac{\partial}{\partial z} \left(A \rho_{\beta} S_{\beta} v_{\beta} \left(h_{\beta} + \frac{v_{\beta}^2}{2} \right) \right) - \sum\nolimits_{\beta} \left(S_{\beta} \rho_{\beta} v_{\beta} g \cos \theta \right) - Q_{ex}$$
[2.20].

Here Q_{ex} is the heat loss/gain of the wellbore per unit length and it is optionally present. When present, it can be either computed by a full numerical approach or by a semi-analytical approach. The angle, θ, denotes the inclination of the wellbore from the vertical, and λ is the area-averaged thermal conductivity of the wellbore taking into account all present fluid phases and possible solid portion. The velocity of each phase, here liquid and gas phase, is computed with the DFM.

2.3.1.2 Two-phase DFM in T2Well-ECO2N

The importance of DFM for modelling wellbore flow in coupled wellbore-reservoir simulators has been already mentioned in previous sections. The basic concept of the DFM is avoiding the complex solving of the momentum equations of two-phase flow, with the simplification of considering the mixture as pseudo-single fluid. Despite DFM neglects some important characteristics of the two-phase flow, it is it's the simplicity that makes it very useful in many engineering applications. In T2Well, DFM is applied to describe single and multiphase flow in the wellbore and obtain advective transport parameters (F_β and u_β).

DFM was first developed by Zubert and Findlay (1965) and over the years, there were many forms of equations in the literature to describe the drift-flux model. Regardless of the numerous equations' forms, the approach is based on the assumption that gas phase flow velocity, v_g, can be related to the volumetric flux of the mixture, j, and the drift velocity of gas, v_d, as:

$$v_g = C_0 \, j + v_d$$
[2.21].

Drift velocity in general describes the relative motion of one phase with respect to the other, while in the case of gas phase it refers to the buoyancy effect (Goda et al., 2003). Parameter C_0 is the profile parameter, also called distribution coefficient, which accounts for the phase concentrations and velocity profiles over the wellbore cross section (Shi et al.,2005a; Pan et al., 2011a).

All the variables in this empirical constitutive relationship must be considered as area-averaged or assumed to be constant over a cross section. The volumetric flux of the mixture is given as:

$$j = S_g v_g + \left(1 - S_g\right) v_l$$
[2.22],

where v_l is the velocity of liquid phase. With the combination of equations 2.21 and 2.22, v_l can be determined as:

$$v_l = \frac{1 - S_g C_0}{1 - S_g} \, j - \frac{S_g}{1 - S_g} v_d$$
[2.23].

As already mentioned, a crucial simplification of DFM is that the momentum equations of two-phase flow in a wellbore can be approximated with a single equation in terms of the mixture

velocity, v_m, and v_d. Detailed development of the single momentum balance for wellbore flow is available in T2Well User guide (Pan et al., 2011a) and it can be summarised as:

$$\frac{\partial}{\partial t}(\rho_m v_m) + \frac{1}{A}\frac{\partial}{\partial z}\left[A(\rho_m v_m + \zeta)\right] = -\frac{\partial p}{\partial z} - \frac{\Gamma f \rho_m |v_m| v_m}{2A} - \rho_m g \cos\theta \qquad [2.24],$$

with ζ denoting the term which takes into account the slip between the two phases and can be defined as:

$$\zeta = \frac{S_g}{1-S_g}\frac{\rho_g \rho_l \rho_m}{\rho_m^{*2}}\left[(C_0 - 1)v_m + v_d\right]^2 \qquad [2.25],$$

where ρ_m^* is the profile-adjusted average density:

$$\rho_m^* = S_g C_0 \rho_g + \left(1 + S_g C_0\right)\rho_l \qquad [2.26].$$

With the determination of the mixture velocity from the equation 2.24, and obtaining the v_d from some empirical relation (as described in Shi et al., 2005), it is possible to compute individual phase velocities with DFM by the flowing equations:

$$v_g = C_0 \frac{\rho_m}{\rho_m^*}v_m + \frac{\rho_l}{\rho_m^*}v_d$$

$$v_l = \frac{\left(1 - S_g C_0\right)\rho_m}{\left(1-S_g\right)\rho_m^*}v_m - \frac{S_g \rho_g}{\left(1-S_g\right)\rho_m^*}v_d \qquad [2.27].$$

What follows is to estimate the value of v_d and C_0. Their values will depend on the flow regime of the two-phase flow since different flow regimes will result in different interfacial interaction. The approach suggested by Shi et al. (2005a), based on the experimental data, is implemented in T2Well for determination of these parameters. First, v_d is calculated as a function of gas saturation and other fluid properties:

$$v_d = \frac{\left(1 - C_0 S_g\right)u_c K\left(S_g, K_u, C_0\right)m(\theta)}{C_0 S_g \sqrt{\rho_g / \rho_l} + 1 - C_0 S_g} \qquad [2.28].$$

Here $m(\theta)$ describes the effect of wellbore inclination as:

$$m(\theta) = m_0 (\cos\theta)^{n_1} (1 + \sin\theta)^{n_2}$$ [2.29],

and m_0, n_1, and n_2 are all fitted parameters. K_u is the Kutateladze number (Richter, 1981), given as a function of Bond number (N_B):

$$K_u = \left[\frac{C_{ku}}{\sqrt{N_B}} \left(\sqrt{1 + \frac{N_B}{C_{ku}^2 C_w}} - 1 \right) \right]^{\frac{1}{2}}$$ [2.30]

with wall friction factor C_w (assumed to be constant in the code, with value 0.008) and C_{ku} parameter, which was taken as a constant value of 142 (Pan et al., 2011a). Bond number is given as:

$$N_B = d^2 \left[\frac{g(\rho_l - \rho_g)}{\sigma_{gl}} \right]$$ [2.31],

where d is wellbore diameter, and σ_{gl} is surface tension between gas and liquid phase.

Parameter u_c denotes the so called "characteristic velocity", which is a measure of bubble rise velocity in a liquid column, given as:

$$u_c = \left[\frac{g\sigma_{gl}(\rho_l - \rho_g)}{\rho_l^2} \right]^{\frac{1}{4}}$$ [2.32].

The role of function $K(\;)$ in equation 2.28 is to make a smooth transition of v_d between two flow stages. More details about the smoothing function for different gas saturation values can be found in T2Well-ECO2N User guide (Pan et al., 2011a).

2.3.1.3 Discretisation

In the wellbore domain, for every Newton-Rapson iteration in TOUGH2, DFM parameters are calculated following the order described in the previous chapter. Development of the momentum conservation equation in time is solved based on a hybrid formulation at the interfaces of neighbouring wellbore elements by a semi explicit approach:

$$v_m^{k+1} = \frac{\left(\frac{\partial P}{\partial z} - \rho_m g \cos\theta\right)^{k+1} + \frac{1}{\Delta t}\rho_m^k v_m^k - \left[\frac{1}{A}\frac{\partial}{\partial z}\left(A\sum_\beta \rho_\beta S_\beta v_\beta^2\right)\right]k}{\frac{\rho_m^{k+1}}{\Delta t} + \frac{f^k \Gamma \rho_m^{k+1}\left|v_m^k\right|}{2A}}$$ [2.33].

Here k and $k+1$ are denoting previous and current time step respectively, and Δt is time step size.

Regarding the component mass and energy balance equations, they are discretised in space using the conventional, fully implicit IFDM scheme of TOUGH2 for the wellbore system, given as:

$$\left[M_i^{\kappa,k+1} - M_i^{\kappa,k}\right]\frac{V_i}{\Delta t} = F_{i,i+\frac{1}{2}}^{\kappa,k+1} - F_{i,i-\frac{1}{2}}^{\kappa,k+1} + Q_i^{\kappa,k+1}$$ [2.34],

where $\kappa = 1, 2, 3$ or 4 (component 4 is energy), and i is the index of the wellbore grid block with the volume V_i.

2.3.1.4 Heat exchange options

There are two available techniques in T2Well to compute heat exchange between the wellbore and surrounding formation: i) numerical (standard) and ii) semi-analytical approach. As in standard TOUGH2 approach, flux terms from the discretised mass and energy balance equation 2.29 are including the heat transport along the connection of wellbore grid blocks' nodes, via both phases. In that case, total heat flux between the nodes n and m can be given as:

$$F_{nm}^3 = A_{nm}\left\{-\lambda\frac{\partial T}{\partial z} + \sum_\beta\left[\left(\rho_\beta S_\beta\left(h_\beta + \frac{v_\beta^2}{2}\right)\right)_{nm+\frac{1}{2}} v_{\beta,nm}\right]\right\}$$ [2.35].

Here λ is area-averaged thermal conductivity of wellbore, including both fluid phases and possible solid portion. Numerical approach of wellbore heat exchange computation necessitates that surrounding formation is explicitly represented in the numerical grid.

In the case of semi-analytical approach, existence of surrounding block is not required, which simplifies the grid generation significantly. Looking back at the equation 2.20 which describes overall one-dimensional energy transport in T2Well, in the case of semi-analytical heat exchange computation approach, heat loss/gain parameter of the i-the wellbore block takes following form:

$$Q_{ex,i} = -A_{wi}\lambda_{fi}\left(\frac{T_i - T_\infty(z)}{r_i f(t)}\right)$$ [2.36],

where A_w is the lateral, connection area between wellbore and surrounding formation, λ_f is the thermal conductivity of the formation surrounding the wellbore, T_i and r_1 are wellbore temperature and radius respectively, while T_∞ is the temperature of the surrounding formation with the respect to the depth z. Time function $f(t)$ is Ramey's wellbore heat loss time function (Ramey, 1962) defined as:

$$f(t) = \ln\left(\frac{2\sqrt{\alpha t}}{r_1}\right) - 0.290$$ [2.37].

In Ramey's function used in T2Well, effect of the wellbore completion is neglected, and α is thermal diffusivity of the formation commonly given as:

$$\alpha = \frac{\lambda_{fi}}{\rho_{fi}c_{fi}}$$ [2.38],

with ρ_f and c_f being bulk formation density and specific heat.

2.3.2 T2Well-ECO2M

T2Well-ECO2M is the test version of T2Well coupled with ECO2M v.2.0 which allows three-phase wellbore-reservoir flow modelling. It has been developed at LBNL and the first mentioning of the new LBNL code version in the literature dates back to 2019, in the work of Oldenburg et al., focused on the simulation of CO_2 phase transition during production from deep reservoirs with CO_2 used for EOR purposes. In the work of Feng et al. (2017), coupling of T2Well and ECO2M was mentioned in the context of CO_2-brine leakage simulation from the wellbore,

following the formulation described by Pan and Oldenburg (2018b), but with implementation of different three-phase DFM approach. The final aim of coupling T2Well-ECO2M in both cases can be summarized as development of the tool which allows simulation of some challenging CO_2 behaviour scenarios, such as simulation of the dynamics of CO_2 injection and leakages through wellbores linked to GHG geological storage in saline aquifers, and CO_2 multiphase flow in injection and production wellbores in EGS exploitation at high temperatures. In the present work, the version developed at LBNL was used and tested for CO_2 injection simulation of several case studies.

As T2Well-ECO2M is a research code still under development, it is not commercially available and there is no available user guide. The main differences in the code when comparing it to the T2Well-ECO2N code version, and instructions for code input file generation, are mainly gathered through private communication with LBNL and direct code application. These main changes and new features available in T2Well-ECO2M will be explained in the following sections. Mass and energy balance formulation, together with discretisation approach, remained the same and the most important changes relate to the application of the three-phase DFM model and additional options regarding the injection conditions regulation and the wellbore-formation heat exchange computation.

2.3.2.1 ECO2M thermodynamics

The first version of the ECO2M module was developed for the application of geological storage in deep-saline aquifers. In general, it includes a detailed description of thermodynamical properties of H_2O-NaCl-CO_2 mixtures (Pruess, 2011), while the fluid-property correlations are the same as in the already mentioned module ECO2N. While ECO2N can represent only single-phase CO_2, ECO2M allows a description of the full spectre of possible CO_2 and CO_2-brine mixture phase conditions and phase transitions. ECO2M is applicable for modelling fluid properties for temperature, pressure and salinity conditions in the range of $-20\ °C \le T \le 110\ °C$, $P \le 600$ bar, and salinity from zero up to full halite saturation. Pure CO_2 properties are obtained from correlations developed and published by Altunin (1975), but these correlations are not directly implemented in ECO2M. Instead, they are gathered in tabular values temperature and pressure depended density,

viscosity, and specific enthalpy of pure CO_2 in a grid form, and provided via a file called CO2TAB. Appropriate property values are obtained by means of bivariate interpolation. The standard CO2TAB data file distributed with ECO2M v.1 covers the range $3.04°C \leq T \leq 103.04°C$ and 1 bar $\leq P \leq 600$ bar.

ECO2M models three mass components (NK=3):

#1: H_2O

#2: NaCl

#3: CO_2

which may partition into 4 phases (NPH=4):

#1: aqueous

#2: liquid CO_2

#3: gaseous CO_2

#4: solid salt.

Figure 3 shows all phase combinations and transitions in a CO_2-H_2O environment. Altogether, there are seven possible phase conditions, but if NaCl ("salt") is added as a third fluid component, the number of possible phase combinations doubles, since in all phase combinations described in Figure 3, there may be an additional phase consisting of halite (solid salt).
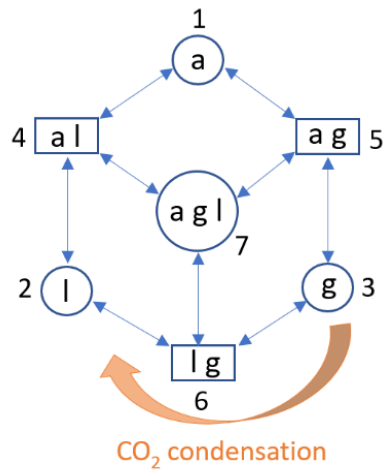
Figure 3: Possible phase combinations and transitions in H_2O-CO_2 system in P-T range of ECO2M; a-aqueous phase, g-gaseous CO_2-rich phase, l-liquid CO_2-rich phase (adapted from Pruess, 2011).

Both liquid and gaseous CO_2 phases may coexist along the CO_2 saturation line (Figure 4) and their coexistence ends at the critical point $(T_{cr}, P_{cr}) = (31.04°C, 73.82$ bar) (Vargaftik, 1975).

For supercritical temperatures ECO2M arbitrarily assigns the single CO_2-rich phase as "liquid" when $P \geq P_{cr}$, and as "gas" when $P < P_{cr}$) as shown in Fig. 4. In fact, in Tab. 3 supercritical conditions are not explicitly indicated. This means also that there should be a direct fictious phase transition between l ⟷ g not shown in Fig. 3.
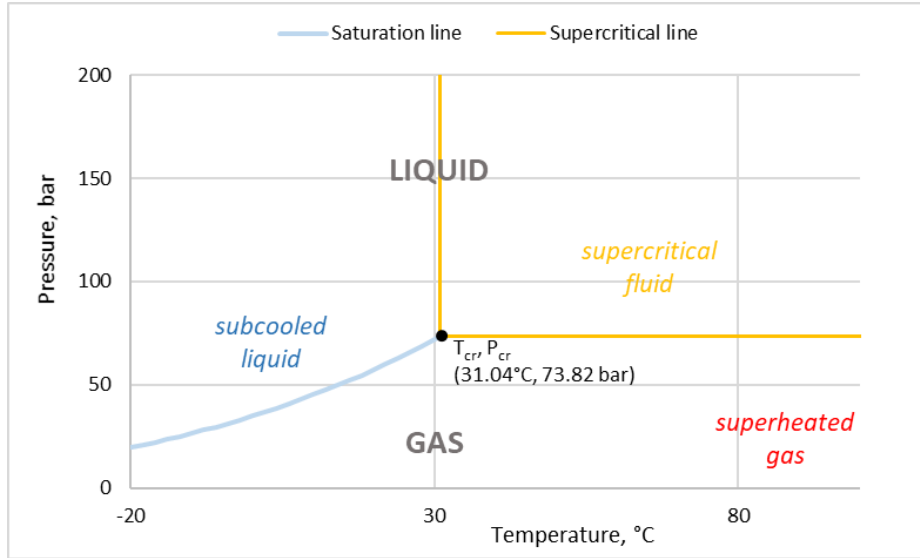
Figure 4*: Phase states of CO_2, with the conventional distinction assumed in ECO2M between liquid and gaseous CO_2 at supercritical temperatures.*

To describe the CO_2-brine flow system in different subdomain parts (wellbore and reservoir grid blocks) and time, it is necessary to set fundamental thermodynamic variables of the system. Four primary variables are required to define the state of the CO_2-H_2O-NaCl mixture, and they depend on the different phase combinations. Identification of the phase combination in the input file for each grid block is managed using a numerical index from 1-7 (Figure 3). The set of primary variables for each phase combination is shown in Table 3.

Table 3*: Primary thermodynamic variables for multiphase H_2O-NaCl-CO_2 mixtures (Pruess, 2011).*

Phase conditions	Index	Primary variables			
		X1	X2	X3	X4
aqueous only	1	P	X_{sm}	X	T
gas only	2	P	X_{sm}	X	T
liquid only	3	P	X_{sm}	X	T

aqueous and liquid	4	P	X_{sm}	S_a	T
aqueous and gas	5	P	X_{sm}	S_a	T
liquid and gas	6	P	X_{sm}	S_g	Y
three-phase	7	P	X_{sm}	S_a	S_g

Thermodynamic variable's indexes listed in the Table 3 designate:

P – pressure (Pa), when several phases are present, P is pressure of the (most) non-wetting phase (liquid or gaseous CO_2);

X_{sm} - salt mass fraction X_s in two-component water-salt system, or solid saturation S_s +10; when $X_{sm} < 0$, it specifies NaCl molality as m = -X_{sm};

X – CO_2 mass fraction;

T – temperature (°C);

S_a – aqueous phase saturation;

S_g – gas phase saturation;

Y – water mass fraction in the two-component H_2O-CO_2 system.

It is possible to notice that for liquid-gas and three-phase conditions, T is not among the primary variables. This is because in the equilibrium between gas and liquid CO_2, T and P are not independent primary variables. Phase conditions for which temperature is not among the primary variables (Index = 6 or 7 in Table 3) may optionally be initialized using T instead of P as the first primary variable. Such conditions are limited to $T \leq T_{cr} = 31.04$°C, and ECO2M recognizes this type of initialization simply from the small numerical value of the first primary variable which would otherwise be P in units of Pa.

Treatment of the dissolved and solid salt in ECO2M, associated with the second primary variable X_{sm}, corresponds to the usual TOUGH2 approach where different numerical ranges are used to

identify different primary variables. In case when no solid salt is present, X_{sm} denotes X_s – the salt mass fraction which refers to the two-component water-NaCl system. But when solid salt is present, X_s is no longer an independent variable since it depends on the solubility of NaCl in the aqueous phase which is a function of temperature. So, in the presence of the solid salt, the numerical range of the second primary variable changes and it will be denoted in the output results as ''solid saturation plus 10'' ($X_{sm} = S_s + 10$, S_s is the fraction of the void space occupied with solid salt) (Pruess, 2011). Treatment of the NaCl in gas and liquid phase is determined by appointed constant threshold value for solubility of NaCl in gas and liquid CO_2 phase, which is in ECO2M by Pruess (2011) set to XCO2eq=1.E-8 kg/kg. So, when the aqueous phase is not present (L, G or L+G), then the NaCl solubility in the G and L phase is less equal to XCO2eq, while higher concentrations will drive the precipitation of solid halite. On the other hand, when the aqueous phase is present, the concentration of NaCl in both G and L phase in equilibrium with the aqueous phase is set in this case to 0. The above treatment of NaCl distribution among the phases at equilibrium suggests potential problems in the mass balance of salt and on the continuity of phase properties at phase transitions.

Regarding the phase change governing, a change of phase composition (appearance or disappearance of a phase) will occur when certain parameters such as mass fractions or fluid pressures move past certain threshold values. For example, if a grid block is in single-phase aqueous condition (INDEX = 1; see Table 3), a transition to two-phase aqueous-liquid conditions (INDEX = 4) should occur when dissolved CO_2 mass fraction exceeds the equilibrium value, $X > X_{aq,l}$. This is valid if we assume that fluid pressure corresponds to liquid CO_2 condition; for lower pressures, the transition would occur to aqueous-gas (Pruess, 2011). As the ''hairtrigger'' threshold criterion proved to cause some unstable behaviour and issues with the convergence of the simulation when phase changes are present, in ECO2M this is avoided by implementation of ''finite-window'' concept for governing the phase change. More details about it can be found in ECO2M user's manual (Pruess, 2011).

2.3.2.2 ECO2M v.2.0

As already mentioned, T2Well has been coupled by Lehua Pan at LBNL with the new ECO2M v.2.0. Since no user guide is at the moment available for ECO2M v.2.0, main differences between the first and new version of ECO2M have been apprehended through the study of the source-code of T2Well-ECO2M and its application. They mainly include:

- extended temperature range to $-20°C \leq T \leq 300°C$, which makes this version suitable for modelling strong temperature drops of CO_2 (with aqueous properties and mutual H_2O-CO_2 solubility computed at the minimum temperature of 3 °C) but also for modelling of EGS with CO_2 as working fluid;
- scaled gas saturation as primary variable in three-phase conditions which main purpose is to remove correlated changes in primary variables. The approach is similar to that used in EWASG module (Battistelli et al., 1997) where 'active saturations' are used to compute the phase characteristic curves when the solid salt phase is present;
- a saturation-weighted-average method to calculate the dissolved CO_2 mass fraction in the aqueous phase and its associated density and specific enthalpy in three-phase conditions to ensure a smooth transition of the properties of the dissolved CO_2 when one of the CO_2 phases disappears;
- a non-iterative calculation of specific enthalpy of dissolved CO_2 under single-phase aqueous conditions to improve convergence during the appearance or disappearance of non-aqueous phases.

As far as the treatment of NaCl equilibrium among the phases is concerned, ECO2M v.2.0 seems to further simplify the treatment used in the previous version by Pruess (2011). Thus, the treatment of NaCl distribution among the phases should be improved following available approaches used in other TOUGH2 EOS modules such as EWASG (Battistelli et al., 1997).

2.3.2.3 Three-phase DFM

Three-phase DFM was developed by Shi et al. (2005b), essentially for modelling of the flow of oil, water, and gas. It was based on the initially developed two-phase DFM (for oil and water). Extension of DFM derived from two-phase to three-phase system will be described referring to documents delivered by LBNL (Pan and Oldenburg, 2018a) and information gathered

through personal communication with the LBNL team. As two-phase DFM has been already described in chapter 2.3., the updated approach for the three-phase system will refer to the previously described formulation.

The approach of the three-phase DFM implemented in T2Well-ECO2M is based on a two-step application of DFM. In the first step, goal is to obtain aqueous v_a and non-aqueous (liquid+gas) v_n phase velocity from the three-phase mixture velocity, v_m. In the second step, DFM approach is reapplied to the mixture of non-aqueous phases, liquid and gas, following the typical DFM formulation for two-phase system.

It will be once again necessary to take into account the spatial discretisation in TOUGH2 and how flux and velocities terms are defined and solved at interfaces between grid cells. Parameters mentioned in the following equations refer to geometry parameters and indexes described in Figure 2.

Solution of the momentum equation of the mixture flow through interface of two adjacent wellbore blocks, n and m, at time level $k+1$ can be given as:

$$\frac{\rho_{nm}^{k+1} v_{nm}^{k+1} - \rho_{nm}^{k} v_{nm}^{k}}{\Delta t} + \delta_{nm}^{k} = -\frac{f_{nm}^{k} \Gamma_{nm} \rho_{nm}^{k+1} v_{nm}^{k+1} \left| v_{nm}^{k} \right|}{2 A_{nm}} - \frac{p_m^{k+1} - p_n^{k+1}}{z_m - z_n} - \rho_{nm}^{k+1} g \cos \theta_{nm} \qquad [2.39],$$

where δ_{nm}^{k} denotes explicit spatial acceleration term, first term from the right part of the equation,

$\dfrac{f_{nm}^{k} \Gamma_{nm} \rho_{nm}^{k+1} v_{nm}^{k+1} \left| v_{nm}^{k} \right|}{2 A_{nm}}$, is semi-implicit friction term, and remaining parameters from the right side

of the equation describe implicit driving force.

Therefore, bulk mass flow rate through interface of n and m at time $k+1$ is given as:

$$q_{nm}^{k+1} = v_{nm}^{k+1} \rho_{nm}^{k+1} = \frac{\dfrac{1}{\Delta t} \rho_{nm}^{k} v_{nm}^{k} - \delta_{nm}^{k} - \left(\dfrac{p_m^{k+1} - p_n^{k+1}}{z_m - z_n} - \rho_{nm}^{k+1} g \cos \theta_{nm} \right)}{\dfrac{1}{\Delta t} + \dfrac{f_{nm}^{k} \Gamma_{nm} \left| v_{nm}^{k} \right|}{2 A_{nm}}} \qquad [2.40],$$

with the first part of the counter and denominator being evaluated at the previous time level, k, while part of the counter inside of the bracket is participating in Newton-Raphson iteration at time level $k+1$ (Pan and Oldenburg, 2018a).

Mixture properties used in momentum equation solution 2.34 can be determined using a mixed-implicit scheme for a three-phase system:

-   for mixture density $\quad \rho_{nm} = \sum_{\beta=1}^{3} S_{nm}^{\beta} \rho_{nm}^{\beta}$;

-   for β phase saturation $\quad S_{nm}^{\beta} = \dfrac{D_n S_m^{\beta} + D_m S_n^{\beta}}{D_n + D_m}$;

-   for β phase density $\quad \rho_{nm}^{\beta} = \dfrac{D_n \rho_m^{\beta} + D_m \rho_n^{\beta}}{D_n + D_m}$;

-   for mixture viscosity $\quad \mu_{nm} = \sum_{\beta+1}^{3} S_{nm}^{\beta} \mu_{nm}^{\beta}$, where individual phase viscosities, μ_{nm}^{β}, are determined using upwind scheme.

Solution of the explicit part of the friction term in the momentum balance equation, $\dfrac{f_{nm}^{k} \Gamma_{nm} \left| v_{nm}^{k} \right|}{2 A_{nm}}$,

depends on the type of flow related to the value of Reynold's number (Pan and Oldenburg, 2018a). The new T2Well code version also allows taking into account additional pressure losses which will occur in presence of complex wellbore geometry where sections of increased friction loss can be approximated by modifying the effective diameter of the wellbore at that particular wellbore section.

In the first part of DFM for a three-phase system where total mixture of three phases is divided into aqueous (a) and non-aqueous part (n-a), the first step is to obtain velocity of the volumetric centre of the mixture:

$$j_{an-a} = \frac{\rho_{an-a}}{\rho_{an-a}^{*}} - \frac{S_{n-a}\left(\rho_a - \rho_{n-a}\right)}{\rho_{an-a}^{*}} v_{d(an-a)} \qquad \text{[2.41]},$$

with ρ_{an-a} mixture density:

$$\rho_{an-a} = \rho_{n-a} S_{n-a} + \left(1 - S_{n-a}\right)\rho_a \qquad \text{[2.42]},$$

and ρ_{an-a}^{*} denoting profile adjusted density of the mixture given as:

$$\rho_{an-a}^{*} = \rho_{n-a} S_{n-a} C_0 + \left(1 - S_{n-a}\right)\rho_a \qquad \text{[2.43]}.$$

42

$v_{d(an-a)}$ and $C_{0(an-a)}$ are drift velocity and profile parameter for first part of DFM application on aqueous and non-aqueous part of the mixture.

In the second step it is possible to calculate non-aqueous phase velocity as:

$$v_{n-a} = C_{0(an-a)} j_{an-a} + v_{d(an-a)}$$ [2.44],

and in third step all required parameters for calculation of aqueous phase are obtained, so it can be given as:

$$v_a = \frac{j_{an-a} - S_{n-a} v_{n-a}}{1 - S_{n-a}}$$ [2.45].

Finally, v_a is used to determine the mass flow (F_{nm}) rate between two adjacent blocks in the wellbore, n and m (Figure 2), while v_{n-a} is used as mixture velocity value in the second part of the DFM approach, to determine the velocity of gas, v_g, and liquid phase, v_l. The second part of the DFM approach follows the same schedule as the first part, therefore, first step includes obtaining volumetric centre of the non-aqueous part of the mixture:

$$j_{gl} = \frac{\rho_{gl}}{\rho_{gl}^*} v_{n-a} - \frac{S_g^* (\rho_l - \rho_g)}{\rho_{gl}^*} v_{d(gl)}$$ [2.46].

In this case, ρ_{gl} is density on non-aqueous mixture:

$$\rho_{gl} = \rho_g S_g^* + (1 - S_g^*) \rho_l$$ [2.47],

ρ_{gl}^* is profile adjusted density of the mixture:

$$\rho_{gl}^* = \rho_g S_g^* C_{0(gl)} + (1 - S_g^* C_{0(gl)}) \rho_l$$ [2.48],

and S_g^* denotes scaled gas saturation $\left(S_g^* = \frac{S_g}{S_g + S_l} \right)$.

$v_{d(gl)}$ and $C_{0(gl)}$ are drift velocity and profile parameter for the second part of DFM application on mixture of non-aqueous phases – liquid and gas.

In the second step it is possible to calculate gas velocity as:

$$v_g = C_{0(gl)} j_{gl} + v_{d(gl)}$$

[2.49],

and in the third step liquid phase velocity given as:

$$v_l = \frac{j_{gl} - S_g^* v_g}{1 - S_g^*}$$

[2.50].

Obtained v_g and v_l are used with v_a, calculated in the first part of DFM approach, to determine mass flow rate through the interface of two adjacent wellbore blocks, F_{nm}, described in equation 2.19. What is missing in both steps is the determination of v_d. It is calculated in the previous time step. For the first part of DFM approach for three-phase system, considering aqueous and non-aqueous part of the fluid mixture, it is determined as:

$$v_{d(an-a)} = \frac{\left(1 - C_{0(an-a)} S_{n-a}\right) u_c \left(\rho_{n-a}, \rho_a, \sigma_{an-a}\right) K \left(S_{n-a}, C_{0(an-a)}, K_u\right)}{C_{0(an-a)} S_{n-a} \sqrt{\rho_{n-a} / \rho_a} + 1 - C_{0(an-a)} S_{n-a}}$$

[2.51],

followed by several adjustments such as in the case of wellbore inclination and scaling to avoid trouble at low pressure values (by factor $0 \leq \left(\frac{p - 1.04e4}{9.0e4}\right)^5 \leq 1$).

In the second part of DFM approach, where non-aqueous mixture part is considered as mixture of liquid and gas CO_2 phase, the drift velocity is determined as:

$$v_{d(gl)} = \frac{\left(1 - C_{0(gl)} S_g\right) u_c \left(\rho_g, \rho_l, \sigma_{gl}\right) K \left(S_g, C_{0(gl)}, K_u\right)}{C_{0(gl)} S_g \sqrt{\rho_g / \rho_l} + 1 - C_{0(gl)} S_{gl}}$$

[2.52].

The same as in the first part of DFM approach, scaling and adjustment is applied for drift flux velocity value. As already mentioned in the chapter 2.3.1.2., K_u is Kutateladze number, function of Bond number. In the case of DFM application on a three-phase system, diameter in the Bond number description (equation 2.31) refers to the diameter of the wellbore occupied by non-aqueous part of the mixture, d_{n-a} (Figure 5).
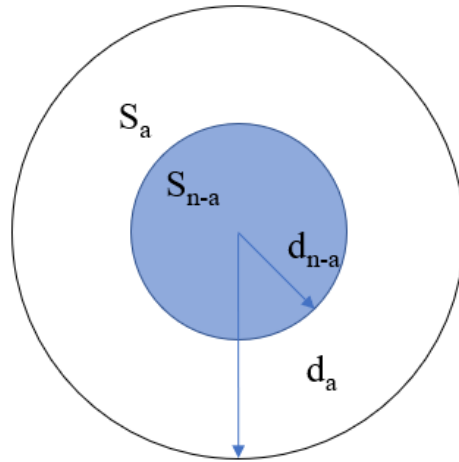
Figure 5*: Phases distribution in wellbore cross-section.*

2.3.2.4 Heat exchange options in T2Well-ECO2M

There are two options to calculate the heat exchange between the wellbore and surrounding formations, numerical and semi-analytical approach. Besides Ramey's method described in chapter 2.3.1.4., alternative formulations for the semi-analytical heat exchange calculation are available in T2Well-ECO2M. T2Well-ECO2M allows two options to use Ramey's method with different time functions *Q3* and *Q3Complete* which were implemented originally in T2Well-EWASG code version (Vasini et al., 2015; 2018), and an additional time-convolution method. These options can be selected by adding dedicated parameters in ROCKS block of the input file, which will be explained in more details in the following subchapter.

Drawbacks of Ramey's method have been discussed in the work of Hasan and Kabir (2002). The remark referred to the results of simulated temperature changes of flowing fluids, which were faster than actually observed, due to neglected heat capacity of the well completion material in Ramey's approach. Moreover, original Ramey's method for wellbore-formation heat exchange calculation works effectively only for times longer than approximately a week, and so is not suitable for the study of short transient phenomena (Vasini et al., 2018). If we assume steady state heat flux through wellbore completion as:

$$dq_1 = 2\pi r_1 U \left(T_1 - T_2\right) dZ \qquad \text{[2.53]},$$

where U is the global heat exchange coefficient of well completion, r_1 is the internal well radius, and T_1 and T_2 are wellbore fluid and wellbore completion temperature respectively. In the combination of equations 2.53, and 2.36 which describes heat loss from the wellbore to the formation, it is possible to get the temperature T_2 at the well completion – rock formation interface:

$$T_2 = \frac{r_1 U \, T_1 f\left(t\right) + \lambda_f T_\infty}{\lambda_f + r_1 U \, f\left(t\right)} \qquad \text{[2.54]}.$$

In this way it is possible to compute the heat flux for unit well length between the wellbore and formation as a function of temperature difference between the wellbore fluid temperature and initial undisturbed formation temperature by substituting T_2 in equation 2.53 with expression form 2.54:

$$dq = \frac{2\pi r_1 \lambda_w U}{\lambda_w + r_1 U \, f\left(t\right)}\left(T_1 - T_\infty\right) dZ \qquad \text{[2.55]}.$$

For the evaluation of global heat exchange coefficient, the full solution developed by Willhite (1967) can be implemented in reduced form, assuming that the internal tubing surface temperature is equal to the flowing fluid temperature, and that the thermal resistance of the tubing and casing is negligible:

$$U = \left[\frac{1}{\left(h_c + h_r\right)} + \frac{r_{to} \ln \dfrac{r_h}{r_{co}}}{\lambda_{cem}} \right]^{-1} \qquad \text{[2.56]}.$$

Here r_{to}, r_h and r_{co} are external tubing radius, external radius of cement sheath and external casing radius respectively, h_c is the natural convection heat transfer coefficient, h_r is the radiation heat transfer coefficient, while λ_{cem} is the thermal conductivity of cement.

In the case of fluid flux directly into a single cemented casing string, the global heat exchange coefficient is given as:

$$U = \frac{\lambda_{cem}}{r_1 \ln \frac{r_2}{r_1}}$$

[2.57].

Instead of Ramey's solution of time function (given in equation 2.37), Vasini et al. (2015) implemented in *Q3* method a time function according to Kanev et al. (1997), who's approach is based on the computation of heat flux at the surface of an infinite cylinder at constant temperature with introduction of dimensionless time, t_D. Here time function solution is given as:

$$\frac{1}{f(t)} = \frac{2}{\ln(4t_D) - 2\gamma} - \frac{\gamma}{\left(\ln(4t_D) - 2\gamma\right)^2}$$

[2.58],

where dimensionless time is equal to $t_D = \frac{\alpha t}{r^2}$, with r denoting wellbore radius, and γ is Euler's constant (0.57722).

Another time function option implemented by Vasini et al. (2018) in *Q3* is the one suggested by Chiu and Thakur (1991) as given below:

$$f(t) = 0.982 \ln\left(1 + 1.81 \frac{\sqrt{\alpha t}}{r_2}\right)$$

[2.59],

which gives a good reproduction of Carslaw and Jager (1959) solution for radial heat conduction from a line source of constant temperature. Here r_2 is wellbore completion radius.

The above time functions are also available inside the *Q3complete* method for wellbore-formation heat exchange calculation using eq. 2.55 by including the steady-state heat conduction through the well completion as described by Ramey (1962) and already implemented in T2Well-EWASG by Vasini et al. (2018).

2.3.2.4.1 Time-convolution method

The semi-analytical time-convolution method for radial, conductive heat exchange between the wellbore and surrounding formation was developed by Zhang et al. (2011). The time-convolution

method implementation in the TOUGH2 family of codes is further described by Finsterle (2017) with respect to the enhancements of the TOUGH2 simulator integrated in iTOUGH2, which is a program for parameter estimation, sensitivity analysis, and uncertainty propagation analysis. This method was already available in T2Well-ECO2M but its activation required certain code modifications which will be explained in the following chapter. Essentially, radial heat transfer with the formation at each time step is calculated by superposition of analytical solutions of heat flow that are dependent on the temperature differences between subsequent time steps. As described by Zhang, evaluation of the heat flux due to unit temperature difference and unit heat exchange surface between wellbore and formation is given for early and late dimensionless time as:

$$q = f_1(t_D)\Delta T = \frac{k\Delta T}{r_0}\left\{(\pi t_D)^{-0.5} + \frac{1}{2} - \frac{1}{4}\left(\frac{t_D}{\pi}\right)^{0.5} + \frac{1}{8}t_D - ...\right\}$$ [2.60],

$$q = f_2(t_D)\Delta T = \frac{2k\Delta T}{r_0}\left\{\frac{1}{\ln(4t_D)-2\gamma} - \frac{\gamma}{\left[\ln(4t_D)-2\gamma\right]^2} - ...\right\}$$ [2.61].

Here f_1 and f_2 are the heat transfer functions which express the amount of the heat flux. As the above equations describe heat flux per unit heat exchange surface, they have to be multiplied by the wellbore element surface ($A_{w(n)} = 2\pi r\,dZ$). Heat transfer functions f_1 and f_2 are approximately the same at the dimensionless time $t_D = 2.8$ and this value is considered as a threshold value to switch from f_1 to f_2.

According to Finsterle (2017), during fluid injection and production, and as a result of the heat exchange processes, temperature changes continuously over time at any point within the wellbore and at the wellbore-formation interface. Based on superposition approach, the radial heat flux across each wellbore element to the surrounding formation is a time-convolution result of varying temperature. The discretized form at each time step can be expressed as:

$$q_{total} = \sum_{i=1}^{d-1} f(t_D - t_i) \cdot \Delta T(t_i)$$ [2.62],

where t_D denotes dimensionless time after d time steps and t_i is the time after i time steps, while solution for f depends on the value of t_D. The temperature difference parameter, $\Delta T\left(t_i\right)$, represents the temperature in the wellbore at time step i, minus the temperature at formation interface at the previous time step, i-1 (i.e. $\Delta T\left(t_i\right) = T_w\left(t_i\right) - T_f\left(t_{i-1}\right)$).

2.4 TOUGH2Viewer

The TOUGH2Viewer software (Bonduà et al., 2012) is an enhanced pre- and post-processor specially designed for results visualisation of TOUGH simulations performed on structured of and fully unstructured 3D Voronoi grids (Bonduà et al., 2015). The structure of TOUGH2Viewer can be divided into four main modules: the input module, visualisation module, editing module, and export module.

In the input module, required data should be uploaded for TOUGH 3D model visualisation. This includes MESH file – ASCII file containing information about the block names and geometric properties (volumes and connection information). For unstructured grid, additional geometric file should be uploaded which, in the case of Voronoi 3D grids, is tough2viewer.dat file, containing additional information about blocks (vertex, faces and face normal). Finally, the output file generated by TOUGH should be uploaded, containing simulation results. It is important to mention that it is possible to proceed with grid visualisation even without output file upload, to visualise the so-called Empty model. This option is very useful for setting the initial conditions of the model in TOUGH2Viewer.

The visualisation module is composed of a set of windows for graphic representation of the grid and visualisation of simulation results in terms of behaviour of different variables through time and space. More details about visualisation functions can be found in the TOUGH2Viewer Quick Tutorial (associated with the software) and the work of Bonduà and Bortolotti (2020). Figure 6 shows an example of numerical model visualisation in TOUGH2Viewer.
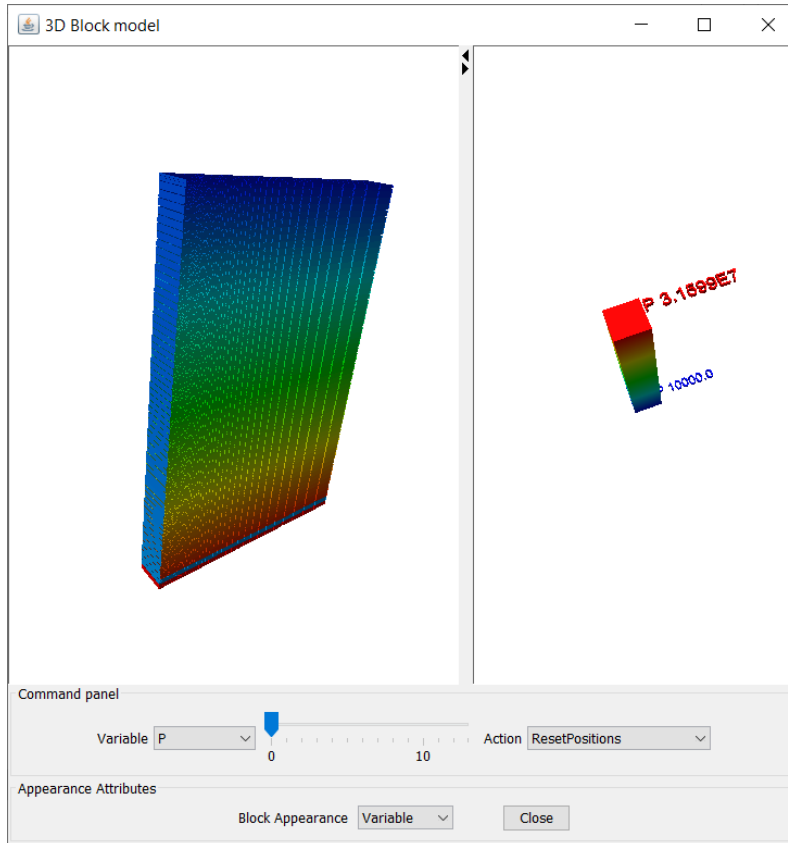
Figure 6: *TOUGH2Viewer 3D block model visualisation*

The editing module allows modification of the properties of single or multiple blocks in terms of volume value and/or rocktype. Moreover, the editing module allows the user to set arbitrary initial conditions for the model. It is possible to set initial conditions for only selected blocks or different rocktypes. Primary variables which should be set in initial conditions depend on the EOS used in the simulation.

Regarding the export module, with numerous export functions, it is important to mention the sub-grid export function which allows the export of only a selected part of the grid, therefore allowing the creation of the new grid which can be again uploaded and edited in TOUGH2Viewer. Moreover, TOUGH2Viewr offers numerical model export, raw data export and manipulated model export. The numerical models created with MESHMAKER (structured 1D or 2D radial grid or 1D, 2D or 3D Cartesian grid) or with VORO2MESH and read by TOUGH2Viewer can be exported in

a format that can be read by Paraview visualisation application as .vtu files (unstructured grid file format).

The last available TOUGH2Viewer version is enhanced in order to allow generation and visualisation of MODFLOW DISU grids and simulation results (Bonduà et al., 2021) and currently, it is the only available free tool dedicated to MODFLOW Voronoi grid generation.

In the scope of this research, TOUGH2Viewer was used as a pre-and-post processor for T2Well-ECO2M in terms of mesh generation and visualisation, initial conditions setting and visualisation and analysis of simulation results.

3 Code improvements and its use

Fundamental instructions on the use of T2Well can be found in the T2Well-ECO2N user guide (Pan et al., 2011a) where a description of input and output file configuration and keywords is explained, along with the procedure for running the executable file. These fundamentals will not be repeated in this study and the reader is advised to find more information in the T2Well-ECO2N user guide. This paragraph will explain differences and new features available in the T2Well-ECO2M code version for generation of an input file and description of injection conditions.

3.1 Compilation

T2Well-ECO2M is a modification and upgrade of T2Well-ECO2N code version, it is composed of a set of Fortran 90 source files grouped in a MS Visual Studio project which can be modified, debugged and compiled under MS Visual Studio integrated with the Intel Parallel Studio XE 2018 update 2 Composer Edition for FORTRAN Window. A list of the source code files for the current T2Well-ECO2M code is given in Table 4.

Table 4: *Source code files for T2Well-ECO2M (adapted from Pan et al., 2011a).*

File name	Description
agra.f	Routine to save a time series of flow rates through user-defined horizons and a routine to save liquid and ga volume vs. time to DOFT file.
CO2Proper_new_well.f	CO_2 properties for ECO2M P&T range.
CO2Proper_old.f	Contain subroutines for CO_2-brine thermodynamic equilibrium
DFM_new.f	Wellbore three-phase flow model definitions, subroutines and functions.
eco2full_well.f	Equation of state (ECO2M v.2.0).
FlowMap.f	Computes Vd in the DFM
FluidPhase.for	Allocation of the phase condition and corresponding index.
HydroFuncs.f	Optional (not used) relative permeability and capillary pressure functions with IFT scaling

InterfacialTension.for	Correlations for interfacial tension of the mixture.
meshm.f	Meshmaker – mesh generation subroutine.
mudfv.f	Compilation of modified TOUGH2 subroutines for wellbore simulation.
proCO2Tab.f	Module for handling table data and interpolations.
radheat.f	Radial heat exchange subroutines.
salt.for	Contains brine and halite correlations.
T2	INCLUDE file with parameters for dimensioning major arrays.
t2cg22x_well.f	TOUGH2 main program.
t2solv.f	Conjugate gradient linear equation solvers.
thermo.inc	Thermodynamic routine constants.

3.2 Input file format

In general, T2Well input files consist of several sections introduce by fixed keywords, describing rocks properties of the system, wellbore properties, the geometry of the mesh, the computational parameters, the initial conditions, etc. Each record in the input file is composed of up to 80 characters, and standard metric units (SI) are adopted, same as in TOUGH2, with temperature characterised in Celsius degrees. An example of the T2Well input file with the addition of the highlighted names of the parameters in the first record of the ROCK type is shown in Figure 7. More information about the parameters in the input file can be found in TOUGH2 and T2Well-ECO2N user guide.

```
*Name_of_the_file.inp
ROCKS----1----*----2----*----3----*----4----*----5----*----6----*----7----*----8
  MAT    NAD  DROK        POR    PER(I)   PER(II)  PER(III)    CWET      SPHT
wells    2 2600.e00    1.0000 0.000e-19 5.000e-14 2.000e-08   2.51e0    920.e-0
    0.0e-10
      7         .457       .01       1.       .01
      8
wellc    2 2600.e00    1.0000 200.0e-09 200.0e-09 200.0e-10  -2.51e0    920.e-0
    0.0e-10
      7         .457       .01       1.       .01
      8

Rock1    2 2600.e00    0.3800 1.00e-13  1.00e-13  1.00e-13    2.51e0    920.0
    0.0e-00
      7         .457       .15       1.       .01
      7         .457      0.14  5.105e-5     1.e11      1.0
Rock2    2 2600.e00    0.1500 1.0e-13   1.0e-13   1.0e-13     2.51      920.
    0.0e-10
      7         .357       .30       1.       .29
      7         .357      0.15  5.105e-5     1.e11      1.0

MULTI----1----*----2----*----3----*----4----*----5----*----6----*----7----*----8
    3    4    3    6
SELEC....2....3....4....5....6....7....8....9...10...11...12...13...14...15...16
    1                                   0    0    0    0    0    0    0    0
         .8        .1       1.2      1.53    0.100  0.046e-3
SOLVR----1----*----2----*----3----*----4----*----5----*----6----*----7----*----8
5  Z1   O0    8.0e-1    1.0e-7
START----1----*----2----*----3----*----4----*----5----*----6----*----7----*----8
----*----1 MOP: 123456789*123456789*1234 ---*----5----*----6----*----7----*----8
PARAM----1----*----2----*----3----*----4----*----5----*----6----*----7----*----8
   29500     5001000300000200   4    3
         4.3200e+7    2.e-1   2.0e+04                9.81       2.0
      1.E-5    1.E00
         0.15000e8                   0.0                  0.0               90.
GENER----1----*----2----*----3----*----4----*----5----*----6----*----7----*----8
*2a 1inj 3                      COM3   1.000e+27.3465E+06


ELEME
*2a 1         wella2.5447E+000.0000E+00      0.0000E+000.0000E+00   -50.000
2Aa 1         wells2.5447E+000.0000E+00      0.0000E+000.0000E+00  -150.000
2Ba 1         wells2.5447E+000.0000E+00      0.0000E+000.0000E+00  -250.000
2Ca 1         wells2.5447E+000.0000E+00      0.0000E+000.0000E+00  -350.000
2Da 1         wells2.5447E+000.0000E+00      0.0000E+000.0000E+00  -450.000
```

Figure 7: Descriptive example of T2Well input file (T2Well-ECO2N).

Input files format of T2Well-ECO2M is the same as for T2Well-ECO2N (Pan et al., 2011a), except for the parts describing fluid properties and primary variables definition which refer to the ECO2M user's guide (Pruess, 2011), and parts noted in this paragraph.

Under the ROCK types dedicated to the wellbore subdomain, which are determined by starting with the letter *w* (e.g. *wells* and *wellc* in Figure 7), T2Well-ECO2M requires inscription of different type of parameters than other T2Well code versions. Parameter *POR* of the wellbore ROCK type,

54

1.0 by default (Figure 6), is used to assign the negative value of wellbore/tubing internal cross section area in T2Well-ECO2M (highlighted in yellow in Figure 8). Parameter *PER(II)* in the same record must determine wellbore wall roughness (highlighted in blue in Figure 8) instead of absolute permeability as in the T2Well-ECO2N version. An example of the ROCKS section for the T2Well-ECO2M input file is given in Figure 8.

```
*Name_of_the_file.inp
ROCKS----1----*----2----*----3----*----4----*----5----*----6----*----7----*----8
wells    2  2600.e00-.45316e-2 0.000e-19 1.000e-5 2.000e-08    2.51e0    920.e-0
   0.0e-10
      7           .457         .01         1.         .01
      8
wellc    2  2600.e00-.45316e-2 200.0e-09 1.000e-5 200.0e-10  -2.51e0    920.e-0
   0.0e-10
      7           .457         .01         1.         .01
      8
Rock1    2  2600.e00    0.3800 1.00e-13 1.00e-13 1.00e-13    2.51e0    920.0
   0.0e-00
      7           .457         .15         1.         .01
      7           .457        0.14 5.105e-5      1.e11       1.0
Rock2    2  2600.e00    0.1500 1.0e-13 1.0e-13 1.0e-13       2.51      920.
   0.0e-10
      7           .357         .30         1.         .29
      7           .357        0.15 5.105e-5      1.e11       1.0
```

Figure 8: An example of the wellbore ROCK's type parameters for T2Well-ECO2M.

3.2.1 Semi-analytical heat exchange method selection

The choice of method for the analytical heat exchange available in T2Well-ECO2M is also determined through modifications in the ROCKS input file section.

Ramey's method for wellbore-surrounding formation heat exchange calculation, as in the previous code version, can be selected by setting the negative value of CWET parameter, which determines formation heat conductivity under fully saturated conditions for wellbore ROCK type (e.g. for ROCK type *wellc* in Figure 7 and 8).

Methods *Q3* and *Q3Complete*, can be selected by the introduction of additional records under wellbore ROCK type and assigning *NAD* = 3 or 4 which will allow reading additional records. An

example of an input file with *Q3* and *Q3Complete* is given in Figure 9. Input file format for *Q3* and *Q3Complete* is the same and method selection will depend on the values on the parameters in the added record.

```
*Name_of_the_file.inp
ROCKS----1----*----2----*----3----*----4----*----5----*----6----*----7----*----8
wells    2  2600.e00    1.0000 0.000e-19 5.000e-14 2.000e-08    2.51e0    920.e-0
    0.0e-10
    7              .457        .01        1.        .01
    8
wellc    3  2600.e00    1.0000 200.0e-09 200.0e-09 200.0e-10   -2.51e0    920.e-0
    0.0e-10
    7              .457        .01        1.        .01
    8
NTEMP   IFL        RWB        UHE        CRHOF        CONDF
      ZF(i)       TF(i)
```

Figure 9: An example of the wellbore ROCK material with selection of Q3/Q3Complete semi-analytical heat-exchange method (without time convolution).

These additional parameters in wellbore ROCKS material are:

NTEMP – number of ZF-TF values used to describe formation static temperature profile which can be different than initial wellbore temperature. Otherwise, when NTEMP is set to 0, static temperature of the formation elements is equal to initial temperature of the wellbore elements;

IFL – the flag to choose between different time functions;

RWB – the outer radius of wellbore completion (m);

UHE – the global heat exchange coefficient of wellbore completion (W/m^2 °C);

CRHOF – the formation heat capacity, including the contribution of both rocks and fluids (J/m^3 °C);

CONDF – thermal conductivity of rock formation (W/°C m);

ZF(i) – the elevation (m), with the same reference used by discretization grid;

TF(i) – static temperature of the formation at the corresponding elevation ZF(i) (°C).

If RWB > 0, the heat exchange calculation is performed including the wellbore completion as described in *Q3Complete* option.

In the current version of T2Well-ECO2M it is possible to choose different time function solutions for *Q3* and *Q3Complete*. By setting different values for IFM it is possible to select following:

IFL=0 – time function solution by Zhang et al. (2011);

IFL=1 – time function according to Kanev et al. (1997);

IFL=2 – time function according to Chiu and Thakur (1991).

Regarding the time-convolution method, to make the algorithm flexible for handling various wellbore configurations and thermal conditions in the rock formation, the code gives the user an option to choose between uniform or depth-dependent formation properties, wellbore radii, and geothermal gradients. Therefore, there are two options to invoke radial heat exchange with time convolution, which can be selected by setting MOP(15)= 5 or 6.

By setting MOP(15) = 5, option for constant wellbore and formation properties is selected and additional ROCK material named **QLOSS** should contain following set of parameters:

DROK: Rock grain density of near wellbore formation;

POR: Wellbore radius;

PER(1):   Reference elevation; specified Z coordinate in block ELEME;

PER(2):   Reference temperature;

PER(3):   Geothermal gradient;

CWET: Heat conductivity of near well formation;

SPHT: Rock grain specific heat of near well formation.

An example of the input file with QLOSS ROCKS material is given in Figure 10.

```
*Name_of_the_file.inp
ROCKS----1----*----2----*----3----*----4----*----5----*----6----*----7----*----8
wells    2  2600.e00-.45316e-2 0.000e-19 1.000e-5 2.000e-08    2.51e0    920.e-0
      0.0e-10
      7           .457          .01         1.         .01
      8
wellc    3  2600.e00-.45316e-2 200.0e-09 1.000e-5 200.0e-10   -2.51e0    920.e-0
      0.0e-10
      7           .457          .01         1.         .01
      8
Rock1    2  2600.e00     0.3800 1.00e-13 1.00e-13 1.00e-13    2.51e0     920.0
      0.0e-00
      7           .457          .15         1.         .01
      7           .457         0.14  5.105e-5    1.e11      1.0
Rock2    2  2600.e00     0.1500 1.0e-13  1.0e-13  1.0e-13     2.51       920.
      0.0e-10
      7           .357          .30         1.         .29
      7           .357         0.15  5.105e-5    1.e11      1.0
QLOSS          2690.0 .03797295        1.5       15.0    0.01499       2.5095 0.97137
```

Figure 10: An example of QLOSS rock domain with time-convolution method parameters.

In case of using the other option, MOP(15)=6, it is possible to consider variable wellbore and formation properties. In that case, it is necessary to provide an external file named *radqloss.dat* which should contain information in following format:

in the first line: **NMATQLOSS**: number of elevations with geometric and thermal data;

Provide NMATQLOSS lines with the following data in free format:

Elevation [m], well radius [m], initial temperature [°C], CWET, DROK, SPHT.

Between elevations, properties are calculated using linear interpolation.

3.2.2 Sinks and sources

T2Well-ECO2M offers the option of setting injection conditions with assigning duration of transitional flow before achieving optimal injection rate and change of injection rate at chosen injection times. This option, invoked with the keyword REGFX, can be included under the standard GENER section which assigns sinks and sources to the model. With REGFX, flow is regulated through a specified connection -regulated interface within the wellbore subdomain

elements. As in TOUGH2, to maintain the desired constant conditions on the upstream block, an infinite volume can be assigned to it.

There are three different cases of REGFX usage with examples and explanation of the parameters given in Figures 11, 12, and 13. A short explanation of the parameters is given highlighted in blue.

```
GENER----1----*----2----*----3----*----4----*----5----*----6----*----7--

REGFX
1                    Injection Interface ID  Cell1Cell2
0.0e-0               Injection rate at time 0.0 s (kg/s)
30.0                 Period of transition (s)
1.000E+01            Mass flow rate at the end of transition period (kg/s)
0                    !<0 indicate limit maximum flow rate
```

Figure 11: REGFX Basic case example.

In the example from Figure 10, injection through interface with ID 1 refers to the first connection interface between the elements of the wellbore model described in CONNE section of the input file. Depending on the geometrical description of the connection interface between the blocks, in the case when direction of the flow is from the Cell2 to Cell1 in connection *Cell1Cell2* it is indicated by negative sign of the flow value.

```
GENER----1----*----2----*----3----*----4----*----5----*----6----*----7----*----8

REGFX
1                    Injection Interface ID  Cell1Cell2
0.0e-0               Injection rate at time 0.0 s (kg/s)
30.0                 Period of transition (s)
1.000E+01            Maximum injection rate kg/s
6                    Number of tabular time (s) and injection rate (kg/s) data
0.00        2.00
43200.00    4.00
86400.00    6.00
129600.00   0.00
216000.00   2.00
259200.00   4.00
```

Figure 12: REGFX Case with tabular flow rates.

59

In the case of REGFX application with tabular flow rates (Figure 12), data highlighted in orange are only place holders and will not have effect on the simulation.

```
GENER----1----*----2----*----3----*----4----*----5----*----6-

REGFX
1                       Injection Interface ID  Cell1Cell2
20.0                    Injection rate at time 0.0 s (kg/s)
120.0                   Period of transition (s)
100.00                  Maximum injection rate (kg/s)
-1                      !<0 indicate limit maximum flow rate
```

Figure 13: REGFX case with limiting flow rate.

In the case from Figure 13, when the last parameter is <0, it indicates that the mass flow rate at the end of the transient period (100 kg/s in this case) is also the maximum flow rate which will not be exceeded during injection period.

3.3 Up-to-date changes in the original T2Well-ECO2M code version and code verification

The Original version of T2Well-ECO2M code developed at LBNL has been shared with the research group of DICAM (University of Bologna), dedicated to geothermal numerical modelling, as a research code version under development, in March, 2020, and has been hitherto modified, updated, and debugged. New features and required code modifications, mainly implemented for simulation of CO_2 injection with phase transition studied in this research, are described in the following paragraphs. A fast check of each code change was done by running the same sample problem consisting of a vertical wellbore CO_2 injection at constant rate and wellhead enthalpy into a 1D radial gas reservoir with closed lateral boundaries. The efficiency of numerical solution was checked by comparing the number of completed time steps and iterations number necessary to

simulate a total of 741 days including: 1-year injection, 1-day shut-in, 1-year injection and 10 days final shut-in.

3.3.1 Additional printouts and correlations updates

In the new updated version of the T2Well-ECO2M code, printout options for the output file tables have been modified in terms of avoiding printout of seldom used variables useful only for the debugging purpose and parameters useful for the analysis of CO_2 phase transition phenomena during the injection added into printout. Among the other parameters, in the default output tables printing of the relative permeabilities and specific enthalpies of all three fluid phases, the density and enthalpy of solid halite, and gas phase velocity have been added. Additionally, when choosing to have printout of an optional table (filed IE(7)>0 of the keyword SELEC of the input file) in the new updated code version, the mass fraction of NaCl in the CO_2 liquid (XSL) and CO_2-rich gas phase (XSG) have been added to the printout, along with the information on the relative permeability (RELP), capillary pressure (PCAP) and permeability reduction (PERMRED) models chosen for each rock domain.

Regarding the updating of the correlations, IAPWS-IF97 (IAPWS, 1997; 2007) correlations for the pure water and steam are available in the current T2Well-ECO2M version. The standard TOUGH2 simulator (Pruess et al., 1999; 2012) implements the IFC (1967) correlations for the saturation pressure, density and enthalpy of water and steam, plus simple correlations for the dynamic viscosity of water and steam. The IAPWS-IF97 correlations for industrial applications have been initially coded into the TOUGH2 environment by Croucher and O'Sullivan (2008) and subsequently by Magnusdottir and Finsterle (2015) for the iTOUGH2 simulator. Croucher and O'Sullivan correlations, integrated with updated correlations for the dynamic viscosity of water and steam (IAPWS, 2008), were implemented in T2Well-EWASG (Vasini et al., 2018) and subsequently imported into the original version of T2Well-ECO2M. But the code modifications required for the use of updated viscosity correlations were missing. In the current version of T2Well-ECO2M, updated correlations for viscosity of water and steam due to IAPWS (2008) have been implemented. The water corelation can be selected in the input file, by denoting the value of **FE(12)** parameter (field of the keyword SELEC) as follows:

FE(12) = 0: IFC67 (DEFAULT);

FE(12) = 1: IAPWS-IF97 (Croucher and O'Sullivan, 2008).

In order to facilitate code maintenance, the IAPWS-IF97 subroutines have been moved into a new source file called IAPWS-IF97.for, which now contains the following subroutines: COWAT97, SUPST97, SAT97, TSAT97, VISH2O, VISH2O97 and THERC_2011.

The new correlation for the brine and halite has been implemented following the correlations derived from Driesner (2007) publication, which were developed for 0-1000°C, 1-5000 bar and NaCl concentration up to halite saturation (Battistelli, 2012). The new brine correlations can be selected in the input file with IE(4)=6 and **IE(15)=5**, which will allow the code to compute both brine density and enthalpy using Driesner's correlations, but also update halite properties. In order to facilitate code maintenance, the new brine and halite correlations have been placed into the existing module called SALT.for, which now contains the following subroutines and functions: SO1, SO2, SATB, VISB, COBRI, DRIESNER, BRINEN, HALITE, HHAL, DHAL, AKREL, TCRIT_BRINE, THERCB.

The T2Well-ECO2M accounts for precipitation of solid halite on the reduction of rock permeability due to the reduction of active porosity, same as in EWASG. In addition to the correlations already implemented in T2Well-ECO2M, new correlations are added, which can be selected by assigning one of the values 4, 5, 6 to the field **IE(11)**. The new correlations are underlined in the list below:

IE(11) =

= 0: PERMEABILITY DOES NOT VARY WITH FLOW POROSITY.

= 1: PERMEABILITY VARIES AS PHIF**FE(1).

= 2: SERIES FRACTURE MODEL.

= 3: SERIES TUBE MODEL.

= 4: Generalized critical porosity model (AKREL*=((PHIN-FE(1))/(1.-FE(1)))**FE(2)).

= 5: Fractures with a linear statistical distribution of apertures (Verma and Pruess, 1988).

= 6: Tubes with a linear statistical distribution of apertures (Verma and Pruess, 1988).

3.3.2 Time-convolution method issues solving

In the original T2Well-ECO2M code version delivered by LBNL, the choice of QLOSSRAD subroutine, corresponding to semi-analytical time convolution approach for wellbore-formation heat exchange, required certain modifications to reach full operativity.

Initially, it was possible to use the time-convolution method only with the absence of wellbore flow. In the input file format, a specific position foreseen to define heat exchange area between wellbore and formation was already used to define the AHT parameter, which should be set to zero in T2Well-ECO2M in order to allow the code recognising wellbore blocks as cylindrical elements with impermeable walls. Now the use of QLOSSRAD, which needs to know the lateral well surface area through the AHT parameter, is allowed by using AHT<0 as a flag.

Additionally, in the original code version, the QLOSRAD subroutine was missing the calculation of heat flux derivative with respect to temperature, required for those thermodynamic conditions for which temperature is not among the primary variables. This happens for ECO2M v.2.0 for conditions 6 (liquid and gas conditions) and 7 (three-phase conditions) (see Table 3). The current code version has heat flux derivatives calculations implemented.

One of the limitations of QLOSSRAD subroutine, and a plan for further improvement, is that it allows either to use a constant wellbore completion and linear formation temperature profile with MOP(15)=5 or assign the same variable wellbore completion and temperature profile with MOP(15)=6 for all wells generated in the model. This represents a quite strong limitation if the code has to be used for field problems in which well have different depths and well completions.

The extension to multiple wells having a variable wellbore completion has been implemented following the same approach already used for the analytical heat exchange calculation using Ramey's equation without time convolution. It is based on the reading of additional input lines by setting NAD ≥3 in the ROCKS blocks belonging to wellbores and on setting a negative thermal conductivity to engage the analytical heat exchange approach.

The time functions corresponding to IFL=1 and 2 were added in QLOSSRAD, making possible the simulation with the time convolution using the following time functions as already available in functions *Q3* and *Q3complete*:

IFL=0   Zhang et al. (2011)

IFL=1   Vasini et al. (2015) after Kanev et al. (1997)

IFL=2   Vasini et al. (2018) after Chiu and Thakur (1991).

Moreover, with the application of the time-convolution approach, it is assumed that there is no thermal resistance between the cased well and the formation. But as explained by Zhang et al. (2011) for time-convolution application in TOUGH2 "*such a resistance can easily be accounted for by inserting a cylindrical element between the wellbore simulator and the radial domain in which the semi-analytical solution is applied. These cylindrical elements would represent, for example, the metal casing, cement and grouting materials, other wellbore installations, and the skin zone; radial and axial heat transfer through these materials and zones will be calculated using the simulator's numerical solution approach, providing the temperature condition at the interface to the formation*".

The proposed approach would offer additional flexibility in solving a more complex heat exchange problems in deep wells with strong change of rates and temperatures and the ability to consider a depth-dependent variation of parameters. This approach was not yet tested with T2Well-ECO2M.

The steady state heat flow through the well completion components in analogy to the implementation in *Q3complete* method has not yet been implemented inside QLOSSRAD.

4 Test injection application and results

In this chapter, principal results of the application of T2Well-ECO2M for coupled-wellbore simulation of CO_2 injection into depleted gas reservoir are presented and discussed. Part of the results has been presented in several conferences attended during Ph.D. research period, GET2020 conference in Strasbourg, France (16-18 November, 2020 – online event) and OMC2021 conference in Ravenna, Italy (28-30, September, 2021).

4.1 Approach applied in development of injection site models

In the coupled wellbore-reservoir CO_2 injection simulation cases described in the following paragraphs, the same general approach was used starting with the development of the conceptual model of the injection site, appropriate mesh generation and simulation of the initial conditions for wellbore and reservoir prior to the injection. Meshes of the injection site models were generated with the MESHMAKER module (more details can be found in the TOUGH2 User's Guide) and afterward visualised and modified in the TOUGH2Viewer pre-post processor. TOUGH2Viewer allows to denote model domains and to give initial properties for different domains which can be exported in form of an INCON file and used for input file generation.

The initial conditions for the injection sites were simulated for a certain period before the injection, long enough to reach steady state of the wellbore-reservoir system. As the T2Well-ECO2M code version allows to work with a mixture of H_2O-CO_2-NaCl, there is no possibility to show the presence of hydrocarbon mixtures. Therefore, in the simulated examples, the reservoir domain is assumed to be initially saturated with CO_2 and residual brine, and the wellbore domain is assumed to be initially filled with CO_2 and a small amount of water to avoid possible numerical issues in the closure of water mass balance. It is assumed that a reservoir initially saturated with CO_2 is an adequate representation of a depleted gas reservoir in CO_2 subcritical conditions, where CO_2 and natural gas have similar thermophysical properties. For that reason, in an analysis of reservoir results for the following injection cases simulated with T2Well-ECO2M, it was not possible to track the gas displacement of in-situ CO_2 by the injected CO_2. However, it was possible

to track other characteristics reservoir fronts such as *thermal front*, which indicates the sharp decline of initial reservoir temperature due to the arrival of cold injected CO_2.

Regarding the injection conditions it is necessary to mention that the injection in T2Well-ECO2M can be modelled essentially with two approaches, or injecting at constant rate, with WH Pressure (WHP) evolution computed by the code, or injecting at constant WHP, with flow rate evolution computed by the code. The evolution of WHP or rate is computed under transient conditions by the code as function of pressure losses within the wellbore and the reservoir. For both approaches it is necessary to assign the heat content of injected CO_2. This is possible with two options, with constant enthalpy or with constant temperature. In these simulations the CO_2 injection at wellhead will be simulated at constant rate and enthalpy, looking at the transient conditions in both the tubing and the reservoir.

4.2 Dedicated case with phase transition

A dedicated case of CO_2 injection into depleted gas reservoir was chosen to show the ability of T2Well-ECO2M to simulate CO_2 phase transition in wellbore and near-wellbore area. While some of the geometrical parameters were arbitrarily chosen according to previous test simulation, Conceptual model and initial conditions, of Pool A sand of Cortemaggiore field (Italy) has been taken as a reference (Giorgis et al., 2007) for reservoir petrophysical parameters, together with the brine salinity and the relationships between porosity reduction due to halite precipitation and permeability reduction. Results of this case were presented at GET2020 conference (Strpić et al., 2020).

4.2.1 Conceptual model and initial conditions

A two-dimensional radial grid, consisting of 8,160 blocks, was built to represent, in a simplified way, the wellbore, reservoir, and wellbore surrounding formation of a CCS injection site model (Figure 14). The 2D model has a total depth of 3,142 m and an external radius of 2,000 m. Wellbore domain (wellb, Figure 14) was schematized as a 3-1/2" API tubing with uniform internal diameter (ID 2,992 inches = 75,99 mm), reaching the depth of 3,092 m at the top of the

reservoir layer. Wellbore is discretized with 67 elements with length gradually increasing from 1 m to 20 m in the upper part (from +2 m to - 47 m) and then uniform elements of 50 m down to the top of reservoir domain. Two 1 m blocks above ground level have been added to represent the wellhead where CO_2 enters the wellbore from a pipeline, in order to have a better control of the upstream conditions (wellhead element wellA, Figure 14). More details about the input parameters can be found in Appendix A.
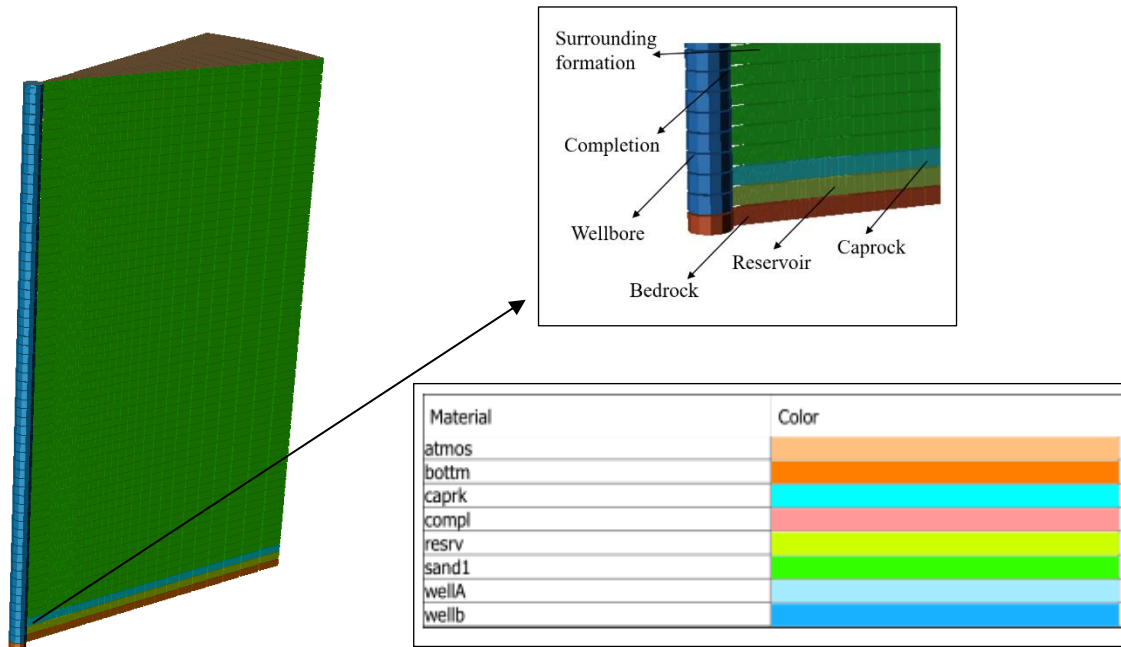

Figure 14: CO$_2$ injection site model with rocktype (material)colour scale. Mesh visualisation (not to scale) is performed with the post-processing tool TOUGH2Viewer (Bonduà et al., 2012).

The remaining 2D domain, which includes the reservoir, the atmosphere above the ground surface (atmos), the well completion domain (compl), the surrounding rock formations (sand1), the caprock (caprk) and bedrock (bottm), is discretized with 119 concentric cylindrical blocks with radius increments increasing logarithmically. Reservoir (resrv) domain has a porosity 0.20 and horizontal permeability of 1.0E-13 m^2. An impermeable layer (bedrock) with a constant temperature of 61.7°C is located below the reservoir formation. The reservoir is assumed to be already filled with CO_2 and a brine phase with 20% saturation and with NaCl content of 50,000

ppm, with initial reservoir pressure 50 bar. Temperature at the wellhead was set to 15°C to represent average annual temperature.

To determine static conditions before the injection, initial conditions simulation was run for period of 10 years. Wellbore was assumed to be filled with CO_2 and a small amount of water (1 ppm) at pressure of 50 bar. Pressure and temperature distribution after 10 years of steady-state simulation are shown in Figure 15, with final WHP 26.7 bar abs.
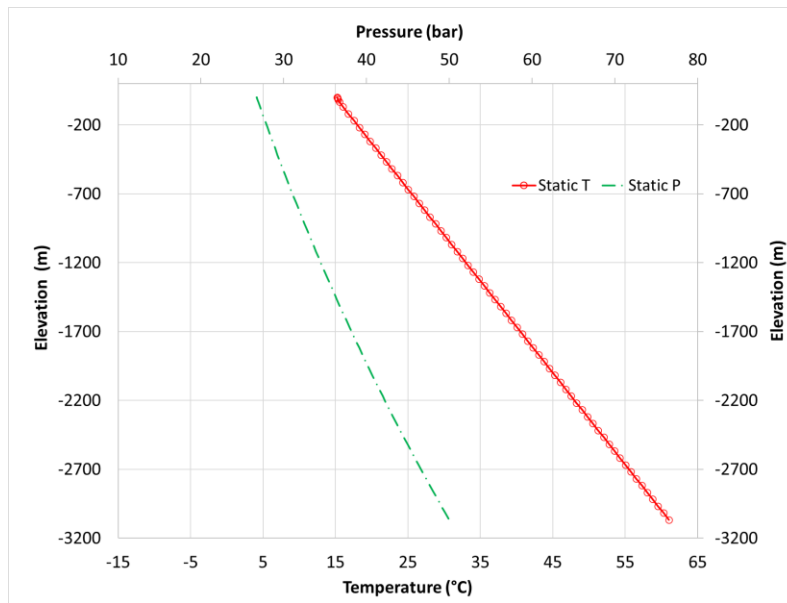
Figure 15: Wellbore static pressure and temperature distribution after 10 years of steady-state simulation.

4.2.2 Injection conditions

CO_2 with just 10 ppm dissolved water, is injected at a constant rate of 10 kg/s and with a constant enthalpy of 239.76 kJ/kg. This enthalpy has been evaluated at 15 °C and 52 bar, which is a pressure slightly higher than the saturation pressure of CO_2 at the chosen temperature. This choice assumes that CO_2 temperature in the upstream pipeline reaches the annual average ground temperature due to heat transfer, while the pressure is at the minimum value necessary to have

liquid CO_2 flowing within the pipeline. Injection at constant rate and enthalpy is simulated for 1 year with the numerical solution of heat exchange with surrounding rock formations.

4.2.3 Results

Evolution of WH and BH conditions at time during the injection, wellbore P and T vertical distribution and reservoir conditions are presented and discussed in the following paragraphs, along with the discussion of the results.

4.2.3.1 Wellbore conditions

Figure 16 shows evolution of WH and BH pressure and temperature conditions during 1 year of CO_2 injection at 10kg/s. An additional time scale with heterogenous units was added for easier managing.
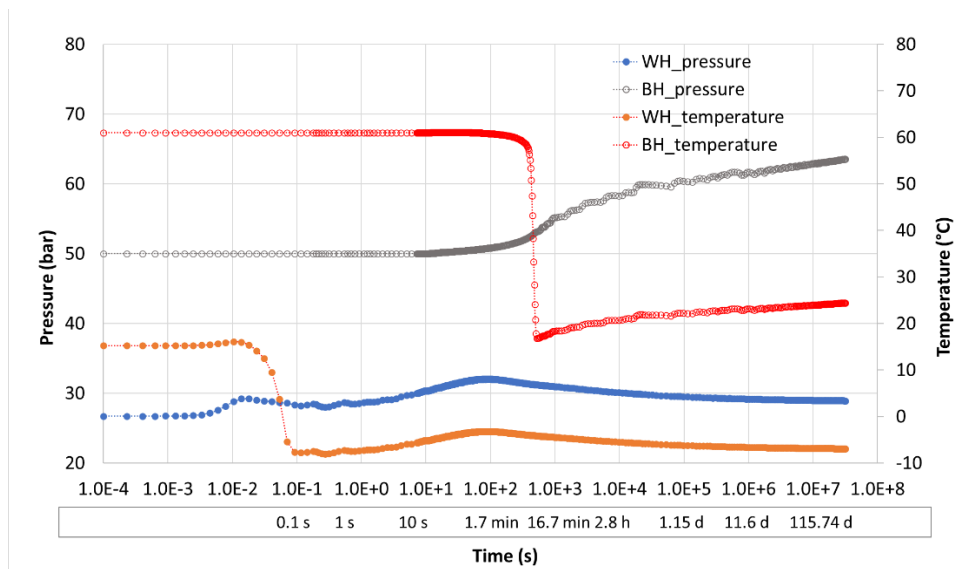

Figure 16*: WH and BH pressure and temperature evolution during 1 year of continuous CO_2 injection at constant WH enthalpy.*

69

From Figure 16, it is possible to notice the temperature drop at the WH and BH. During the first second of injection, WHT drops from 15°C to a minimum of -8°C (the simulation assumes the rate instantaneously reach 10 kg/s) and remains below 0°C (Figure 16). The WHT changes with WHP along the saturation line due to fluid flashing, with fluid cooling as the WHP declines below the value at which the injection enthalpy has been computed. As the static WHP is 26.7 bar, a significant pressure drop occurs with respect to the 52 bar assumed in the upstream. In practice, if single-liquid CO_2 flow is desired within the pipeline during the whole injection operations (which is common practice), throttling is necessary at WH, which generates a strong CO_2 expansion with related cooling due to fluid flashing. The reason for strange step-wise BH pressure and temperature behaviour will be explained in the following paragraph related to the reservoir conditions analysis.

To get a better view of thermodynamic conditions within the wellbore and presumptive CO_2 phase transition, pressure and temperature phase diagram (Figure 17) and pressure and temperature wellbore profiles (Figure 18) were studied for different injection times.
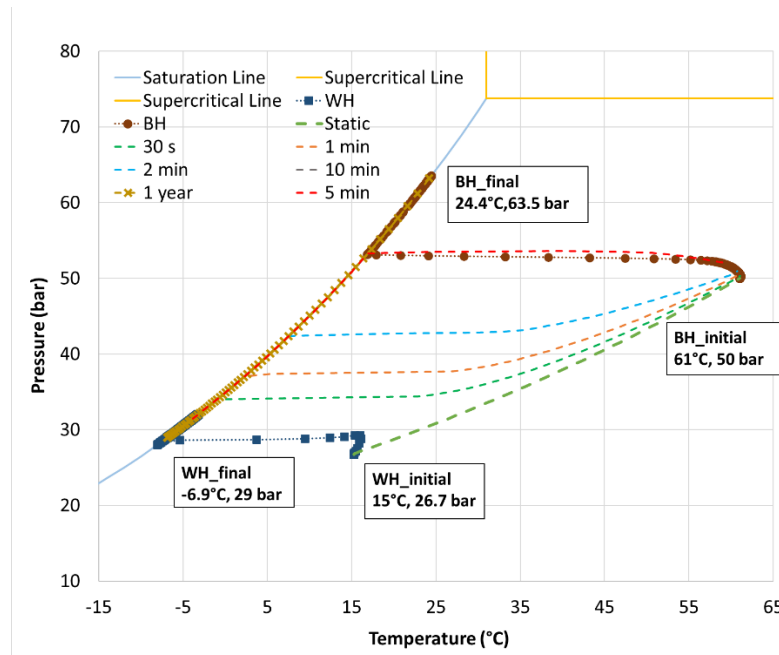

Figure 17: *P-T diagram with the CO_2 saturation line, the time evolution of WH and BH conditions and PT profiles along the wellbore at selected injection times.*

It is possible to notice that two-phase CO_2 conditions appear at the WH almost instantaneously with the start of injection, and after 10 minutes are present in the whole wellbore, as 10 min PT profile at Figure 17 is completely overlapping with CO_2 saturation line.
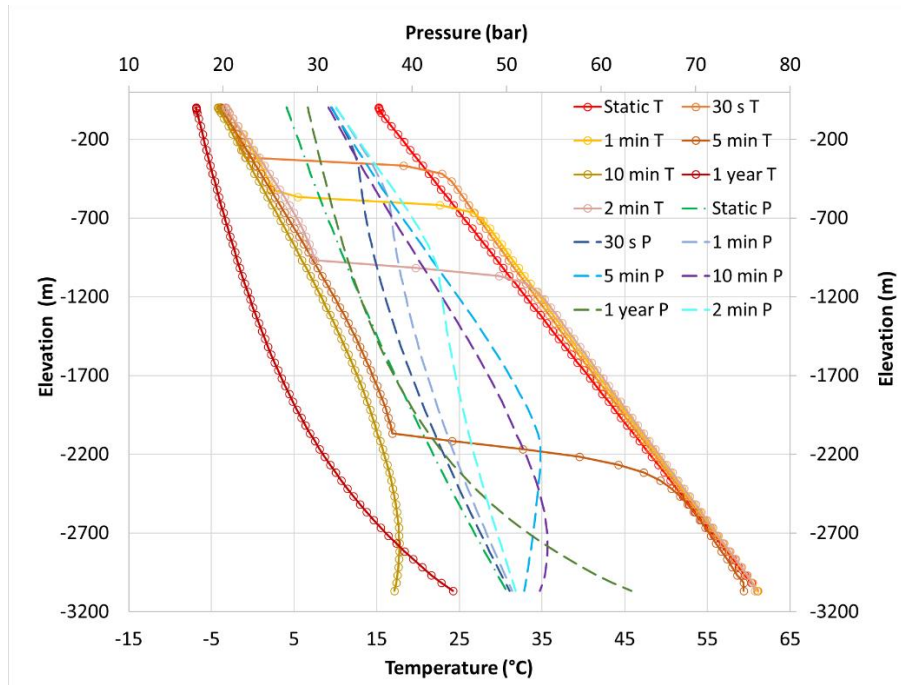
Figure 18: Vertical distribution of temperature and pressure inside the wellbore at selected injection times.

The same behaviour can be noticed in the Figure 18 showing the vertical distribution of wellbore temperature and pressure at selected injection times, where starting from the static temperature (bright red marker curve) wellbore temperature drops with the arrival of the cold CO_2 front. It is possible to follow the phase transition from single to two-phase CO_2 condition evolving inside of the wellbore with two-phase condition present in the whole wellbore after 10 minutes of the injection (dark yellow marker curve).

Even though the WHT is below 0 °C during the whole 1-year injection period, there is no danger of hydrate formation within the wellbore because dry CO_2 is injected and the aqueous phase does not evolve along the wellbore. The injected CO_2 encounters the aqueous phase in the reservoir, where hydrate formation may occur. In Figure 19, according to Akinfiev and Diamond

71

(2010), for pressure above 50 bar, as in this case, hydrate phase formation requires temperatures below about 11 °C.
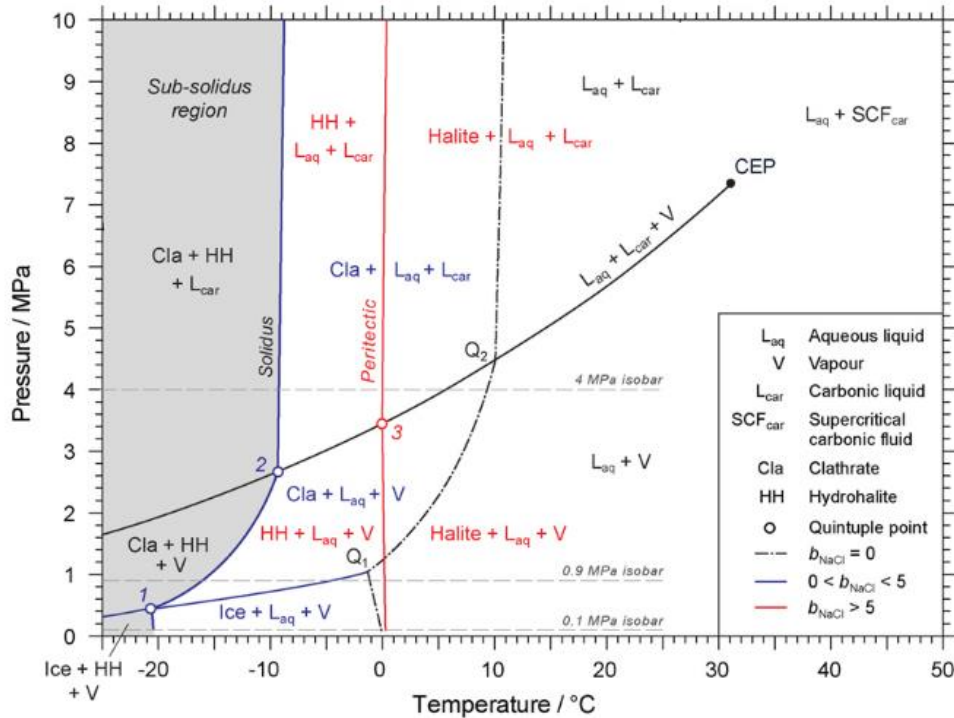
Figure 19: *T–P projection of stable phase relations in the CO_2–H_2O–NaCl system within the low-T low-P region (Akinfiev and Diamond (2010)).*

As seen in Figure 16, BHT drops for almost 45°C with the arrival of the cold injected fluid after about 10 minutes injection, reaching a minimum temperature of 17 °C, staying above the hydrate formation limit.

4.2.3.2 Reservoir conditions

Moving from the lateral boundary towards the wellbore, the following characteristic reservoir fronts can be observed (Figure 20):

- the thermal front, where the initial reservoir T sharply declines due to the arrival of cold injected CO_2;

- the CO$_2$ condensation front (3-phase front), linked to the thermal front, where a large fraction of the gaseous CO$_2$ condenses;

- the evaporation front, where the water contained in the brine is evaporated by the injected undersaturated CO$_2$;

- the halite precipitation front, where the brine becomes oversaturated in NaCl at local T conditions and solid halite (SS) precipitates within the porous medium;

- a secondary CO$_2$ condensation front, where additional gaseous CO$_2$ condenses to provide the heat necessary for the water evaporation.
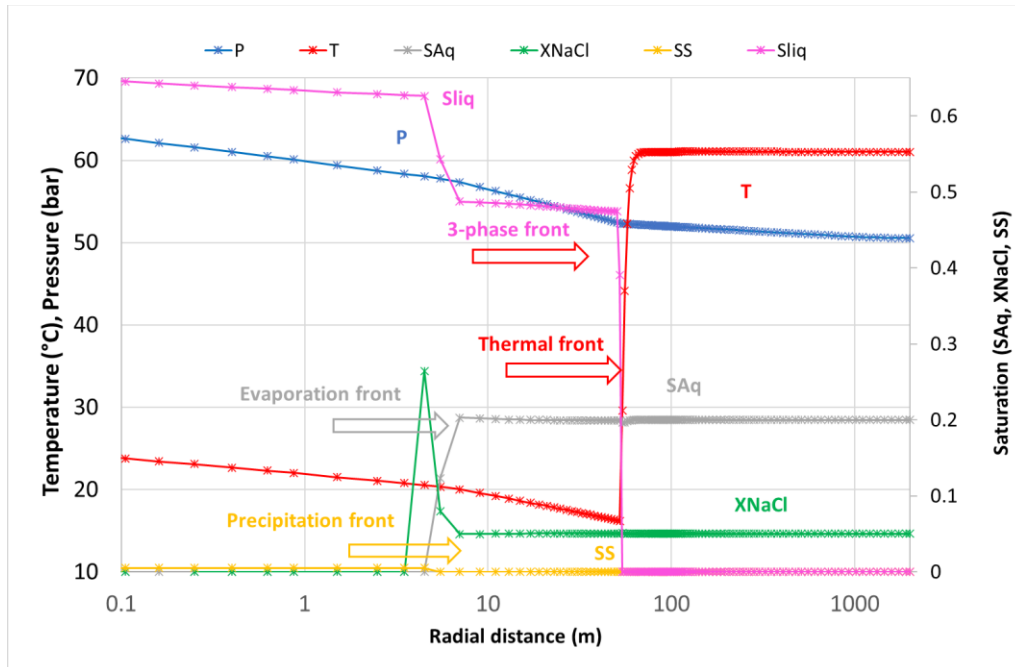
***Figure 20**: Radial distribution of the main reservoir parameters after 1 year of continuous CO$_2$ injection.*

Thorough analysis of the interdependent wellbore and reservoir conditions showed that the step changes of BHP and BHT in Figure 16 are the result of phase transition from single gas to two-phase CO$_2$ in the reservoir at the primary CO$_2$ condensation front. The transition is accompanied by a local sharp change of phases saturation and the related sharp decrease of overall

73

CO_2 mobility which needs a step increment of P to maintain the constant mass rate radial flow any time the transition occurs in a new element. In practice, the relative permeability increment of the CO_2 liquid phase does not compensate for the drastic reduction of gaseous CO_2 relative permeability. This is proved by running an additional simulation considering only first 20 blocks of reservoir domain, excluding wellbore domain and running simulation with direct injection from the first reservoir block. CO_2 was injected at the average flowing enthalpy of the BH for one week (Figure 21).
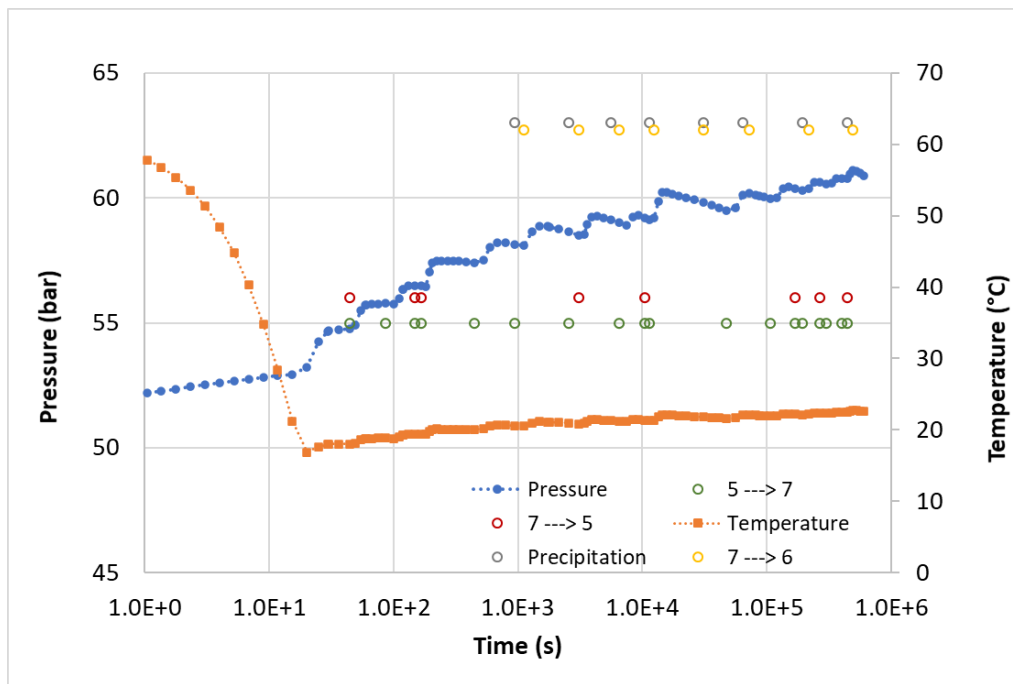
Figure 21: Pressure and temperature of injection block during 1 week of continuous CO_2 injection with indication of phase transitions (5 → 7, 7 → 5, 7 → 6) and NaCl precipitation.

As it can be seen from Figure 21, time of phase transition (evolution of liquid CO_2 5 → 7) inside of near-wellbore area is associated with the occurrence of a pressure step-wise behaviour. It is assumed that the characteristic 3-phase relative permeability curves used were presenting some subtle issues linked to their continuity and derivability. This issue was already highlighted by Battistelli (2020) such as those about 3-phase Stone's I relative permeability model (Stone, 1970) that was used in these simulations. It is believed that the observed numerical step changes of BHP

and BHT might be reduced by using more appropriate 3-phase relative permeability functions. In particular the standard relative permeability curves used in TOUGH2 have been developed for almost immiscible fluid phases, like gas and water. In this case, the gas and liquid CO_2 phases have properties that converge at the same value at the CO_2 critical point. Thus, a miscible approach for the relative permeability and capillary pressure curves might be necessary to better simulate the occurrence of CO_2 vaporization/condensation fronts. This improvement of the T2Well-ECO2M code will be the subject of future studies.

The secondary increment of the CO_2 liquid phase (Figure 20) is related to the evaporation of brine whose pore volume is occupied by both gaseous and liquid CO_2, but with a higher saturation increment of the latter. The heat necessary for the water vaporization is then provided by the partial condensation of the gaseous CO_2, where localized step T changes was not allowed due to the CO_{2_liq} - CO_{2_gas} equilibrium.

Looking at the 1-year P distribution within the reservoir shown in Figure 10, 3 regions can be observed corresponding to (i) the near-wellbore two-phase CO_2 dry zone, (ii) the intermediate 3-phase zone, and (iii) the two-phase gaseous CO_2 – brine zone at initial reservoir T where the CO_2 was simply displaced towards the lateral boundary. Within the first two zones i) and ii), T and P spatial distributions are strongly related because of the multiphase CO_2 conditions. The additional T reduction of flowing CO_2 with respect to BHT is then related to the pressure reduction needed to support the radial flow of injected two-phase CO_2.

The solid saturation (SS), or the saturation of solid halite phase, is present just around the injection wellbore within a distance of about 5 m. SS reaches a value of about 5.0E-3 which can be easily computed considering the amount of NaCl initially dissolved in the brine, the brine density and saturation, and the final density of solid halite. In the present model the brine is at irreducible saturation (SAq=0.2). Thus, the brine is immobile even during CO_2 injection. The NaCl initially contained in a grid element precipitate into the same element, and this is the reason for a constant SS value. These small SS values give a permeability reduction having a negligible effect on the pressure gradient of the near wellbore area.

5 Time-convolution method application

Thermal effects present during the CO_2 injection and CO_2 phase transition inside of the wellbore are result of several processes. The final wellbore temperature distribution during the steady-state injection will depend on the pressure drop and JT's effect, friction losses and wellbore-formation heat exchange. T2Well-ECO2M offers a numerical and a semi-analytical approach to calculate heat exchange between the wellbore and surrounding formation. Although the full numerical approach is the most accurate, it requires building and solving spatial grids with many additional discretisation elements just for the modelling of heat conduction. The advantage of using the semi-analytical approach is to allow a smaller effort in terms of model grid generation and input preparation by limiting the number of grid elements, and consequently, a strong reduction of CPU execution time. However, it is crucial to determine proper equivalent thermal properties to be used in the analytical solution that conveniently reproduce those of the surrounding formations given in full numerical approach.

As explained in paragraph 2.3.1.4, the semi-analytical approach for wellbore heat exchange in T2Well-ECO2M is based on the Ramey's method with or without time-convolution. In order to test the time-convolution approach which is for the first time available in T2Well code, simulation results of using numerical and time convolution approach for computation of heat exchange between the wellbore and formation were compared with reference to the simulation of dry CO_2 injection. Comparison was done for the model and conditions presented in previous chapter, which is simulated using fully numerical approach. Results of the comparison were presented at Offshore Mediterranean Conference 2021 (Ravenna, Italy). For the purpose of comparison of the numerical and semi-analytical approach, efforts were made to have equivalent thermal properties in both models, therefore thermal properties of fully numerical model from case presented in paragraph 4.2 have been slightly modified. Detailed list of input parameters for fully numerical and semi-analytical model is given in Appendix A. Initial conditions and injection conditions for the case with semi-analytical, time-convolution approach for wellbore-formation heat exchange are same as in fully numerical model from paragraph 4.2, and conceptual model of the injection site is shown in Figure 22.
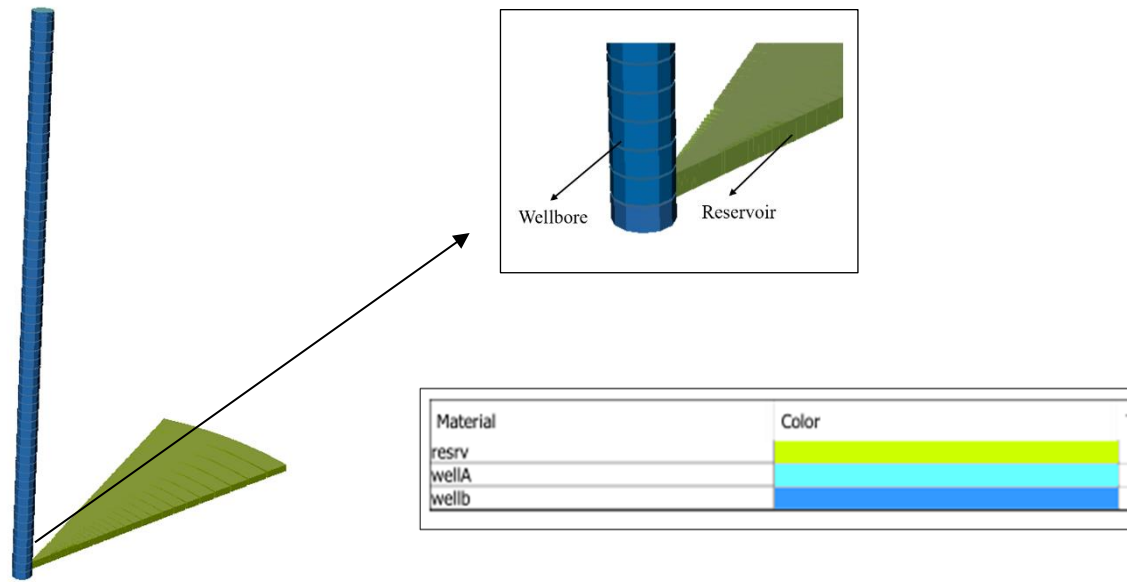
Figure 22: *CO$_2$ injection site model for semi-analytical (time-convolution approach) simulation with rocktype (material) colour scale. Mesh visualisation (not to scale) is performed with the post-processing tool TOUGH2Viewer (Bonduà et al., 2012).*

As in fully numerical model (Figure 14), wellA denotes wellhead element added for a better control of upstream conditions. In comparison with the model from Figure 14, which is required in fully numerical approach simulation, in case of semi-analytical approach wellbore-formation heat exchange model consists of only wellbore and reservoir domain, with an associated grid of only 186 blocks.

5.1 Results of comparison

Execution time for the simulation with fully numerical heat exchange calculation was 364 s, while for the simplified model with semi-analytical heat exchange it was only 9 s (2.47%). The simulations results are compared looking at the evolution of WH and BH conditions as function of time, at the evolution of P&T wellbore flowing profiles on the phase thermodynamic diagram (P-T diagram), and at the spatial distribution of reservoir conditions.

77

5.1.1 Wellbore conditions

Figure 23 shows the comparison of the evolution of WH and BH conditions during 1 year of CO_2 injection for the numerical heat exchange solution (##_num) and the time-convolution semi-analytical approach (##_s-a).
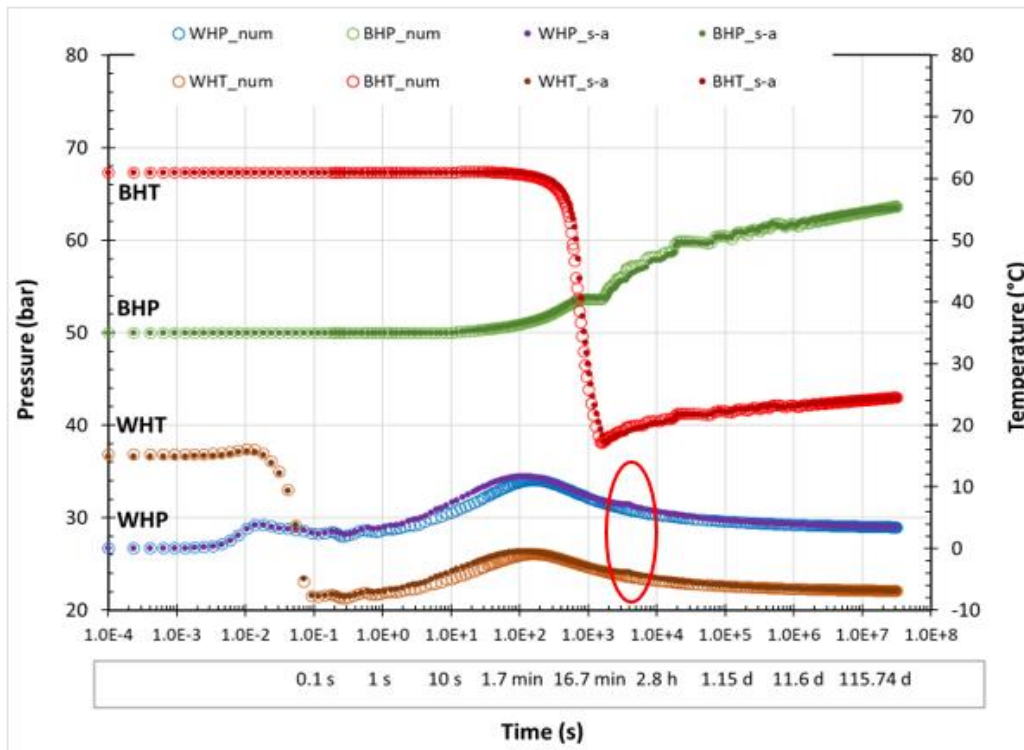
Figure 23*: WH pressure and temperature and BH pressure and temperature during 1 year of continuous CO_2 injection at 10 kg/s and constant WH enthalpy, for numerical (##_num) and semi-analytical (##_s-a) solution of wellbore-formation heat exchange.*

The small spike visible on the curves of semi-analytical solution for WHP and WHT shown in Figure 22 at around 4,000 s (red frame), is caused by the switch between two different equations (Equation 2.60 and 2.61) for the time function used by Zhang et al. (2011).

Results of pressure and temperature phase diagrams of wellbore conditions for different injection times for fully numerical approach and semi-analytical approach of wellbore-formation computation are shown in Figure 24 and 25 respectively.
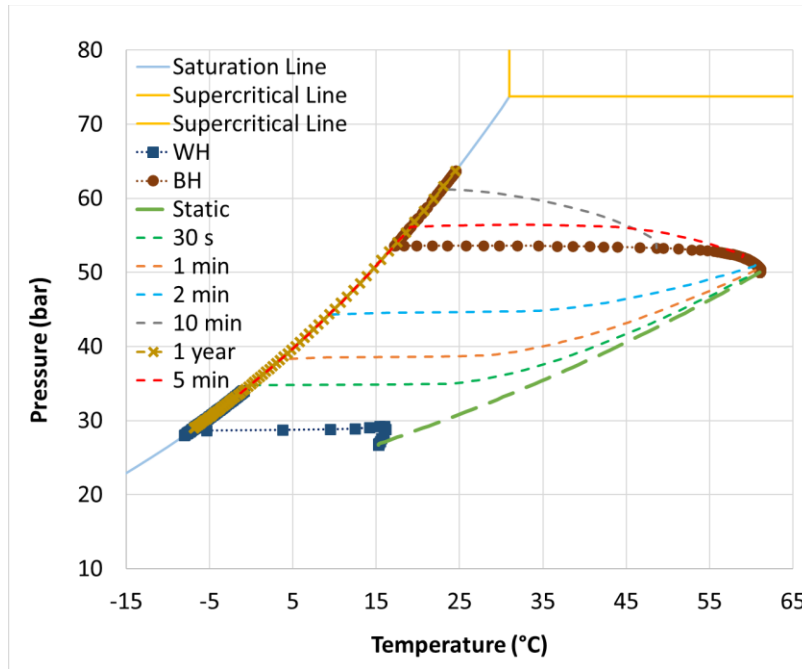
Figure 24: P-T diagram with the CO_2 saturation line, the time evolution of WH and BH conditions and PT profiles along the wellbore at selected injection times for the numerical case.
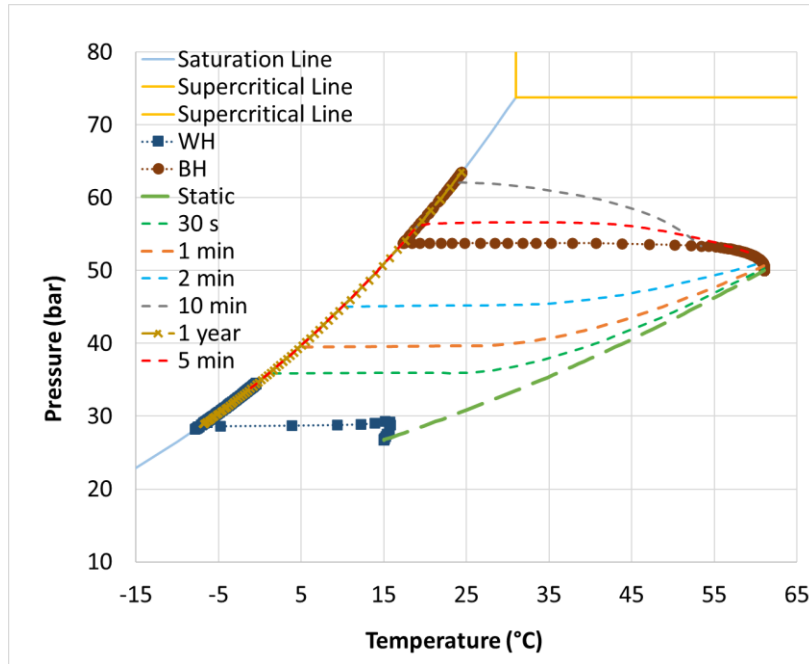
Figure 25*: P-T diagram with the CO_2 saturation line, the time evolution of WH and BH conditions and PT profiles along the wellbore at selected injection times for the semi-analytical case.*

Pressure and temperature wellbore vertical profiles results for different injection times for fully numerical and semi-analytical case are shown in Figure 26 and 27.
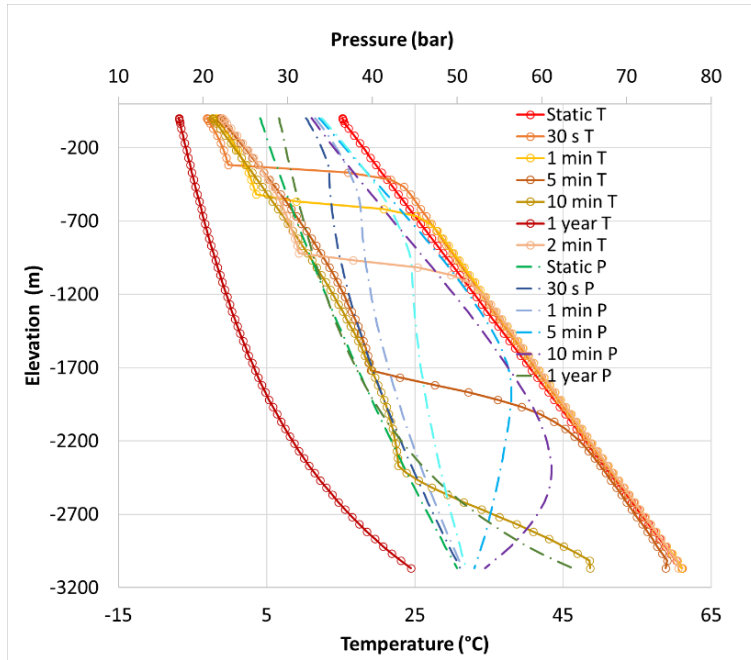
Figure 26*: Vertical distribution of flowing pressure and temperature inside the wellbore at different injection times for numerical case.*
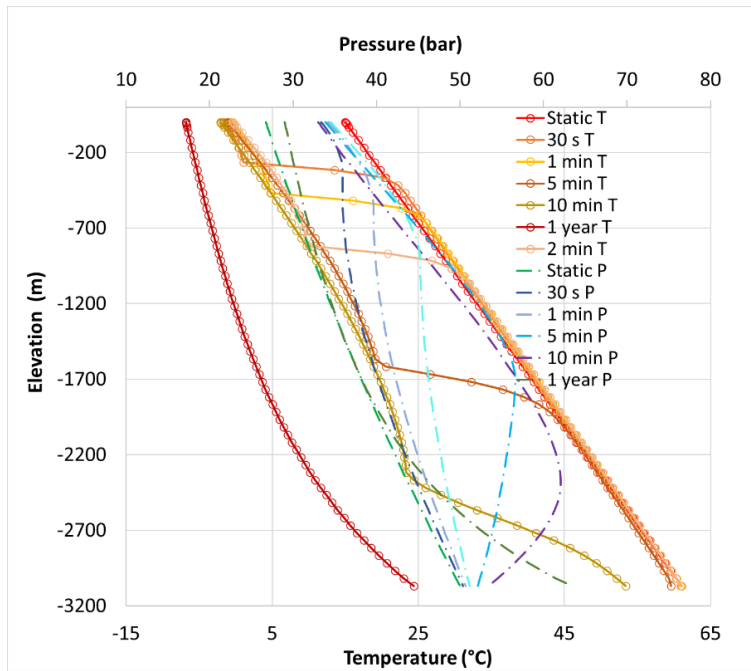
Figure 27*: Vertical distribution of flowing pressure and temperature inside the wellbore at different injection time for semi-analytical case.*

Wellbore conditions result prove to be in a good agreement. Small discrepancies can be noticed mostly during the first 10 minutes of injection when most of wellbore transients are experienced (Figure 24/25 and Figure 26/27).

5.1.2 Reservoir conditions

Figure 27 shows comparison of results for radial distribution of characteristic reservoir fronts for fully numerical (##_num) and semi-analytical approach (##_s-a) after 1 year of continuous CO_2 injection.
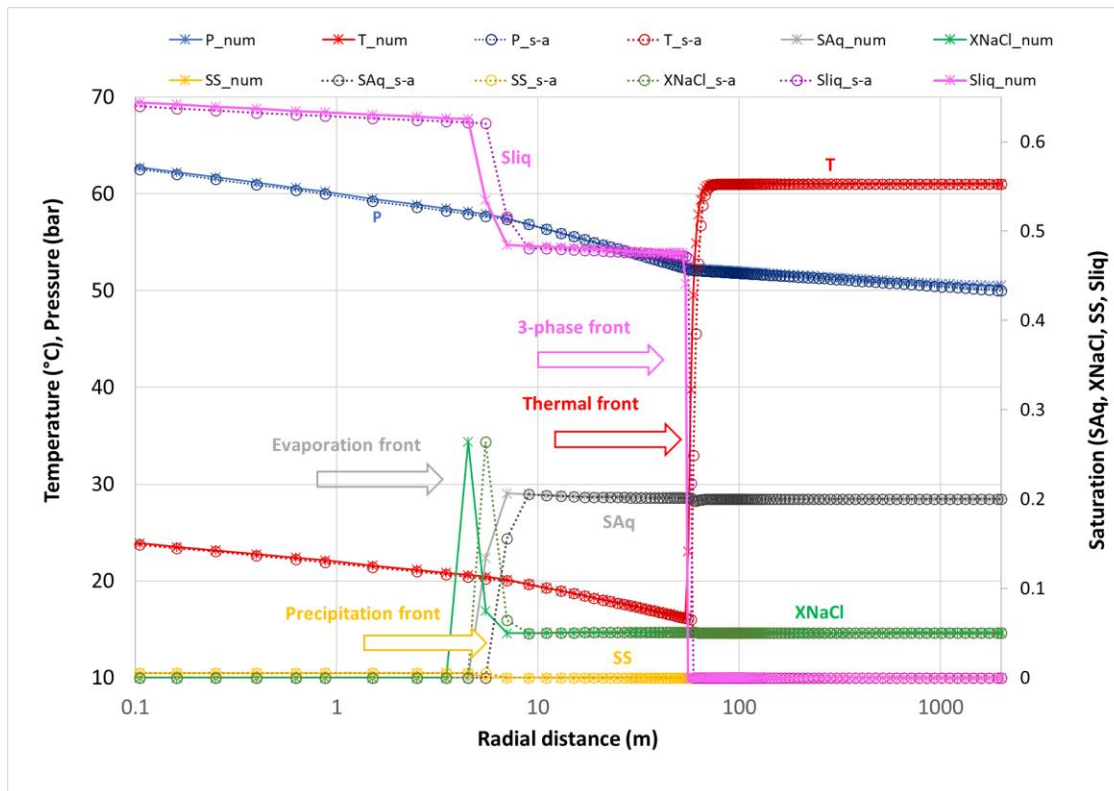
Figure 28*: Comparison of radial distribution (logarithmic scale) of main reservoir parameters after 1 year of continuous CO_2 injection for the full numerical (##_num) and semi-analytical (##_s-a) case.*

Considering the good fit of wellbore conditions for numerical and semi-analytical approach of wellbore-formation heat exchange calculation, expectedly, reservoir parameters are also in a good

agreement with main differences restricted to the location of dynamic fronts of SAq, XNaCl and Sliq.

As it could be seen from the presented comparison, semi-analytical time convolution option for wellbore-formation heat exchange calculation in T2Well-ECO2M proved to give results which are in a good agreement with, the most accurate, numerical results. In the same time, application of time-convolution approach requires less effort in terms of model grid and input file generation, with significant reduction in CPU execution time, which was only 2,47% of the time necessary for execution of fully numerical case. Therefore, time convolution approach proves to be valuable option for preliminary analysis of the thermal effect during CO_2 injection, especially to eliminate some safety concerns connected with the strong temperature drops and/or hydrate formation.

In the same time, it is necessary to keep in mind that even though time-convolution approach does not require spatial discretization of the formation domain, it is crucial to determine accurate equivalent thermal properties to be used in semi-analytical solution. These thermal properties should reproduce those of wellbore surrounding formations that can be composed of multiple subdomains over the wellbore depth.

6 Conclusions

The objective of this study was to modify the T2Well-ECO2M code and test it on dedicated realistic cases to evaluate the performance of the software for simulating the CO_2 phase transition and heat exchange with the surrounding formation during the transient wellbore flow during the CO_2 injection into depleted gas reservoirs. The main simulation goal was to detect the effects of two-phase conditions inside of the wellbore and whether such conditions during the whole injection period would jeopardize injectivity or cause some safety concerns. Among the factors effecting the temperature of CO_2 inside of the wellbore, special attention was given to the contribution of wellbore-formation heat exchange during multiphase CO_2 injection in terms of testing and modification of available heat-exchange options available in T2Well-ECO2M. Moreover, as T2Well-ECO2M is a research code, the original version shared by LBNL was improved and debugged in many aspects to be suitable for simulation of various conditions of multiphase CO_2 injection.

T2Well-ECO2M research code proved to be able to model coupled wellbore-reservoir processes, including multiphase wellbore flow caused by flashing of injected CO_2. Although originally designed for simulation of CO_2 injection into deep saline aquifers and modelling of EGS, it is assumed that it can give a good insight into processes occurring during multiphase CO_2 injection into depleted gas reservoirs. Thermophysical properties of natural gas in depleted reservoirs are similar to those of CO_2-rich mixtures, therefore, assuming that the reservoir is already saturated with CO_2 (and irreducible brine) allows one to study wellbore transients and near wellbore conditions with limited errors with respect to the real case scenario. Considering that the critical conditions mostly occur during start-up and shut-in operations and transient fluid flow, T2WELL-ECO2M proved to be a valuable tool for assessing the safety of further injection and safety concerns connected with the effect of a strong temperature drop on casings and cement sheaths. Moreover, from the here presented results of injection into reservoir with characteristics of depleted gas reservoirs, it can be noticed that is it possible to maintain CO_2 injection under two-phase wellbore conditions during the entire period of injection. A thorough analysis of BH pressure step-wise changes (Figure 16) indicated a connection with CO_2 phase transition in near-wellbore area which confirmed that wellbore and reservoir flow should not be analysed individually but as interrelated. Not only that wellbore conditions directly affect the fluid entering in to the reservoir,

but also what happens in near-wellbore zone has an effect on wellbore BH conditions. Non-isothermal conditions inside of the wellbore, as already mentioned, are a combination of several coupled effects. Therefore, for the real case scenario and such a narrow frame of BH temperature to stay above hydrate formation conditions as it is the case in chapter 4, it is necessary to have accurate wellbore modelling accounting for diameter changes, wellbore wall roughness, completion characteristics and surrounding formation thermal properties.

Accurate modelling of BH conditions potentially allows more flexibility in choice of upstream conditions.

The new updated code version has showed to be a robust and performing wellbore-reservoir simulator that can be also used to simulate the CO_2 injection into depleted gas reservoirs. It now offers the choice of additional printouts in the output file, updates of outdated correlations and various semi-analytical wellbore-formation heat exchange options. Some of these options were revamped in the current code version, such as *Q3* and *Q3Complete* subroutines, while the time-convolution method was modified and tested and is ready to use. When compared to fully numerical approach of wellbore to formation heat exchange solution, the new time-convolution approach implemented in T2Well-ECO2M proved to provide solutions in good agreement and with a reduction of the computation time.

6.1 Ongoing and future research

This study is just a scratch of all possibilities that T2Well-ECO2M can offer. Going through an extensive literature review of studies and available software gathered in this research, and recognition of the importance of coupled-wellbore reservoir simulation along with non-isothermal wellbore conditions during CO_2 injection, T2Well-ECO2M proves to be a valuable tool in the field of CCS. A part of ongoing research is to verify the performance of T2Well-ECO2M, for simulation of multiphase CO_2 wellbore flow, through a reproduction of the literature cases studying multiphase wellbore flow with classical wellbore simulators. Despite the good simulation performance showed by new improved version of T2Well-ECO2M, as an extension of the presented research, future work could be dedicated to further improvement of the time-convolution method to model different wellbore completion and temperature profiles in case of multiple

wellbores present in the model and the effect of thermal resistance between the wellbore and formation domain.

Again, one of the possibilities, already studied by Oldenburg and Pan (2019) from LBNL, could be adding surface equipment into the model. In their study, they use T2Well coupled with a preliminary version of the EOS module able to simulate multiphase CO_2 flow to simulate onshore and offshore wellbore CO_2 blowout caused by breached surface/subsea pipe. This approach in further studies would allow to analyse the magnitude of temperature drop effect during CO_2 blowouts on upstream equipment.

Considering the possible applications of T2Well-ECO2M, part of the future work could be to test the code on simulation of EGS. Another interesting field of application could be the modelling of CO_2 injection in hydrothermal reservoirs which is now under study in order to reduce the GHG emissions deriving from the utilisation of currently exploited geothermal fields.

While working on this research, there has been a continuous effort to gather as much as possible user experience and create T2Well-ECO2M user's guide which would give basic instruction about the input file generation and gather all differences with so far available T2Well code version. Moreover, there is a continuous effort in improving and modifying the TOUGH2Viewer pre-and-post processing tool to allow reading new output formats and to facilitate the analysis of simulation results, such as a direct plot of pressure and temperature relations on the CO_2 phase diagram.

7 References

- Akinfiev, N.N., Diamond, L.W., Thermodynamic model of aqueous CO_2-H_2O-NaCl solutions from -22 to 100°C and from 0.1 to 100 MPa, Fluid Phase Equilibria, 2010, 295, pp. 104 -124.
- Altunin, V.V., Thermophysical Properties of Carbon Dioxide. Publishing House of Standards, 1975, pp. 551, Moscow (in Russian).
- Ames, W.F., Numerical Methods for Partial Differential Equations. Barnes and Noble, New York, 1969.
- Ampelli, C., Perathoner, S., Centi. G., CO_2 utilization: an enabling element to move to a resource- and energy-efficient chemical and fuel production, Philosophical Transactions of Royal Society A, 2015.
- Asamoto, S., Le Guen, Y., Poupard, O., Capra, B., Well integrity assessment for CO_2 injection: a numerical case study on thermo-mechanical behavior in downhole CO_2 environments, Engineering Computations, 30 (6), 2013, pp. 842-853.
- Bacci, G., Korre, A., Durucan, S., An experimental and numerical investigation into the impact of dissolution/precipitation mechanisms on CO_2 injectivity in the wellbore and far field regions, International Journal of Greenhouse Gas Control, 5(3), 2011.
- Bachu, S., Bonijoly, D., Bradshaw, J., Burruss, R., Holloway, S., Christensen, N.P., Mathiassen, O.M., CO_2 storage capacity estimation: Methodology and gaps, International Journal of Greenhouse Gas Control, 1 (4) 2007, pp. 430-443
- Bahonar, M., Azaiez, J., Zhangxing J. C., "Transient Nonisothermal Fully Coupled Wellbore/Reservoir Model for Gas-Well Testing, Part 1: Modelling", Journal of Canadian Petroleum Technology, 50, 2011, pp. 37–50.
- Barker, D.J., Turner, S.A., Napier-Moore, P.A, Clark, M.,Davison, J.E., CO_2 Capture in the Cement Industry, Energy Procedia, 1(1), 2009, pp. 87-94.
- Basirat, F., Yang, Z., Bensabat, J., Levchenko, S., Pan L., Niemi, A., Characterization of CO_2 self-release during Heletz Residual Trapping Experiment I (RTE I) using a coupled wellbore-reservoir simulator, International Journal of Greenhouse Gas Control, 102, 2020
- Battistelli, A. and Marcolini, M., TMGAS: a new TOUGH2 EOS module for the numerical simulation of gas mixtures injection in geological structures, International Journal of Greenhouse Gas Control, 2009, 3, pp. 481-493.
- Battistelli, A., Calore, C., Pruess, K., The simulator TOUGH2/EWASG for modelling geothermal reservoirs with brines and a non-condensable gas, Geothermics, 26(4), 1997, pp. 437-464.
- Battistelli, A., Carpita, M., Marcolini, M., Thermal effects and coupled wellbore – reservoir flow during GHG injection in depleted gas reservoirs, Processes and Technologies for a Sustainable Energy, Ischia, June 27-30, 2010.
- Battistelli, A., Ceragioli, P., Marcolini, M., Injection of Acid Gas Mixtures in Sour Oil Reservoirs: Analysis of Near-Wellbore Processes with Coupled Modelling of Well and Reservoir Flow, Transport in Porous Media, 2011, 90(1), pp. 233-251.

- Battistelli, A., Finsterle, S., Marcolini, M., Pan, L., Modeling of coupled wellbore-reservoir flow in steam-like supercritical geothermal systems, Geothermics, 86, 2020
- Battistelli, A., Improving the treatment of saline brines in EWASG for the simulation of hydrothermal systems. Proceedings, TOUGH Symposium 2012, Lawrence Berkeley National Laboratory, Berkeley, California, September 17–19, 2012.
- Battistelli, A., Analysis of wellbore flow of two-phase CO_2 mixtures using the T2Well coupled wellbore-reservoir simulator, Final Technical Report. DICAM Dept., University of Bologna, Contract Rep. N. 67 – Prot. N. 2130., 2020.
- Birkholzer, J.T., Nicot, J.P., Oldenburg, C.M., Zhou, Q., Kraemer, S., Bandilla, K., Brine flow up a well caused by pressure perturbation from geologic carbon sequestration: Static and dynamic evaluations, International Journal of Greenhouse Gas Control, 5(4), 2011, pp. 850-861.
- Boot-Handford, M.E., Abanades, J.C., Anthony E.J., Blunt, M.J., Brandani S., Dowell, N.M., Fernández, J.R., Ferrari, M-C., Gross, R., Hallett, J.P., Haszeldine, R.S., Heptonstall, P., Lyngfelt, A., Makuch, Z., Mangano, E., Porter, R.T.J., Pourkashanian, M., Rochelle, G.T., Shah, N., Yaoa, J.G., Fennell P.S., Carbon capture and storage update, Energy & Environmental Science, 1, 2014.
- Bonduà, S., Battistelli, A., Berry, P., Bortolotti, V., Consonni, A., Cormio C., Geloni, C., Vasini, E.M., 3D VORONOI PRE-AND POST-PROCESSING TOOLS FOR THE MODELING OF DEEP SEDIMENTARY FORMATIONS WITH THE TOUGH2 FAMILY OF CODES, Proceedings, TOUGH Symposium 2015, Lawrence Berkeley National Laboratory, Berkeley, California, September 28-30, 2015.
- Bonduá, S., Berry, P., Bortolotti, V., Cormio, C., TOUGH2Viewer: A post-processing tool for interactive 3D visualization of locally refined unstructured grids for TOUGH2, Computers & Geosciences, 46, 2012, pp. 107-118.
- Bonduà, S., Bortolotti V., Strpić, K., VORO2MESH and TOUGH2Viewer for MODFLOW User Manual, DICAM softwares, 2021.
- Bonduà, S., Bortolotti V., TOUGH2Viewer 2.0: A multiplatform tool for fully 3D Voronoi TOUGH grids, SoftwareX, 12, 2020.
- Budinis, S., Krevor, S., Dowell, N.M., Brandon, N., Hawkes, A., An assessment of CCS costs, barriers and potential, Energy Strategy Reviews, 22, 2018, pp. 61-81.
- Carey, J.W., Svec, R., Grigg, R., Zhang, J., Crow, W., Experimental investigation of wellbore integrity and CO_2-brine flow along the casing-cement microannulus. International Journal of Greenhouse Gas Control, 4, 2010, pp. 272–282
- Carslaw, H.S., Jaeger, J.C., Conduction of Heat in Solids, 2nd Edition - Oxford: Clarendon Press, 1959.
- Chang, Y.B., Lim, M.T., Pope, G.A., Sepehrnoori, K., CO_2 Flow patterns under multiphase flow: heterogeneous field-scale conditions. SPE Reservoir Engineering, 1994, pp. 208–216.
- Chierici, G.L., The Simulation of Reservoir Behaviour Using Numerical Modelling. In: Principles of Petroleum Reservoir Engineering. Springer, Berlin, 1995, pp. 123-150.

- Chiu, K., Thakur, S.C., Modeling of Wellbore Heat Losses in Directional Wells Under Changing Injection Conditions. Paper 22870-MS, SPE Annual Technical Conference and Exhibition, 6-9 October 1991, Dallas, Texas, 1991.
- Collins, R.E., Flow of fluids through porous materials, Reinhold Publishing Co., New York, 1961
- Cooper, C., A technical basis for carbon dioxide storage, Energy Procedia, 1, 2009, pp. 1727-1733.
- Corey, A.T., The Interrelation Between Gas and Oil Relative Permeabilities, Producers Monthly,19, 1954, pp. 38-41.
- Croucher, A., Waiwera user guide – Release 1.2.1., University of Auckland, Geothermal Institute, 2020.
- Croucher, A.E. and O'Sullivan, M.J., Application of the computer code TOUGH2 to the simulation of supercritical conditions in geothermal systems. Geothermics, 2008, 37, pp. 622–634.
- Cuéllar-Franca, R.M. and Azapagic, A., Carbon capture, storage and utilisation technologies: A critical analysis and comparison of their life cycle environmental impacts., Journal of CO_2 Utillization, 2015, 9, pp. 82–102.
- da Costa, P.V.M., da Costa, A.M., Meneghini, J.R., Nishimoto, K., Assi, G., Ebecken, N.F.F., Pinguelli Rosa, L., Miranda, A.C.D.O., Goulart, M.B.R., Bergsten, A., Brandão, C., World's First Carbon Sequestration Project in Salt Caverns Built Offshore in Ultra Deep Water in Brazil, Proceedings of the ASME 2020 39th International Conference on Ocean, Offshore and Arctic Engineering, Volume 1: Offshore Technology,August 3–7, 2020.
- Da Silva, D.V.A and Jansen, J.D., A Review of Coupled Dynamic Well-Reservoir Simulation, IFAC-Papers OnLine, 48(6) 2015, pp. 236-241.
- De Andrade, J., Torsæter, M., Todorović, J., Opedal, N., Stroisz, A., Vrålstad, T., Influence of casing centralization on cement sheath integrity during thermal cycling, IADC/SPE Drilling Conference and Exhibition, Society of Petroleum Engineers, 2014.
- Driesner, T., The system H_2O–NaCl. Part I: Part II: Correlations for molar volume, enthalpy, and isobaric heat capacity from 0 to 1000°C, 1 to 5000 bar, and 0 to 1 XNaCl, Geochimica et Cosmochimica Acta, 2007, 71, pp. 4902–4919.
- Ebigbo, A., Class, H., Helmig, R. CO_2 leakage through an abandoned well: problem-oriented benchmarks. Computational Geoscience, 11, 2007, pp. 103–115.
- Fagin, R.G. and Stewart, C.H., A New Approach to the Two-Dimensional Multi-phase Reservoir Simulator, Society of Petroleum Engineers Journal, 6, 1966, pp. 175-182.
- Falta, R., Pruess, K., Javandel, I., and Witherspoon, P., Numerical Modeling of Steam Injection for the Removal of Nonaqueous Phase Liquids from the Subsurface. 1. Numerical Formulation, Water Resources Research, 28(2), 1992, pp. 433–449.
- Feather, B.M. and Archer, R.A., Enhanced Natural Gas Recovery by Carbon Dioxide Injection for Storage Purposes, 17th Australasian Fluid Mechanics Conference Auckland, New Zealand, 5-9 December 2010.

- Feng, G., Xu, T., Tian, H., Lu, M., Connell, L.D., Lei, H., Shi, Y., Three-phase non-isothermal flow behavior of CO_2-brine leakage from wellbores, International Journal of Greenhouse Gas Control, 64, 2017, pp. 183-193.
- Finsterle, S., Enhancements to the TOUGH2 Simulator Integrated in iTOUGH2. LBNL report, 2017, LBNL-7016E.
- Ge, M., and Friedrich J., 4 Charts Explain Greenhouse Gas Emissions by Countries and Sectors, World Research Institute, 2020.
- Giorgis T., Carpita M., Battistelli A., 2D modeling of salt precipitation during the injection of dry CO_2 in a depleted gas reservoir. Energy Conversion and Management, 2007, 48 (6), pp. 1816-1826.
- Goda, H., Hibiki, T., Kim, S., Ishii, M., Uhle, J., Drift-flux model for downward two-phase flow, International Journal of Heat and Mass Transfer, 2003, 46(25), pp. 4835–4844.
- Hadgu, T., R. W. Zimmerman, R.W., Bodvarsson G.S., Coupled reservoir-wellbore simulation of geothermal reservoir behavior, Geothermics, 24(2), 1995, pp.145-166.
- Han, J., Carey, J.W., Zhang, J., Degradation of Cement–Steel Composite at Bonded Steel–Cement Interfaces in Supercritical CO_2 Saturated Brines Simulating Wellbore Systems, CORROSION/2012, NACE, Houston, TX, 2012.
- Hannis, S., Lu, J., Chadwick, A., Hovorka, S., Kirk, K., Romanak, K., Pearce J., CO_2 Storage in Depleted or Depleting Oil and Gas Fields: What can We Learn from Existing Projects?, Energy Procedia, Volume 114, 2017, pp. 5680-5690.
- Hasan, A.R, Kabir, C.S., Fluid Flow and Heat Transfer in Wellbores. Society of Petroleum Engineers, Richardson, Texas, 2002.
- Heathman, J., Critical Application Cementing–Redefining the Issues, Society of Petroleum Engineers - Distinguished Lecturer Series, Richardson, TX, USA, 2007.
- Hertzberg, M., Siddons, A., Schreuder H., Role of greenhouse gases in climate change, Energy and Environment, 28(4), 2017.
- Hsu, C.F., Morell, J.I., Falls, A.H., Field-scale CO_2-flood simulations and their impact on the performance of the Wasson Denver Unit, SPE Symposium on Reservoir, 12–15 February 1995, San Antonio.
- Hu, L., Pan, L., Zhang, K., Modeling brine leakage to shallow aquifer through an open wellbore using T2WELL/ECO2N, International Journal of Greenhouse Gas Control, 9, 2012, pp. 393-401.
- IAPWS 2011, Release on the IAPWS Formulation 2011 for the Thermal Conductivity of Ordinary Water Substance, IAPWS R15-11, September 2011.
- IAPWS, Release on the IAPWS Formulation 2008 for the Viscosity of Ordinary Water Substance, Berlin, Germany September 2008.
- IAPWS, Release on the IAPWS Industrial Formulation 1997 for the Thermodynamic Properties of Water and Steam. Erlangen, Germany, 1997.
- IAPWS, Revised Release on the IAPWS Industrial Formulation 2007 for the Thermodynamic Properties of Water and Steam, IAPWS Release, Switzerland, 2007.
- IFC, A Formulation of the Thermodynamic Properties of Ordinary Water Substance. IFC Secretariat, Düsseldorf, Germany, 1967.

- IPCC (2005) Special report on carbon dioxide capture and storage, Metz, B., Davidson, O., de Coninck, H.C., Loos, M., Meyer, L.J., (eds) Prepared by Working Group III of the Intergovernmental Panel on Climate Change. Cambridge University Press, Cambridge, United Kingdom/New York, NY, USA
- IPCC, 2007: Climate Change 2007: Synthesis Report, Bernstein, L., Bosch, P., Canziani, O., Chen, Z., Christ, R., & Riahi, K.
- IPCC, 2018: Global Warming of 1.5°C. An IPCC Special Report on the impacts of global warming of 1.5°C above pre-industrial levels and related global greenhouse gas emission pathways, in the context of strengthening the global response to the threat of climate change, sustainable development, and efforts to eradicate poverty [Masson-Delmotte, V., P. Zhai, H.-O. Pörtner, D. Roberts, J. Skea, P.R. Shukla, A. Pirani, W. Moufouma-Okia, C. Péan, R. Pidcock, S. Connors, J.B.R. Matthews, Y. Chen, X. Zhou, M.I. Gomis, E. Lonnoy, T. Maycock, M. Tignor, and T. Waterfield (eds.)].
- Jiang, X., A review of physical modelling and numerical simulation of long-term geological storage of CO_2, Applied Energy, 88(11), 2011, pp.3557-3566.
- Jung, Y., Pau, G.S.H., Finsterle, S., Doughty, C., TOUGH3 User's Guide version 1.0, LBNL-2001093, Lawrence Berkeley National Laboratory, California, 2018.
- Kaldi, J., Daniel, R., Tenthorey, E., Michael, K., Schacht, U., Nicol, A., Underschultz, J., Backe, G., Containment of CO_2 in CCS: Role of Caprocks and Faults, Energy Procedia, 37, 2013, pp. 5403-5410.
- Kanev, K., Ikeuchi, J., Kimura, S., Okajima, A., Heat loss to the surrounding rock formation from a geothermal wellbore, Geothermics, 1997, 26(3), pp. 329-349.
- Kapusta, S.D. and Canter, S.C., Corrosion Control in CO_2 Enhanced Oil Recovery, CORROSION/94, NACE, Houston, 1994.
- Karimi, F. and Khalilpour, R., Evolution of carbon capture and storage research: trends of international collaborations and knowledge maps, International Journal of Greenhouse Gas Control, 37, 2015, pp. 362-376.
- Katz, D.L. and Lee, R.L., Natural gas engineering, McGraw-Hill, New York, 1990.
- Klinkby, L., Nielsen, C.M., Krogh, E., Smith, I.E., Palm, B., Bernstone, C., Simulating rapidly fluctuating CO_2 flow into the Vedsted CO_2 pipeline, injection well and reservoir, Energy Procedia 4, 2011, pp. 4291-4298.
- Ladbrook, B., Smith, N., Pershad, H., Harland, K., Slater, S., Holloway, S., Kirk, K., CO_2 Storage in Depleted Gas Fields. IEA Technical Report, 2009.
- Lavrov, A. and Torsæter, M., Thermal stresses in annular cement, Physics and Mechanics of Primary Well Cementing, Springer, 2016, pp. 93-101.
- Lei, H., Cai, Y., Lu, M, Li, X., Connell L.D., A study on the thermal-hydrodynamical-coupled CO_2 flow process in the Ordos CCS-geological-formation, International Journal of Greenhouse Gas Control, 95, 2020.
- Leung, D.Y.C., Caramanna, G., Maroto-Valer, M.M., An overview of current status of carbon dioxide capture and storage technologies, Renewable and Sustainable Energy, Renewable and Sustainable Energy Reviews, 2014, 39, pp. 426–443.

- Lindeberg, E., Modelling pressure and temperature profile in a CO_2 injection well, Energy Procedia, 4, 2011, pp. 3935–394.
- Livescu, S., Durlofsky, L.J., Aziz, K., Ginestra, J.C., A fully-coupled thermal multiphase wellbore flow model for use in reservoir simulation, Journal of Petroleum Science and Engineering, 71(3–4), 2010, pp. 138–146.
- Lu, M. and Connell, L.D. Non-isothermal flow of carbon dioxide in injection wells during geological storage, International Journal of Greenhouse Gas Control, 2008.
- Lu, M. and Connell, L.D., The transient behaviour of CO_2 flow with phase transition in injection wells during geological storage – Application to a case study, Journal of Petroleum Science and Engineering, 124, 2014, pp. 7-18.
- Magnusdottir, L. and Finsterle, S., iTOUGH2-EOS1SC: Multiphase Reservoir Simulator for Water under Sub- and Supercritical Conditions, User's Guide. LBNL Report LBNL-7017E, 2015.
- Mann, M.E., Greenhouse gas, Encyclopedia Britannica, 19 March 2019, https://www.britannica.com/science/greenhouse-gas. (last accessed 8 February 2021).
- Miller, C.W., Wellbore Storage Effect in Geothermal Wells, Society of Petroleum Engineers Journal, 20(6), 1980, pp. 555–566.
- Munkejord, S.T., Bernstone, C., Clausen, S., de Koeijer, G., Mølnvik, M.J., Combining thermodynamic and fluid flow modelling for CO_2 flow assurance, Energy Procedia, 63 2013, pp. 2904-2913.
- Munkejord, S.T., Hammer, M., Depressurization of CO2-rich mixtures in pipes: Two-phase flow modelling and comparison with experiments, International Journal of Greenhouse Gas Control, 37, 2015, pp. 398-411.
- Oddie, G., Shi, H., Durlofsky, L.J., Aziz, K., Pfeffer, B., Holmes, J.A., Experimental study of two and three phase flows in large diameter inclined pipes, Intonational Journal of Multiphase Flow 29(4), 2003, pp. 527–558.
- Narinesingh, J. and Alexander, D., CO_2 Enhanced Gas Recovery and Geologic Sequestration in Condensate Reservoir: A Simulation Study of the Effects of Injection Pressure on Condensate Recovery from Reservoir and CO_2 Storage Efficiency, Energy Procedia, 63, 2014, pp. 3107-3115.
- Oldenburg, C. M., Pan, L., Porous media compressed-air energy storage (PM-CAES): theory and simulation of the coupled wellbore reservoir system, Transport in Porous Media, 2013.
- Oldenburg, C.M., Joule-Thomson cooling due to CO_2 injection into natural gas reservoirs, TOUGH2 Symposium 2006 Proceedings, Lawrence Berkeley National Laboratory, Berkeley, California, May 15–17, 2006.
- Oldenburg, C.M., Pan, L., Zhou, Q., Dobeck, L., Spangler, L., On producing CO_2 from subsurface reservoirs: simulations of liquid-gas phase change caused by decompression, Greenhouse Gas Science and Technology, 9, 2019, pp. 194–208.
- Oldenburg, C.M. and Pan, L., Simulation Study Comparing Offshore Versus Onshore CO_2 Well Blowouts, offshore Technology Conference, Houston, Texas, USA, 6 – 9 May 2019.

- Pan, L. and Oldenburg C.M., T2Well: Derivation of (1) the 1D multiphase momentum equation for wellbore flow and (2) a two-step approach for 3-phase DFM, presentation, Lawrence Berkeley National Laboratory, July 2018a.
- Pan, L. and Oldenburg, C., Modeling Transient Leakage Signals from Abandoned Wells with T2Well: Effects of Plug Gap Aperture, 14th Greenhouse Gas Control Technologies Conference Melbourne, 21-26 October 2018b.
- Pan, L. and Oldenburg, C.M., T2Well—An integrated wellbore–reservoir simulator, Computers & Geosciences, 65, 2014, pp. 46–55.
- Pan, L., Freifeld, B., Doughty, C., Zakem, S., Sheu, M., Cutright, B., Terrail, T., Fully coupled wellbore-reservoir modelling of geothermal heat extraction using CO_2 as the working fluid, Geothermics, 53, 2015a, pp. 100-113.
- Pan, L., Oldenburg, C., Pruess, K., Wu, Y.S., Transient CO_2 leakage and injection in wellbore-reservoir systems for geologic carbon sequestration, Greenhouse Gases: Science and Technology 1(4), 2011b.
- Pan, L., Oldenburg, C.M., Wu, Y.S., Pruess, K., T2Well/ECO2N Version 1.0: Multiphase and Non-Isothermal Model for Coupled Wellbore-Reservoir Flow of Carbon Dioxide and Variable Salinity Water, Report LBNL-4291E, 2011a.
- Pan, L., Spycher, N., Doughty, C., Pruess, K., ECO2N V2.0: A TOUGH2 Fluid Property Module for Mixtures of Water, NaCl, and CO_2, Earth Sciences Division, Lawrence Berkeley National Laboratory University of California, Berkeley, 2015b, LBNL-6930E.
- Panday, S., Forsyth, P., Falta, R., Wu, Y., and Huyakorn, P., Considerations for robust compositional simulations of subsurface nonaqueous phase liquid contamination and remediation, Water Resources Research, 31(5), 1995, pp. 1273–1289.
- Paterson, L., Lu, M., Cornell, L.D., Ennis-King J. Numerical Modeling of Pressure and Temperature profiles Including Phase Transition in Carbon Dioxide Wells. SPE Annual Conference 2008, Denver Colorado.
- Peaceman, D.W., Fundamentals of Numerical Reservoir Simulation, Elsevier, Amsterdam, The Netherlands, 1977.
- Peery, J.H. and Herron, E.H., 1969. Three-Phase Reservoir Simulation. Journal of Petroleum Technology, 21, 1969, pp. 211-220.
- Pekot, L.J., Petit, P., Adushita, Y., Saunier, S., De Silva, R., Simulation of two-phase flow in carbon dioxide injection wells, SPE Offshore Europe Oil and Gas Conference and Exhibition, Paper SPE 144847, Society of Petroleum Engineers, Aberdeen, 2011, pp. 94–106.
- Pham, V.T.H., CO_2 storage – Simulations for forecasting the behavior of injection CO_2 in geological formations, Dissertation for the degree of Philosophiae Doctor, Department of geoscience, University of Oslo, Norway, 2012.
- Piao, J., Han, W.S., Choung, S., Kim, K-Y., Dynamic Behavior of CO_2 in a Wellbore and Storage Formation: Wellbore-Coupled and Salt-Precipitation Processes during Geologic CO_2 Sequestration, Geofluids, 2018.

- Pires, J.C.M., Martins, F.G., Alvim-Ferraz, M.C.M., Simões, M., Recent developments on carbon capture and storage: An overview, Chemical Engineering and Design, 2011, 89, pp. 1446-1460.
- Pruess, K., ECO2N: A TOUGH2 Fluid Property Module for Mixtures of Water, NaCl, and CO_2, Earth Sciences Division, Lawrence Berkeley National Laboratory University of California, Berkeley, 2005, LBNL-57952.
- Pruess, K., Garcia J., Multiphase flow dynamics during CO_2 disposal into saline aquifers, Environmental Geology, 42, 2002, pp. 282–295.
- Pruess, K., Oldenburg, C., Moridis, G.J., TOUGH2 User's Guide, Version 2.1, Report LBNL-43134, Lawrence Berkeley National Laboratory, Berkeley, California, 2012.
- Pruess, K., Oldenburg, C.M., Moridis, G.J., TOUGH2 User's Guide Version 2. Report, LBNL-43134, Lawrence Berkeley National Laboratory, California, 1999.
- Pruess, K., On CO_2 fluid flow and heat transfer in the subsurface, flowing leakage from the from the geological storage reservoir, Environmental Geology, 54, 2007, pp. 1677-1686.
- Pruess. K., ECO2M: A TOUGH2 Fluid Property Module for Mixtures of Water, NaCl, and CO_2, Including Super- and Sub-Critical Conditions, and Phase Change Between Liquid and Gaseous CO_2, Report LBNL-4590E, 2011.
- Rafieea, A., Khalilpour, K.R., Milani,d D., Panahie, M., Trends in CO_2 conversion and utilization: A review from process systems perspective, Journal of Environmental Chemical Engineering, 6(5), 2018, pp. 5771-5794.
- Ramey, H.J., Heat losses during flow of steam down a wellbore. Journal of Petroleum Technology, 1965, pp. 845-851.
- Raza, A., Gholami, R., Rezaee, R., Bing, C.H., Nagarajan, R., Hamid M.A., CO_2 storage in depleted gas reservoirs: A study on the effect of residual gas saturation, Petroleum, Volume 4, Issue 1, 2018, pp. 95-107.
- Raza, A., Gholami, R., Rezaee, R., Rasouli, V., Rabiei, M., Significant aspects of carbon capture and storage – A review, Petroleum, 5(4), 2019, pp. 335-340.
- Raza, A., Rezaee, R., Gholami, R., Bing, C.H., Nagarajan, R., Hamid, M.A., A screening criterion for selection of suitable CO_2 storage sites, Journal of Natural Gas Science and Engineering, 28, 2016, pp. 317-327.
- Richter, H.J., Flooding in tubes and annuli, International Journal of Multiphase Flow, 7(6), 1981, pp. 647-659.
- Ritchie, H. and Roser, M., CO_2 and Greenhouse Gas Emissions, Published online at OurWorldInData.org. Retrieved from: 'https://ourworldindata.org/co2-and-other-greenhouse-gas-emissions' (2017 published, revised in 2020) [Online Resource] (last access 10 February, 2021).
- Rodosta, T. D., Litynski, J. T., Plasynski, S. I., Hickman, S., Frailey, S., Myer, L., U.S. Department of Energy's site screening, site selection, and initial characterization for storage of CO_2 in deep geological formations. Energy Procedia 4, 2011, pp. 4664–4671.

- Roussanaly, S., Berghout, N., Fout, T., Garcia, M., Gardarsdottir, S., Nazir, S.M., Ramirez, A., Rubin, E.S., Towards improved cost evaluation of Carbon Capture and Storage from industry, International Journal of Greenhouse Gas Control, 106, 2021.
- Roy P., Morris J.P., Walsh S.D.C., Iyer J., Carroll S., Effect of thermal stress on wellbore integrity during CO_2 injection, International Journal of Greenhouse Gas Control, 77, 2018, pp. 14-26.
- Roy, P., Morris, J.P., Walsh, S.D.C, Iyer, J., Carroll, S., Todorovic, J., Gawel, K., Torsæter, M., Assessment of thermal stress on well integrity as a function of size and material properties, Energy Procedia, 114 ,2017, pp. 5241-5248.
- Sacconi, A., Mahgerefteh, H., Modelling start-up injection of CO_2 into highly-depleted gas fields, Energy, 191, 2020.
- Samuel, R., Mahgerefteh, H., Transient Flow Modelling of Start-up CO_2 Injection into Highly-Depleted Oil/Gas Fields, International Journal of Chemical Engineering and Applications, 8(5), 2017, pp. 319-326.
- Scherer, G.W., Kutchko, B., Thaulow, N., Duguid, A., Mook, B., Characterization of cement from a well at Teapot Dome Oil Field: implications for geologic sequestration. International Journal of Greenhouse Gas Control, 5, 2011, pp.115–124.
- Shi, H., Holmes, J. A., Durlofsky, L.J., Aziz, K., Diaz, L., Alkaya, B., Oddie, G., Drift-Flux Modeling of Two-Phase Flow in Wellbores. SPE Journal, 10(01), 2005a, pp. 24–33.
- Shi, H., Holmes, J., Diaz, L., Durlofsky, L.J., Khalid, A., Drift-Flux Parameters for Three-Phase Steady-State Flow in Wellbores, SPE Journal, 10, 2005b, pp. 130–137.
- Potdar, S.R. and Vishal, V., Trapping Mechanism of CO_2 Storage in Deep Saline Aquifers: Brief Review, In book: Geologic Carbon Sequestration, Springer, 2016.
- Smit, B., Reime, J.R., Oldenburg, C.M., Bourg, I.C., Introduction to Carbon Capture and Sequestration, Imperial College Press, 2014.
- Stephen A. Rackley, Carbon Capture and Storage, Butterworth-Heinemann, 2017
- Stone, H.L., Probability Model for Estimating Three-Phase Relative Permeability, Journal of Petroleum Technology, 1970, 249, pp. 214-218.
- Strpić, K., A. Battistelli, A., Bonduà, S., Bortolotti, V., Macini, P., Pan L., Modeling of Transient Multiphase Flow in a CO_2 Injection Well with the Wellbore-Reservoir Coupled Simulator T2Well-ECO2M, Proceedings, 1st Geoscience & Engineering in Energy Transition Conference 16-18 November 2020, Strasbourg, France, 2020.
- Strpić, K., A. Battistelli, A., Bonduà, S., Bortolotti, V., Macini, P., Pan L., Evaluation of time-convolution approach for modelling heat exchange between wellbore and formation during multiphase CO_2 injection with T2Well-ECO2M, Proceedings, Offshore Mediterranean Conference 28-30 September 2021, Ravenna, Italy.
- Tian, Z-H., and Yang Z-L., Scenarios of Carbon Emissions from the Power Sector in Guangdong Province, Sustainability, 8(9), 2016.
- Todorović, J., Gawel, K., Lavrov A., Torsæter, M., Integrity of downscaled well models subject to cooling, SPE Bergen One Day Seminar, Society of Petroleum Engineers 2016.

- Torsen, A.O., Smistad, H.J., Tveit, H., Hansen, O.C., Bjørtuft, V.G., Furuvik, N.C.I., Moldestad, B.M.E., Simulation of CO_2 storage in the North Sea, Linköping Electronic Conference Proceedings, 2018, pp. 255-262.
- UNFCCC 2015, Paris Agreement. Decision 1/CP.17. http://unfccc.int/resource/docs/2015/cop21/eng/l09r01.pdf, UNFCCC document FCCC/CP/2015/L.9/Rev.1.
- Vargaftik, N.B., Tables on the thermophysical properties of liquids and gases, 2nd edition, Wiley, New York, 1975.
- Vargaftik, N.B., Vinograd.ov, Y.K., Yargin, V.S., Handbook of physical properties of liquids and gases, 3rd edition, Begell House, New York, 1996.
- Vasini, E.M., Battistelli, A., Berry, P., Bonduà, S., Bortolotti, V., Cormio, C., Pan, L. Interpretation of production tests in geothermal wells with T2Well-EWASG. Proceedings, TOUGH Symposium 2015. LBNL, Berkeley, California, September 28-30, 2015.
- Vasini, E.M., Battistelli, A., Berry, P., Bonduà, S., Bortolotti, V., Cormio, C., Pan, L. Interpretation of production tests in geothermal wells with T2Well-EWASG. Geothermics, 2018, 73, pp. 158-167.
- van Genuchten, M.Th., A Closed-Form Equation for Predicting the Hydraulic Conductivity of Unsaturated Soils, Soil Science Society, 44(5), 1980, pp. 892 – 898.
- Verma, A. and Pruess, K., Thermohydrologic conditions and silica redistribution near high-level nuclear wastes emplaced in saturated geological formations, Journal of Geophysical Research, 1988, 93, pp. 1159-1173.
- Wan, N.-H., Wang, L.-S., Hou, L.-T., Wu, Q.-L., Xu, J.-Y., Modeling Transient Flow in CO_2 Injection Wells by Considering the Phase Change, Processes, 9(12), 2021.
- Wang, J., Ryan D., Anthony, E.J., Wildgust, N., Aiken, T., Effects of Impurities on CO_2 Transport, Injection and Storage, Energy Procedia, 4, 2011, pp. 3071-3078.
- Watson, T.L. and Bachu, S., Evaluation of the Potential for Gas and CO_2 Leakage Along Wellbores, E&P Environmental and Safety Conference, Galveston, Texas, U.S.A., March 2007.
- Weideman B.L., Investigation of Cased Wellbore Integrity in the Wabamun Area Sequestration Project, Missouri University of Science and Technology, 2014
- Willhite, G.P., Over-all Heat transfer coefficients in steam and hot water injection wells, Continental Oil Co. Ponca City Okla, May, 1967.
- Yashvardhan, V., Vikram, V., Ranjith P. G., Sensitivity Analysis of Geomechanical Constraints in CO_2 Storage to Screen Potential Sites in Deep Saline Aquifers, 3, 2021.
- Yoro, K.O. and Daramola, M.O., Chapter 1 - CO_2 emission sources, greenhouse gases, and the global warming effect, Advances in Carbon Capture, Woodhead Publishing, 2020, pp. 3-28.
- Zhang, K., Ling, L., Wang, Y., Modeling approaches for wellbore boundary conditions for simulation of CO_2 geologic sequestration in saline aquifers, Proceedings, TOUGH Symposium 2012, Lawrence Berkeley National Laboratory, Berkeley, California, September 17-19, 2012.

- Zhang, Y., Pan, L., Pruess, K., Finsterle, S., A time-convolution approach for modeling heat exchange between a wellbore and surrounding formation, Geothermics, 2011, 40, pp. 261–266.
- Zhao, R. and Cheng, J., Effects of temperature on salt precipitation due to formation dry-out during CO_2 injection in saline aquifers, Greenhouse Gases: Science and Technology, 7(4), 2017.
- Zhao, R. and Cheng, J., Non-isothermal modeling of CO_2 injection into saline aquifers at a low temperature. Environmental Earth Science 73(9), 2015, pp. 5307-5316
- Zhu, Q., Developments on CO_2-utilization technologies, Clean Energy, 3(2), 2019, pp. 85–100.
- Zubert, N. and Findlay, J.A., Average Volumetric Concentration in Two-Phase Flow Systems, Journal of Heat Transfer, 87, 1965.

Appendix A. Input Parameters

A1. Dedicated case with phase transition

```
*numerical_model* - 2-D reservoir model
MESHMAKER1----*----2----*----3----*----4----*----5----*----6----*----7----*----8
RZ2D
RADII
   10
     0.   0.037973     0.06      0.09      0.12      0.20      0.30      0.50
   0.75       1.0
EQUID
    5           1.
EQUID
    5           2.
LOGAR
   50          1.E2
LOGAR
   50          2.E3
EQUID
    1          1.0E-3
LAYER----1----*----2----*----3----*----4----*----5----*----6----*----7----*----8
   68
     1.        1.        2.       10.       10.       20.       50.       50.
       50.       50.       50.       50.       50.       50.       50.       50.
       50.       50.       50.       50.       50.       50.       50.       50.
       50.       50.       50.       50.       50.       50.       50.       50.
       50.       50.       50.       50.       50.       50.       50.       50.
       50.       50.       50.       50.       50.       50.       50.       50.
       50.       50.       50.       50.       50.       50.       50.       50.
       50.       50.       50.       50.
ENDFI
```

Figure A1: Input file for MESHmaker for 2D radially symmetric grid of injection site model presented in paragraph 4.2.

Table A1: Input parameters for dedicated model with phase transition (paragraph 4.2)

Wellbore		
Internal diameter	2.99	inch
Wall roughness	1.E-5	m
Depth of tubing installation	3092.0	m
Rock grain density of wellbore surrounding*	2385.0	kg/m^3
Thermal conductivity of wellbore surrounding*	2.50	W/(m°C)

Rock grain spec. heat*	1000.0	J/(kg°C)
Completion domain		
Rock grain density	2690.0	kg/m^3
Porosity	1.E-10	-
Abs. permeability (x,y.z)	1.E-20, 1.E-20, 1.E-20	m^2
Thermal conductivity	1.4	W/(m°C)
Rock grain spec. heat	400.0	J/(kg°C)
Surrounding formation		
Rock grain density	2690.0	kg/m^3
Porosity	0.05	-
Abs. permeability (x,y.z)	5.E-15, 5.E-15, 5.E-15	m^2
Thermal conductivity	2.50	W/(m°C)
Rock grain spec. heat	920.0	J/(kg°C)
Temperature distribution	15.2°C @ 0 m 61.7°C @ 3142 m (bedrock)	
Pressure distribution	Hydrostatic pressure gradient	
Caprock and bedrock		
Rock grain density	2600.0	kg/m^3
Porosity	0.01	-
Abs. permeability (x,y.z)	1.0E-19, 1.0E-19, 1.0E-18	m^2
Thermal conductivity	2.30	W/(m°C)
Rock grain spec. heat	920.0	J/(kg°C)
Relative permeability: Corey's curves (1954) S_{lr}, S_{gr}	0.40, 0.05	
Capillary pressure: van Genuchten (1980) λ, S_{lr}, $1/P_0$, P_{max}, S_{ls}	0.44380, 8.01E-2, 5.792e-07, 5.E7, 1.0	
Atmosphere (0 m - +2 m)		
Rock grain density	2600.0	kg/m^3
Porosity	0.90	-
Abs. permeability (x,y.z)	1.0E-19, 1.0E-19, 1.0E-18	m^2
Thermal conductivity	2.30	W/(m°C)
Rock grain spec. heat	99920.0	J/(kg°C)
Reservoir		
Reservoir thickness	50.0	m
Rock grain density	2690.0	kg/m^3
Porosity	0.20	-
Abs. permeability (x,y.z)	1.0E-13, 1.0E-13, 1.0E-14	m^2
Thermal conductivity	2.30	W/(m°C)
Rock grain spec. heat	920.0	J/(kg°C)
Initial (residual) brine saturation	0.20	-
Brine salinity	50,000	ppm

Relative permeability: Stone's 1st three-phase method (modified) (1970) S_{ar}, S_{lr}, S_{gr}, n	0.20, 0.05, 0.05, 3	
Capillary pressure: van Genutchen (1980) λ, S_{lr}, $1/P_0$, P_{max}, S_{ls}	0.30, 0.00, 1.105E-4, 1.E7, 0.999	

*required parameters for wellbore rocktype definition
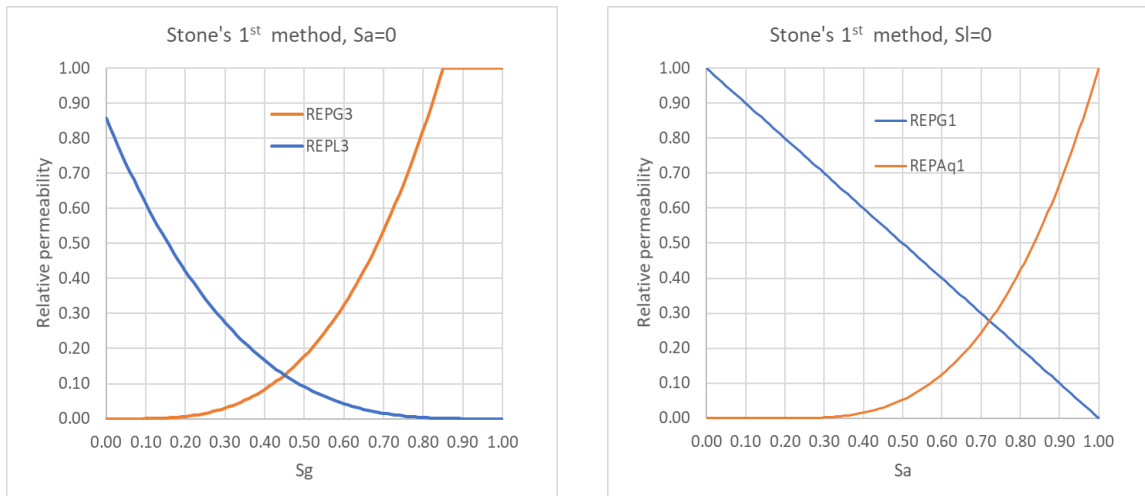
A1.1 Characteristic curves

Figure A2: *Stone's first three-phase method for gas (REPG3) and liquid (REPL3), and gas (REPG1) and water (REPAq1) relative permeability computed with T2Well-ECO2M with parameters presented in Table A1 for reservoir domain.*
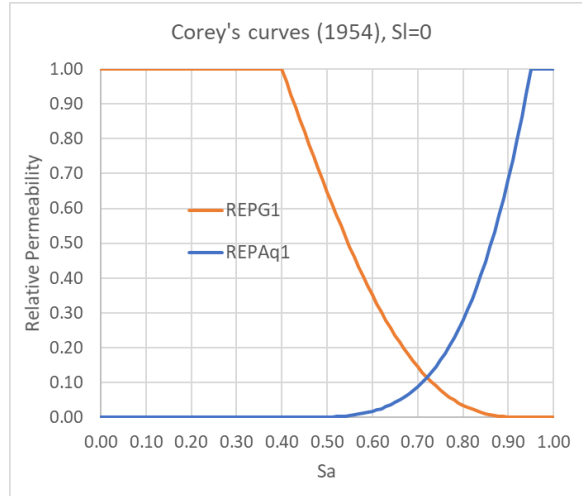
Figure A3: *Corey's curves for gas (RPG1) and aqueous (RPAq1) relative permeability computed with T2Well-ECO2M with parameters presented in Table A1 for caprock and bedrock domain.*
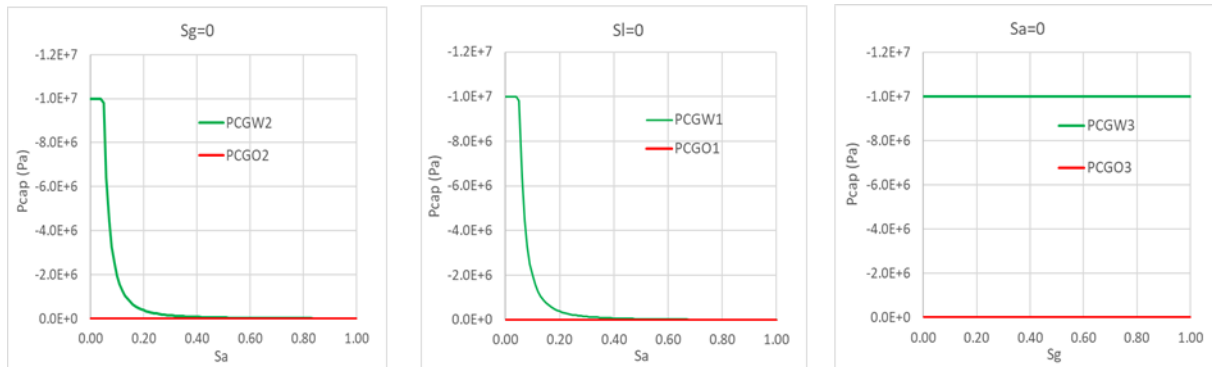
Figure A4: Capillary pressure curves for three-phase system with van Genuchten model (parameters presented in Table A1 for reservoir domain).
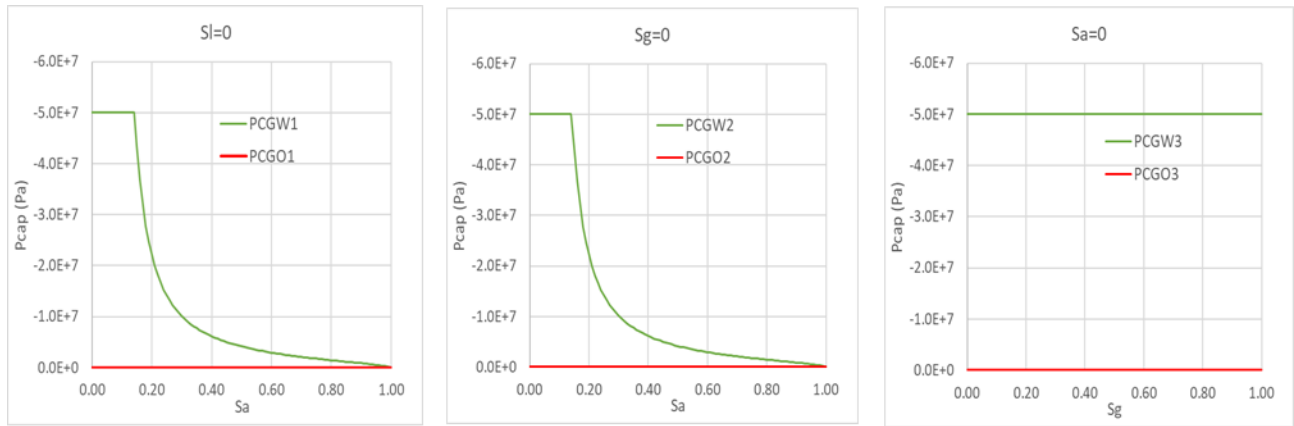
Figure A5: *Capillary pressure curves for three-phase system with van Genuchten model (parameters presented in Table A1 for caprock and bedrock domain).*

A1.2 Boundaries

Top and bottom boundaries of reservoir domain are impervious. At the top, there is the athmosphere layer with high thermal capacity (99920.0 J/(kg°C)) to ensure constant temperature of 15°C. The bottom-most layer, bedrock, is at the constant temperature of 61.7°C. The lateral boundary of the reservoir is closed and insulated.

A2. Time-convolution method application

```
*semianalytical_model* - 2-D reservoir model
MESHMAKER1----*----2----*----3----*----4----*----5----*----6----*----7----*----8
RZ2D
RADII
   2
      0.  0.037973
LAYER----1----*----2----*----3----*----4----*----5----*----6----*----7----*----8
  67
       1.        1.        2.       10.       10.       20.       50.       50.
      50.       50.       50.       50.       50.       50.       50.       50.
      50.       50.       50.       50.       50.       50.       50.       50.
      50.       50.       50.       50.       50.       50.       50.       50.
      50.       50.       50.       50.       50.       50.       50.       50.
      50.       50.       50.       50.       50.       50.       50.       50.
      50.       50.       50.       50.       50.       50.       50.       50.
      50.       50.       50.       50.       50.       50.       50.       50.
      50.       50.       50.
ENDFI
```

Figure A6: *Input file for MESHmaker for 2D radially symmetric grid of injection site model presented in chapter 5.*

Table A2: *Input parameters for model with fully numerical wellbore to formation heat exchange from comparison in chapter 5.*

Wellbore		
Internal diameter	2.99	inch
Wall roughness	1.E-5	m
Depth of tubing installation	3092.0	m
Rock grain density of wellbore surrounding*	2385.0	kg/m^3
Thermal conductivity of wellbore surrounding*	2.50	W/(m°C)
Rock grain spec. heat*	1000.0	J/(kg°C)
Completion domain		
Rock grain density	2690.0	kg/m^3
Porosity	1.E-10	-
Abs. permeability (x,y.z)	1.E-20, 1.E-20, 1.E-20	m^2
Thermal conductivity	2.50	W/(m°C)
Rock grain spec. heat	920.0	J/(kg°C)
Surrounding formation		

Rock grain density	2690.0	kg/m^3
Porosity	0.05	-
Abs. permeability (x,y.z)	5.E-15, 5.E-15, 5.E-15	m^2
Thermal conductivity	2.50	W/(m°C)
Rock grain spec. heat	920.0	J/(kg°C)
Temperature distribution	15.2°C @ 0 m 61.7°C @ 3142 m (bedrock)	
Pressure distribution	Hydrostatic pressure gradient	
Caprock and bedrock		
Rock grain density	2690.0	kg/m^3
Porosity	0.01	-
Abs. permeability (x,y.z)	1.0E-19, 1.0E-19, 1.0E-18	m^2
Thermal conductivity	2.50	W/(m°C)
Rock grain spec. heat	920.0	J/(kg°C)
Relative permeability: Corey's curves (1954) S_{lr}, S_{gr}	0.40, 0.05	
Capillary pressure: van Genuchten (1980) λ, S_{lr}, $1/P_0$, P_{max}, S_{ls}	0.44380, 8.01E-2, 5.792e-07, 5.E7, 1.0	
Atmosphere (0 m - +2 m)		
Rock grain density	2600.0	kg/m^3
Porosity	0.90	-
Abs. permeability (x,y.z)	1.0E-19, 1.0E-19, 1.0E-18	m^2
Thermal conductivity	2.50	W/(m°C)
Rock grain spec. heat	99920.0	J/(kg°C)
Reservoir		
Reservoir thickness	50.0	m
Rock grain density	2690.0	kg/m^3
Porosity	0.20	-
Abs. permeability (x,y.z)	1.0E-13, 1.0E-13, 1.0E-14	m^2
Thermal conductivity	2.30	W/(m°C)
Rock grain spec. heat	920.0	J/(kg°C)
Initial (residual) brine saturation	0.20	-
Brine salinity	50,000	ppm
Relative permeability: Stone's 1st three-phase method (modified) (1970) S_{ar}, S_{lr}, S_{gr}, n	0.20, 0.05, 0.05, 3	
Capillary pressure: van Genutchen (1980) λ, S_{lr}, $1/P_0$, P_{max}, S_{ls}	0.30, 0.00, 1.105E-4, 1.E7, 0.999	

* required parameters for wellbore rocktype definition

Table A3: Input parameters for model with semi-analytical (time-convolution) wellbore to formation heat exchange from comparison in chapter 5.

Wellbore		
Internal diameter	2.99	inch
Wall roughness	1.E-5	m
Depth of tubing installation	3092.0	m
Rock grain density of wellbore surrounding*	2385.0	kg/m^3
Thermal conductivity of wellbore surrounding*	2.50	W/(m°C)
Rock grain spec. heat of wellbore surrounding*	1000.0	J/(kg°C)
Reservoir		
Reservoir thickness	50.0	m
Rock grain density	2690.0	kg/m^3
Porosity	0.20	-
Abs. permeability (x,y.z)	1.0E-13, 1.0E-13, 1.0E-14	m^2
Thermal conductivity	2.30	W/(m°C)
Rock grain spec. heat	920.0	J/(kg°C)
Initial (residual) brine saturation	0.20	-
Brine salinity	50,000	ppm
Relative permeability: Stone's 1st three-phase method (modified) (1970) S_{ar}, S_{lr}, S_{gr}, n	0.20, 0.05, 0.05, 3	
Capillary pressure: van Genutchen (1980) λ, S_{lr}, $1/P_0$, P_{max}, S_{ls}	0.30, 0.00, 1.105E-4, 1.E7, 0.999	
QLOSS**		
Rock grain density of wellbore surrounding	2690.0	kg/m^3
Wellbore radius	0.037973	m
Reference depth (z coordinate)	1.5	m
Reference temperature	15	°C
Thermal conductivity of wellbore surrounding	2.50	W/(m°C)
Rock grain specific heat of wellbore surrounding	950.971376	J/(kg°C)

* required parameters for wellbore rocktype definition

**QLOSS -required parameters for time-convolution method for wellbore to formation heat exchange, with constant wellbore and formation properties (MOP(15)=5)